Development of Advanced Control Methods Applicable to Industrial Processing Systems

Song Xu

Gunma University

February 2020

Abstract

With the fast development of science and technology, industrial processes such as thermal process, manufacturing process, production process and so on are becoming more and more important, and have higher requirement for the operation performance. Thermal processing system, as one of the most complex processes, has a wide range of applications in the industrial field especially in the food process. For the multi-point (multi-input multi-output) thermal processing systems, temperature control is playing a more and more important role in its application. The proportional-integral-derivative (PID) control technologies have been widely used for most of the industrial processes. However, due to the nonlinearity and large dead time of the temperature control objects, the performance of PID-only control system may not satisfy the expected requirements. Also, the coupling influence and dead time difference in the multi-point temperature system have a significant effect to the transient response of each point.

Two advanced control methods are proposed in this thesis to deal with the two shortcomings mentioned above, respectively. For the coupling influence and dead time difference in the multi-point temperature control system, a pole-zero cancellation method is proposed. While for the nonlinearity and large dead time of the control objects, a reference-model-based artificial neural network (NN) method is proposed.

1) Pole-zero cancellation method for multi-point temperature control system

The proposed method is one kind of the model-based advanced control method. In order to realize the model-based advanced control, the system identification method was performed to obtain the plant model of the control object. The detailed introduction of the system identification method for first order plus time delay (FOPTD) system has been presented. Based on the identified plant model, the multi-input multi-output (MIMO) PI control system was designed as such. Due to the strong coupling effect of the controlled object, the decoupling compensation was added into the MIMO PI control system. The experiments for the MIMO PI control system with and without decoupling compensation were then carried out. Upon these foundations, the pole-zero cancellation method has been proposed for the MIMO temperature

control system to ensure proper transient response and to provide more closely controlled temperatures. In the proposed method, the temperature difference and transient response of all points can be controlled by considering the delay time difference and coupling term together with matrix gain compensation, and by investigating the pole-zero cancellation with feedforward reference model to the control loop. The simulations were carried out in the MATLAB/SIMULINK environment, and the experiments were performed based on the DSP controlled system platform. The effectiveness of the proposed pole-zero cancellation method was evaluated by comparing the results to those of a well-tuned conventional PI control system and PI plus decoupling compensation system.

2) Reference-model-based Artificial NN control method for temperature control system

In this method, a reference-model-based artificial neural network (NN) control method has been proposed for the temperature control system. Several types of neural network structure and activation function are investigated, and the multi-layer NN structure is chosen with the ReLU function as its activation function. The control system is driven by using the error signal between system output and reference model output as the teaching signal of the NN controller. The proposed method is a reference-model-based NN system combined with I-PD control structure. The reference model and I-PD parameters are designed based on the FOPTD system. The simulation was carried out in MATLAB/SIMULINK environment to evaluate the control performance of the proposed method by comparing with the conventional feedback error learning NN control system. The effectiveness of the proposed method has been evaluated by focusing on the overshoot and transient response of the controlled system. As a result, the robustness of the proposed reference model-based NN control method for the plant perturbation and disturbance has been successfully verified. In addition, the recurrent type NN structure was then introduced to the control system, and simulations were carried out to compare with the feedforward type NN control system. Finally, the experiments of the proposed control method have been carried out on a DSP-based temperature system platform. The results are quantitively evaluated by taking the transient response into account.

ACKNOWLEDGMENT

TABLE OF CONTENT

Chapter 1

Introduction

1.1 Introduction

With the development of the science and technology, the requirements of the fierce competition, resources and environment in the contemporary world market are pushing the world's process industry to pursue advanced control and make full use of information and computer technology, so that enterprises continue to increase their ability to respond to the market, including organizing and adjust the production in time according to the market needs; fully tap the production potential; improve the efficiency; reduce the consumption; ensure the quality; control the three wastes; ensure the safety; reduce the inventory; accelerate the capital turnover and achieve the overall optimization of the production process and business process. In recent years, it has become a standard development model for computer applications that with adopted highly reliable, intelligent instrumentation, distributed control systems and advanced process control strategies to achieve optimization at all levels, and then promote management information systems, organize computer-integrated management and control integration.

In the current industrial process, traditional control is still used in over 95% of the loops. The extensive application of control is related to its simple design and relatively easy parameter setting. It can indeed meet the requirements of most simple control loops. However, for more and more complex industrial processes, especially the existence of large pure time delay, large inertia, and nonlinear systems, it is often difficult for control to meet the requirements of control quality one. Therefore, it is hoped that the quality of control can be improved through the application of advanced control methods.

Advanced control in the 19th century mainly refers to those algorithms and strategies that are different from conventional PID control. From the beginning of the 20th century, with the

widespread application of training and computer technology, blank motion control has developed greatly. Advanced process control (APC) has rich content and wide coverage, including predictive control, adaptive control, and robust control, etc. It is a powerful means of tapping potentials and improving efficiency on the basis of existing devices and foundations. It can help companies to significantly reduce production costs from a control perspective, and improve product output and quality. This effectively improves the competitiveness of the enterprises.

As an important branch of advanced process control, predictive control is a new type of computer control algorithm that appeared in the European and American industrial fields in the mid to late 19th century.

Since predictive control technology has been proposed, it has been favored by the process control community for its excellent control performance. Predictive control requires a dynamic model of the processing system, but only emphasizes the function of the model and does not pay attention to its structural form. It maintains the controlling idea based on optimization but restricts the optimization to the limited time domain, which is conducive to solving the constrained multi-objective multi-degree-of-freedom optimization closed-loop in the control process through online iterative optimization and feedback correction. Also, it is used to timely correct the effects of modeling errors and other uncertain factors, so it has a strong ability to adapt to complex environments. Because of the above advantages and the flexibility of predictive control when dealing with multi-objects optimization control problems with constraints, it naturally becomes one of the most effective methods for multi-variable constraint control of the complex industrial processes.

1.2 Overview of advanced control technology

1.2.1 Development of advanced control technology

Since the development of the third-generation control theory in the twentieth century, high-tech development and research departments have organically combined the chemical

engineering, process control theory, instruments, and computers to design a new type of multi-input multi-output advanced control software, which can solve the non-controllable chemical process problems such as non-linear, time-varying, large time lag, and improve the operating performance of the device, so as to achieve the effect energy saving and consumption reduction to improve the overall economic benefit of the device, this technology is so-called advanced control technology. Through reasonable configuration, the advanced control (APC) technology can realize closed-loop online applications.

The design idea of the advanced control is based on multi-variable estimation. The process model is used to predict the output of the future moment. The process model is corrected by the difference between the actual output of the object and the model's predicted output, so that several variables to be controlled are controlled in one desired industrial control point and the whole devise is pushed to the best state. At present, advanced control technology not only continuously introduces new results in theory but also has achieved remarkable results in practical production applications.

Advanced control such as model recognition and optimization algorithms are different from conventional control, but the effect of these control is not just a computer control algorithm. Although there is still no clear definition, its task is clear, that is, it is used to deal with the problems of complex systems with conventional control effects. The advanced nature of these control methods should be reflected in the following aspects:

1). Unlike conventional control, advanced control is usually a model-based control strategy, such as model predictive control. At present, intelligent control technologies such as expert control, neural network control, fuzzy control and improve methods of predictive based control are becoming an important development direction of advanced control.

2). Advanced control is usually used to deal with complex process control problems, such as large time delays, multi-variable failures, various constraints on the control variables, etc. Advanced control is a dynamic coordinated constraint control based on conventional single-loop control and can make the control system adapt to the dynamic characteristics and operational requirements of the actual industrial production process.

3). The real-time advanced control requires sufficient computing power to support it. Because

3

the advanced control is affected by the complexity of the control algorithm and the computer hardware, most of the advanced control algorithms are usually implemented on the host computer of the computer control system.

1.2.2 Classification of process control strategies

The well-known process control expert D. E. Seborg classified the process control strategies into five categories.

1) Conventional control strategies which include manual control, PID control, and ratio, cascade, feed-forward, etc.

2) Advanced control—Classic methods, such as gain adjustment, delay time compensation, and decoupling control.

3) Advanced control—popular methods, such as model predictive control, internal model, self-adaptive, statistical quality, etc.

4) Advanced control—Potential technologies, such as optimal control, nonlinear control, expert control, neural network control, fuzzy control, etc.

5) Advanced control—The latest progress, such as robust control, H_∞ control, U integration, etc.

Different researchers and research purposes will produce different views about what exactly should be included in advanced control technology. But it is certain that controller parameter self-tuning, adaptive control, model prediction, etc. should be the main content of advanced control technology at this stage.

1.2.3 Models of industrial processes

According to the requirements of the control, the model must contain information that can predict the consequences of changing the operating conditions of the process and can be roughly divided into four models depending on the method used.

1) Mechanism model: For those objects with clear processes and obvious characteristics, a set of differential equations can be used to describe its dynamic process. The mechanism model

is usually established according to the basic principles of chemistry or physics. The final model depends on the system, and if the concentrated parameters are represented by centralized parameters, the distributed parameters are represented by the partial differential equations. And ordinary differential equations are described in a one-dimensional manner, usually time partial differential equations are described in state space. Generally speaking, distributed parameter models are more complex and more cumbersome. By simplifying some assumptions, a series of ordinary differential equations can be used to represent the distributed parameter model, both of which can be subdivided into linear and nonlinear. In many cases, due to time and capital constraints, the development mechanism model is not realistic, especially when the object process is fuzzy or the obtained equations are complex and cannot be solved, the black box model empirical model established using the data from the object has advantages.

2) Black box model: The black-box model simply describes the functional relationship between the input and the output of the system. It is established by analyzing the historical production data of the actual soil process and using appropriate mathematical methods. Compared with the mechanism model, the function parameters of the black box model have no trends of the process behavior, then the method of the black-box model is also effective, and the cost of developing the black box model is often lower than the mechanism.

3) Qualitative models: In the industrial process, there are many objects that involve heat transfer, mass transfer and chemical reactions. Due to their non-linearity, complex mechanisms, difficult detection and uncertainty, it is difficult to establish a suitable mathematical model. In this case, establish a qualitative model can be one choice. The simplest form of the qualitative model is a rule-based model that uses "if-then-else" to describe process behavior. These rules come from human experts. Similarly, genetic algorithms and rule induction techniques can also be applied to process data to generate these described rules.

4) Statistical model: Due to the uncertainty of the process systems, statistical methods become necessary. This technology has been widely used in statistical data analysis, information theory, strategy theory and decision system theory. The probability model is characterized by the probability density function of the variables. It gives the possibility of a certain value of the variables. The correlation model can be obtained by monitoring the changes

of the variables and then quantifying the similarity between them.

1.3 Intelligent control method

As one of the important directions for the modern advanced control technology, intelligent control methods have become a very active and challenging field in today's world automation disciplines. Also, it represents one of the latest directions in the development of science and technology of today's industrial control.

1.3.1 Definition of intelligent control

Intelligent control is the product of the intersection of artificial intelligence and control theory and is an advanced stage of the development of classical control theory. Its ability and level of problem-solving are significantly higher than those of conventional control. Its core task is to use human-like intelligent control decision-making to control systems with complexity and uncertainty.

1.3.2 Characteristics of intelligent control

The main characteristics of intelligent control can be concluded as four main points:

1) The intelligent control has effective global control and strong fault tolerance for uncertain systems.

2) The intelligent control is a multi-modal combination control method which is combined with the qualitative decision-making and quantitative control.

3) The intelligent control can analyze and synthesize the system from the perspective of system function and overall optimization to achieve predetermined goals. It has the good self-organizing ability.

4) The intelligent control system is a hybrid control process that can process information with mathematical operation, logic and knowledge reasoning methods.

1.3.3 Areas of intelligent control

Then main areas of intelligent control can be divided into three parts: Fuzzy control, Neural networks, Genetic algorithms and Expert control.

1.3.3.1 Fuzzy control

The concept of "Fuzzy sets" was first proposed in 1965 by L. A. Zadeh, an expert in Automatic Control Theory, University of California. Fuzzy control is a kind of control based on fuzzy reasoning and imitating human thinking. It is a kind of control for objects that are difficult to establish accurate mathematical models. The root of its successful application is that fuzzy logic itself provides language information for experts to construct linguistic information and transform it into control strategies. A fuzzy controller is shown in Figure 1-1. The fuzzy controller has several components:

- The rule-base is a set of rules about how to control.
- Fuzzification is the process of transforming the numeric input into a form that can be used by the inference mechanism.
- The inference mechanism uses information about the current inputs (formed by fuzzification), decides which rules apply in the current situation, and forms conclusions about what the plant input should be.
- Defuzzification converts the conclusions reached by the inference mechanism into a numeric input for the plant.
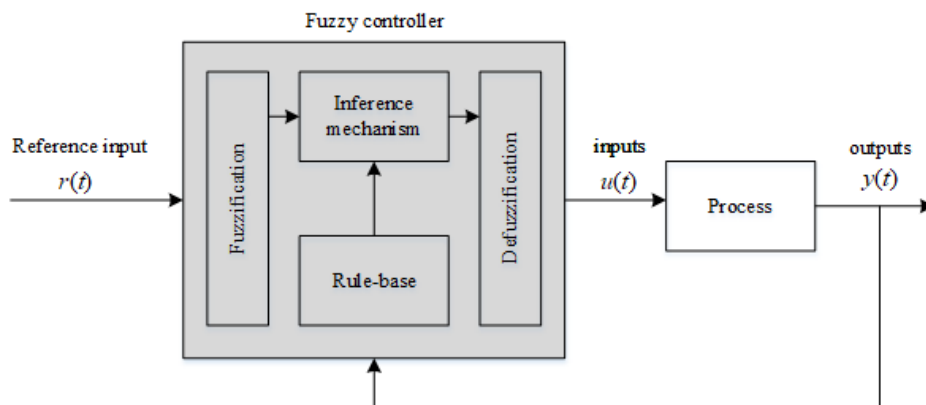
Figure 1-1 Fuzzy control.

7

1.3.3.2 Neural networks

Neural network control is an intelligent control and identification method based on a structure that mimics the physiological structure of the human brain as shown in Figure 1-2.
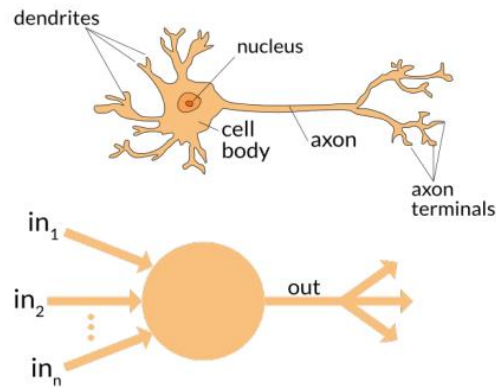
Figure 1-2 Physiological structure of the neuron.

With the continuous deepening of the application research of artificial neural networks, new models are continuously introduced. In the field of intelligent control, the most widely used are the BP network and the Hopfield network. Compared with the conventional control method the neural network has the following important characteristics:

➢ Non-linearity, the neural network can fully approximate any non-linear function in theory.

➢ Parallel distributed processing, the neural network has a highly parallel structure and parallel implementation capabilities, which makes it have a greater degree of fault tolerance and strong data processing capabilities.

➢ Learning and self-adaptability, neural networks can learn and remember the information provided by the knowledge environment.

➢ Multivariable processing. Neural networks can naturally process multi-input signals and have multi-outputs. It is very suitable for multi-variable systems.

At present, neural networks have been successfully applied in many fields such as signal processing, system identification and optimization, pattern recognition, fault diagnosis and robotics. It will have great and far-reaching significance for the development and application of intelligent control.

However, we also see that there are still many problems in the theory and design methods of neural network control for further research, mainly the analysis methods of artificial neural network system stability, the selection and optimization of neural network structure and size, the convergence and real-time problems of learning and control algorithms, and how to apply neural network theory to specific control systems to improve performance, etc.

1.3.3.3 Genetic algorithms

A genetic algorithm (GA) is a computational model that simulates the natural evolution and biological mechanism of Darwin's biological evolution theory. It is a method to search for the optimal solution by simulating natural evolution of organisms. The main strategy of its operation is to establish the solution set of the population of potential problems of the control object to achieve the encoding of genes. Individuals realize coding, as a combination of multiple genes, from which to start solving a certain gene combination. Just as the adjustment of black hair is a strange thing determined by a certain segment of the chromosome in each subject.

The genetic algorithm also implements the process of mapping phenotype genes to coding and then solving. The main features of the genetic algorithm are:
- ➢ Take the coding of decision variables as the operation object.
- ➢ Use the objective function value directly as the search information.
- ➢ Simultaneous multi-point search of solution space.
- ➢ Use adaptive probability search technology.

1.3.3.4 Expert control

Expert control developed in the field of artificial intelligence is a technology of knowledge-based intelligent computer programs. The essence of expert control is based on various knowledge of control objects and control laws, and it is necessary to use this knowledge in an intelligent way in order to obtain the optimization and practicality of the control system as much as possible. One simple expert control system is shown in Figure 1-3.
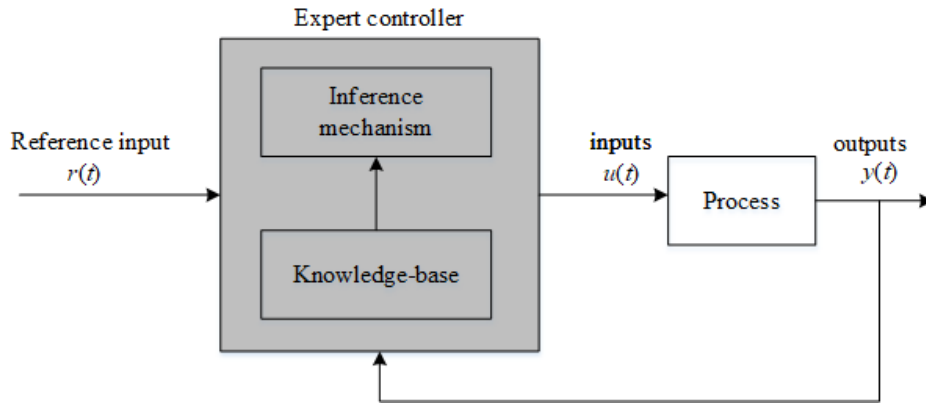
Figure 1-3 Expert control.

Expert systems generally consist of a knowledge base, an inference engine, an explanation mechanism, and a knowledge acquisition system. The knowledge base is used to store the empirical knowledge, principle knowledge, feasible operations and rules of experts in a certain field. The original knowledge can be modified and expanded through the knowledge acquisition system. The inference engine solves the current problem according to a certain inference strategy based on the system information and the knowledge in the knowledge base. The interpretation mechanism explains the knowledge found and provides a human-machine interface for the user.

The characteristics of the expert control are as follows:

1) With domain expert-level expertise, capable of symbol processing and heuristic reasoning.

2) Have the ability to acquire knowledge, have flexibility, transparency and interaction.

1.4 Temperature control in industrial process

Temperature control is a common control object in industrial process control and accounts for a considerable proportion of industrial production energy consumption. There many areas where temperature control is required and different industries have different requirements for temperature control. The quality of temperature control directly affects the quality and production efficiency of industrial products. For example, in the beer fermentation process, the proper temperature can greatly increase the speed of beer fermentation and improve production efficiency, the product distillation process requires a higher temperature. Different products

may be obtained at different temperatures. The stable temperature can not only speed up the product separation process, but it can also increase the purity of the product. Improving the temperature control of the heating furnace in steel rolling will not only reduce energy consumption, improve production efficiency, but also reduce the occurrence of defective products in steel rolling.

In short, temperature control is one of the most important control objects in industrial processes. Improving the performance of temperature process control is of great significance to industrial production.

The characteristics of temperature control are as follows:

1) Large inertia: Inertia is a property that anything has to maintain its original motion or static state. The inertia of a thing is often related to its quality and its nature. Temperature is a manifestation of the intensity of the molecular motion of an object. It is often because of the slower heat transfer and its larger range of action. It is not easy to change its original temperature, that is, it shows large inertia.

2) Non-linearity: Non-linearity is a situation where the input and output are not proportional. Temperature and energy are in a linear relationship, but the temperature change is often due to different fuel combustion values, changes in the composition of the heated object or uneven heat dissipation and heating factors, which presents an uncertain characteristic of the relationship between the temperature change and the input given quantity, that is, nonlinear features

3) Large time lag: Because the control of temperature is often not the control of one point of temperature, but the control of the whole thing or a wide range of temperature, the process of temperature rise is often a process from local to overall, so from heating to temperature, the change often takes a certain time, that is, the temperature change has a large lag.

Due to these features of temperature control, coupled with different control objects, difference control accuracy and control requirements, the method of temperature control is also different. The conventional control method is PID control, in order to improve the adaptive range of PID control, fuzzy control and PID control method are combined to generate the fuzzy PID control algorithm. In order to improve the robustness of the controller and the adaptability

11

when the model is changed, a predictive control algorithm can also be introduced. For control objects with coupling effects, decoupling compensation can be applied to reduce the influence between coupling terms. For large time lags. Smith predictive compensation can also be used for control.

In this research, focused on the temperature control system, two main advanced control methods will be proposed: 1) Model-based Pole-Zero cancellation method for the multi-point temperature control system. 2) Model-Free reference model-based artificial neural network control method for the temperature control system with large time lag.

1.5 Main objective

This study will focus on the application of advanced control methods and its application in temperature control systems, and can be mainly divided into two parts: 1) Model-Based Pole-Zero Cancellation Control Method for Multi-point temperature control system. 2) Model-Free Reference-Model-Based Neural Network Method for temperature control system with large lag. The entire thesis can be divided into four chapters.

Chapter 1: Introduction. In this chapter, a brief overview of the advanced control and its historical development is introduced. The models of the industrial processes and their characteristics are presented. The intelligent control method and the overview of its main areas are introduced. At last, the temperature control system characteristics and difficulties in temperature control are performed.

Chapter 2: The Model-Based Pole-Zero Cancellation method for multi-point temperature control system is introduced including system identification, parameter autotuning, decoupling compensation and pole-zero cancellation control. The presentation flows through theoretical analysis and system simulation to real process experiments. Both simulation and experimental results are finally compared to the conventional PI control system to verify the efficiency of the proposed method.

Chapter 3: The Model-free reference-model-based artificial neural network control method for temperature control system with large time lag is introduced. The systematical introduction of several neural network types is done and the simulations are carried out to evaluate the

control efficiency of the proposed method. The experiments are carried out on a DSP based temperature control platform. The results are compared to the conventional I-PD control system to verify the control efficiency of the proposed method.

Chapter 4: The research content of this topic is summarized, and the remaining problems are pointed out, which lays the foundation for further research in the future.

Reference

[1] Lúa. A. Zotică. R C, Skogestad. S, Optimal Operation with Changing Active Constraint Regions using Classical Advanced Control, IFAC-Papers OnLine, 2018, 51, 18, 440-445.

[2] Bagheri. M, Akbari. A, Mirbagheri. S. A, Advanced control of membrane fouling in filtration systems using artificial intelligence and machine learning techniques: A critical review, Process Safety and Environmental Protection, 2019, 123, 229-252,

[3] Jin. S, Zhao. B. T, Su. Y. X, Advanced control of NO emission from algal biomass combustion using loaded iron-based additives, Energy, 2019, 185, 229-238.

[4] Tahir. F, Mercer. E, Lowdon. I, Lovett. D, Advanced process control and monitoring of a continuous flow micro-reactor, Control Engineering Practice, 2018, 77, 225-234.

[5] Shao. G. D, Latif. H, Villalba. C. M, Denno. P, Standards-based integration of advanced process control and optimization, Journal of Industrial Information Integration, 2019, 13, 1-12.

[6] Zhou. Y, Lorenz T, Advanced-step multistage nonlinear model predictive control: Robustness and stability, Journal of Process Control, 2020, 85, 15-29.

[7] Choi. J. S, Kim. K. M, Changes in infection control policies and advancing infection control advanced practice nurse education in the Republic of Korea, American Journal of Infection Control, 2019.

[8] Zhou. J, Lorenz T, Advanced-step multistage nonlinear model predictive control: Robustness and stability, Journal of Process Control, 2019, 84, 192-206.

[9] Manoli. K, Sarathy. S, Maffettone. R, Domenico Santoro, Detailed modeling and advanced control for chemical disinfection of secondary effluent wastewater by peracetic acid, Water Research, 2019, 153, 251-262.

[10] Zhou. P, Lu. S, Yuan. M, Chai. T, Survey on higher-level advanced control for grinding circuits operation, Powder Technology, 2016, 288, 324-338.

[11] Sangi. R, Müller. D, A novel hybrid agent-based model predictive control for advanced building energy systems, Energy Conversion and Management, 2018, 178, 415-427.

[12] Lv. Y, Qian. S, Du. S, Chen. J, Zhou. J, Xu. C, Coupling feedback genetic circuits with growth phenotype for dynamic population control and intelligent bioproduction, Metabolic Engineering, 2019, 54, 109-116.

[13] Joyce. P, Gustafsson. H, Engineering intelligent particle-lipid composites that control lipase-mediated digestion, Advances in Colloid and Interface Science, 2018, 260, 1-23.

[14] Morillo. D, Olaby. O, Granero. M. A, Physiological closed-loop control in intelligent oxygen therapy: A review, Computer Methods and Programs in Biomedicine, 2017, 146, 101-108.

[15] Khayyam. H, Ranjbarzadeh. H, Marano. V, Intelligent control of vehicle to grid power, Journal of Power Sources, 2012, 201, 1-9.

[16] Zhang. L, Zhou. L, Ren. L, Lai. L, Modeling and simulation in intelligent manufacturing", Computers in Industry, 2019, 112, 103-123.

[17] Ma. H, Yu. C, Dong. L, Fu. Y, Shuai. C, Sun. H, Zhu. X, Review of intelligent well technology, Petroleum, 2019.

[18] Magdi. S, Nezar. M, Mohamed. I, Adaptive intelligent techniques for microgrid control systems: A survey, International Journal of Electrical Power & Energy Systems, 2017, 90, 292-305.

[19] Dai. Y, Zhu. Z, Shan. Z, Cheng. Z, A Survey on Intelligent Screening for Diabetic Retinopathy, Chinese Medical Sciences Journal, 2019, 34, 2, 120-132.

[20] Cao. H, Zhang. X, Chen. X, The concept and progress of intelligent spindles: A review, International Journal of Machine Tools and Manufacture, 2017, 112, 21-52.

[21] Alessa. D, Jason. DM, Micro needling Options for Skin Rejuvenation, Including Non–temperature-controlled Fractional Microneedle Radiofrequency Treatments, Facial Plastic Surgery Clinics of North America, 2020, 28, 1, 1-7.

[22] Petrie. M. D, Wildeman. A. M, Bradford. J. B, Hubbard. R. M, A review of precipitation and temperature control on seedling emergence and establishment for ponderosa and lodgepole pine forest regeneration, Forest Ecology and Management, 2016, 361, 328-338.

[23] Zhou. J. K, Claridge. D. E, PI tuning and robustness analysis for air handler discharge air temperature control, Energy and Buildings, 2012, 44, 1-6.

[24] Xu. X, Zhong. X, Deng. S, Zhang. X, A review on temperature and humidity control methods focusing on air-conditioning equipment and control algorithms applied in small-to-medium-sized buildings, Energy and Buildings, 2018, 162, 163-176.

[25] Michael. J. F, Myron. P. Z, Climate change and biological control: the consequences of increasing temperatures on host–parasitoid interactions, Current Opinion in Insect Science, 2017, 20, 39-44.

[26] Zhang. T, Liu. X, Jiang. Y, Development of temperature and humidity independent control (THIC) air-conditioning systems in China—A review, Renewable and Sustainable Energy Reviews, 2014, 29, 793-803.

[27] Bakir. T, Bonnard. B, Rouot. R, Geometric optimal control techniques to optimize the production of chemical reactors using temperature control, Annual Reviews in Control, 2019, 48, 178-192.

[28] Shaterabadi. Z, Nabiyouni. Z, Soleymani. M, Physics responsible for heating efficiency and self-controlled temperature rise of magnetic nanoparticles in magnetic hyperthermia therapy, Progress in Biophysics and Molecular Biology, 2018, 133, 9-19.

[29] Sevil. Ç, Zehra. Z, Hale. H, Mustafa. A, Optimal temperature control in a batch polymerization reactor using fuzzy-relational models-dynamics matrix control, Computers & Chemical Engineering, 2006, 30, 9, 1315-1323.

[30] Michael. W, Temperature Control of Premature Infants in the Delivery Room, Clinics in Perinatology, 2006, 33, 1, 43-53.

Chapter 2

Pole-Zero Cancellation Method for MIMO Temperature Control System

2.1 Experimental setup

Before the control method is designed and applied, the experimental setup needs to be introduced first. The designed method will be applied to the experimental setup shown in Figure 2-1. It includes a digital signal processor (DSP) as the temperature controller. The system has four coupled channels. Each channel has two independent heaters and one temperature sensor. The temperature sensor transforms the temperature (0-400degree Celsius) into an output voltage (0-10VDC). The heaters are controlled by the solid-state relay (SSR has shown in Figure 2-1), and the SSR is driven by pulse width modulation (PWM) signals. The temperature can be controlled through the duty ratio of the PWM signals.
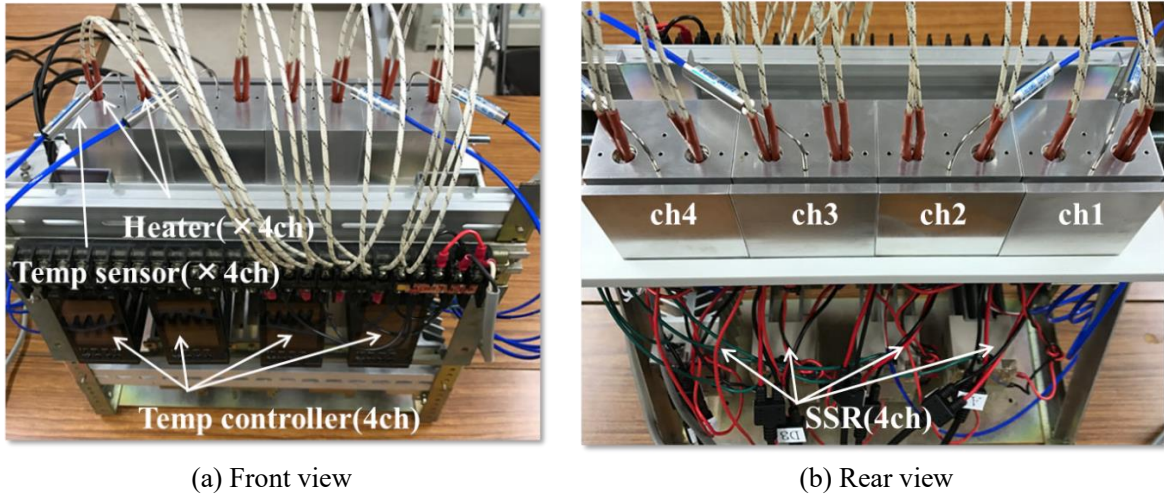

(a) Front view   (b) Rear view

Figure 2-1 Experimental setup.

2.2 System identification

In order to realize precise temperature control by the model-based advanced control method, the mathematical model of the control object needs to be obtained, thus, the system identification needs to be carried out.

2.2.1 System identification methods

System identification is based on the input and output time functions of the system to determine the mathematical model describing the behavior of the system. It is a branch of modern control theory. The main problem of analyzing the system is to determine the output signal according to the input time function and the characteristics of the system. The conventional system identification methods can be divided into three categories:

1). **Step response method**: This method generally refers to the output (response) of the system when the input is a step function in units.

2). **The least-squares (LS) method**: This method is a conventional data processing method. But because the least-squares estimation is non-uniform and biased, so in order to overcome its shortcomings, there have formed a number of identification methods based on the least-squares method.

3). **Maximum likelihood method**: The maximum likelihood method (ML) has very good performance for special noise models, and has good theoretical guarantees. But the calculation cost is large, and may get the local minimum of the loss function.

2.2.2 Step response system identification method

For our control object, the temperature system is a non-linear and time-continuous system, thus, the step response system identification method has been introduced. The theoretical of the step response identification is performed as follows.

In general, the numerator and denominator of the transfer function of a closed-loop system are polynomial of s, which can be written as Eq. (2-1)

$$\phi(s) = \frac{C(s)}{R(s)} = \frac{b_m s^m + b_{m-1} s^{m-1} + \cdots + b_1 s + b_0}{a_n s^n + a_{n-1} s^{n-1} + \cdots + a_1 s + a_0} \tag{2-1}$$

The Eq. (2-1) can be expressed as the product of the following factors as Eq. (2-2).

$$\phi(s) = \frac{C(s)}{R(s)} = \frac{K\prod\limits_{i=1}^{m}(s - z_i)}{\prod\limits_{i=1}^{n}(s - s_i)} \tag{2-2}$$

In practical control systems, all closed-loop poles are usually different. Therefore, when the input is a unit step function, the output can be expressed as Eq. (2-3)

$$C(s) = \frac{K\prod\limits_{i=1}^{m}(s - z_i)}{\prod\limits_{j=1}^{q}(s - s_j)\prod\limits_{k=1}^{r}(s^2 + 2\zeta_k\omega_k s + \omega_k^2)} \cdot \frac{1}{s} \tag{2-3}$$

Where q and r satisfy the relationship as shown in Eq. (2-4).

$$q + 2r = n \tag{2-4}$$

In the equation, q is the number of real poles, r is the logarithm of conjugate complex poles. Assuming that $0 < \zeta < 1$, extend Eq. (2-3) into the partial fractions as Eq. (2-5):

$$C(s) = \frac{A_0}{s} + \sum_{j=1}^{q}\frac{A_j}{s - s_j} + \sum_{k=1}^{r}\frac{B_k s + C_k}{s^2 + 2\zeta_k\omega_k s + \omega_k^2} \tag{2-5}$$

Assuming that all initial conditions are zero, inverse Laplace transform of Eq. (2-5) can be used to obtain the unit step response of higher-order systems as shown in Eq. (2-6).

$$h(t) = A_0 + \sum_{j=1}^{q}A_j e^{s_j t} + \sum_{k=1}^{r}B_k e^{-\zeta_k\omega_k t}\cos(\omega_k\sqrt{1 - \zeta_k^2})t +$$

$$\sum_{k=1}^{r}\frac{C_k - B_k\zeta_k\omega_k}{\omega_k\sqrt{1 - \zeta_k^2}}e^{-\zeta_k\omega_k t}\sin(\omega_k\sqrt{1 - \zeta_k^2})t, t \geq 0 \tag{2-6}$$

From Eq. (2-6), the time response of the higher-order system is composed of the time response function terms of the first-order system and the second-order system. At the same time, Eq. (2-1) can be written as Eq. (2-7).

$$G(s) = \frac{B(s)}{A(s)} = \frac{b_m s^m + b_{m-1} s^{m-1} + \cdots + b_1 s + b_0}{a_n s^n + a_{n-1} s^{n-1} + \cdots + a_1 s + a_0}$$

$$= \frac{b_m s^m + b_{m-1} s^{m-1} + \cdots + b_1 s + b_0}{\prod\limits_{i=1}^{q}(s + p_i)\prod\limits_{j=1}^{r}\left(s^2 + 2\zeta_j \omega_{nj} s + \omega_{nj}^2\right)}$$

$$= \sum_{i=1}^{q} \frac{k_{1i}}{s + p_i} + \sum_{k=1}^{r} \frac{k_{2j}}{s^2 + 2\zeta_j \omega_{nj} s + \omega_{nj}^2}$$

$$= \sum_{i=1}^{n} \frac{K_i}{T_i s + 1} + \sum_{j=1}^{m} \frac{K_{n+j}\omega_j^2}{s^2 + 2\zeta_j \omega_j s + \omega_j^2}$$

$$m < n, q + 2r = n$$

(2-7)

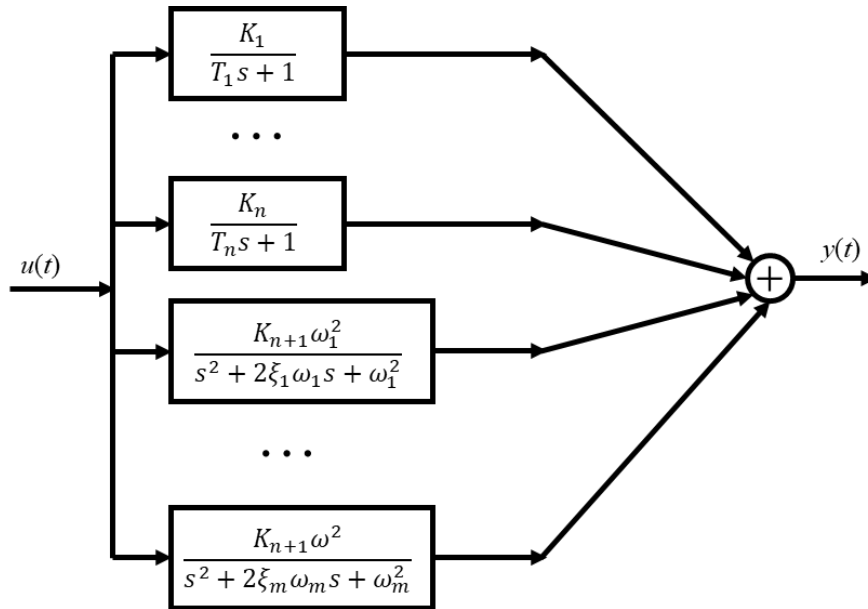According to this equation, a high order system can be decomposed into Figure 2-2.

Figure 2-2 Decomposition of higher-order linear system model.

To sum up, an estimation model of a higher-order system can be obtained by paralleling several first-order and second-order typical links, and the step response of the parallel model is used to approximate the step response of the actual system, thereby obtaining the mathematical model of the actual system.

Furthermore, the third-order and lower-order estimation models are combined through first-order and second-order typical links and the shape of the decomposition curve of the system model is adjusted by adjusting parameters to continuously approximate the step response of the higher-order system. The step response of the original high-order system is small compared to the error. Depending to the input and output characteristics, it can reflect the overall

characteristics of the original system. So that the third-order and lower-order systems can be used to equivalent high-order systems to find the transfer function.

2.2.3 Time domain analysis of linear systems

The evaluation of control system performance is divided into dynamic performance indicators and steady-state performance indicators. The dynamic performance indicators can reflect the response speed and damping range of the system, while steady-state performance indicators can reflect the control accuracy and anti-disturbance ability of the system. In practical applications, the commonly used dynamic performance indicators are mostly rising time t_r, which is a measure of the response speed of the system, overshoot $\delta\%$ that evaluates the degree of damping of the system. The adjustment time t_s is a comprehensive index that reflects both the response speed and degree of damping.

2.2.3.1 First-order systems

A typical first-order system can be expressed as Eq. (2-8).

$$G(s) = \frac{K}{Ts + 1}$$ (2-8)

The steady-state gain K determines the steady-state response value, and the time constant T determines the step response speed. The larger T is, the slower the response and the longer the rising time.

2.2.3.2 Identification method for first-order system

From Eq. (2-8), the system identification algorithm for the first-order system is as follows:
1) Steady-state gain K

$$K = y(\infty) - y(0)$$ (2-9)

In this equation, $y(\infty)$ represent the steady-state value of the step response and $y(0)$ represents the initial value.

2) Time constant T

Next, we need to find the coordinate point on the step response curve when the output changes to 95% of the final value. Its corresponding time is the adjustment time, which according to the dynamic performance index of the first-order system, it is known that t_s is three times of T, thus time constant T can be obtained as:

$$T = \frac{t_s}{3} \tag{2-10}$$

2.2.3.3 Verification of identification accuracy

In order to verify the identification method of the first-order system, the simulation has been carried out. Assuming that the identified system transfer function is as Eq. (2-11):

$$P(s) = \frac{5}{100s + 1} \tag{2-11}$$

A step signal is applied at the initial moment of the simulation, the simulation result is shown in Figure 2-3 and the identified system transfer function is as Eq. (2-12), the fitness is defined as the squared error between the system response and the identified system response.
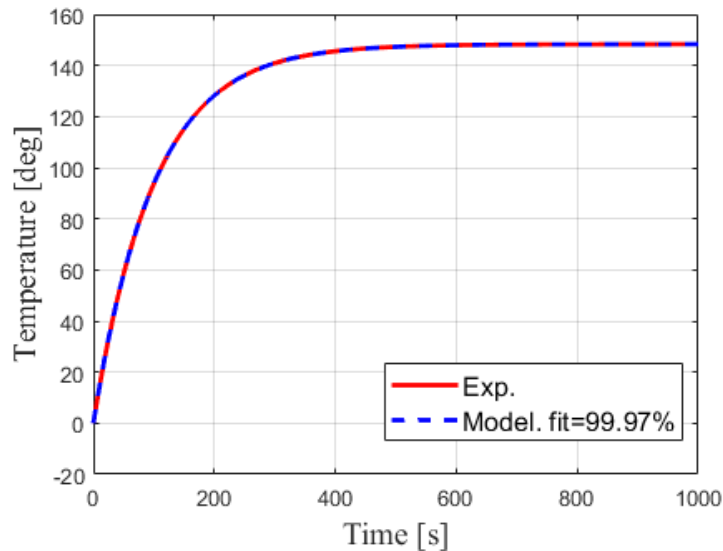

Figure 2-3 Identification result of first-order system.

$$P(s) = \frac{5}{99.973s + 1} \tag{2-12}$$

21

2.2.4 System identification of first-order plus time delay

2.2.4.1 Identification algorithm

In the temperature control system, the dead time is very large and can't be ignored, thus the above identification method needs to be improved. The typical identification structure of a linear plus delay time system is shown in Figure 2-4.
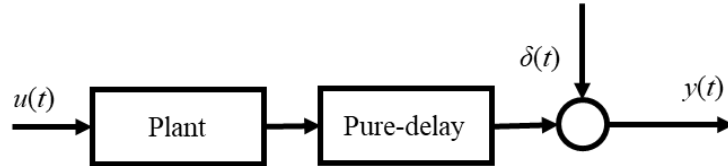

Figure 2-4 Typical identification structure of open-loop plant.

A linear single input single output system with pure delay time can be described as follows:

$$a_n y^{(n)}(t) = b_m u^{(m)}(t-\delta) + e(t) \tag{2-13}$$

$$a_n = [a_n, a_{n-1} \cdots a_0] \in R^{1\times(n+1)} \tag{2-14}$$

$$b_m = [b_m, b_{m-1} \cdots b_0] \in R^{1\times(m+1)} \tag{2-15}$$

$$y^{(n)}(t) = \left[y^{(n)}(t), y^{(n-1)}(t) \cdots y^{(0)}(t) \right] \in R^{1\times(n+1)} \tag{2-16}$$

$$u^{(m)}(t-\delta) = \left[u^{(m)}(t-\delta), u^{(m-1)}(t-\delta) \cdots u^{(0)}(t-\delta) \right] \in R^{1\times(m+1)} \tag{2-17}$$

Where, $y(i)$ and $u(i)$ respectively indicate the ith order differentials of y and u, $e(t)$ is the error term. Perform the Laplace transform at both sides of the above equation, the Eq. (2-18) can be obtained.

$$a_n s^n Y(s) = b_m s^m U(s) e^{-\delta s} + c_{n-1} s^{n-1} + E(s) \tag{2-18}$$

$Y(s)$, $U(s)$ and $E(s)$ are the Laplace transform of $y(t)$, $u(t)$ and $e(t)$, respectively. And at the same time the following equation can also be obtained as is shown in Eq. (2-19):

$$a_n s^n Y(s) = b_m s^m U(s) e^{-\delta s} + c_{n-1} s^{n-1} + E(s) \tag{2-19}$$

The element c_{n-1} captures the initial conditions and is defined as:

$$c_{n-1} = [c_{n-1}, c_{n-2} \cdots c_0] \in R^{1\times n} \tag{2-20}$$

$$c_{n-i} = h_i y^{(n-1)}(0), i = 1...n \tag{2-21}$$

$$h_i = \left[0^{1\times(n-i)} a_n \cdots a_{n-(i-1)} \right] \in R^{1\times n} \tag{2-22}$$

$$y^{(n-1)}(0) = \left[y^{(n-1)}(0), y^{(n-2)}(0) \cdots y(0) \right]^T \tag{2-23}$$

A filter with dynamic integration and order lag term is introduced to form an iterative algorithm to estimate model parameters and pure lag time simultaneously. The filter used in this paper has the following form of transfer function as shown in Eq. (2-24):

$$P(s) = \frac{1}{sA(s)} \tag{2-24}$$

Among them, $A(s)$ is the denominator of the process transfer function. The function of the integration link is to decouple the pure lag from the dynamic parameters of the model. The function of the $1/A(s)$ term is to avoid the direct differential effect of the noise signal. Add the filtering terms $P(s)$ on both sides of Eq. (2-24), and get the formula as Eq. (2-25).

$$a_n s^n P(s) Y(s) = b_m s^m P(s) U(s) e^{-\delta s} + c_{n-1} s^{n-1} P(s) + E(s) P(s) \tag{2-25}$$

Using partial fraction expansion, the filter's transfer function can be expanded as follows:

$$\frac{1}{sA(s)} = \frac{C(s)}{A(s)} + \frac{1}{s} \tag{2-26}$$

Among them, $C(s) = -(a_n s^{n-1} + a_{n-1} s^{n-2} + \cdots a_1)$, defining that $Y^I(s) = Y(s)/A(s)$, $Y(s) = Y(s)/A(s)$, use the same notation for $U(s)$ to transform the estimated equations into standard least squares form:

$$\underline{Y}^I(s) = -\bar{a}_n s^{n-1} \underline{Y}(s) + \bar{b}_m s^{m-1} U(s) e^{-\delta s} + b_0 \left[C(s) U(s) + U^I(s) \right] e^{-\delta s} + c_{n-1} s^{n-1} P(s) + \xi(s) \tag{2-27}$$

Where $\bar{a}_n$ is a_n removes the last item, $\bar{b}_m$ is b_m removes the last item, and $\bar{b}_m \in R^{1\times m}$

For the step input, if the step amplitude is h, that is $u(t) = u_r(t) - u_{ss} = h$, we can obtain Eqs. (2-28) and (2-29), respectively:

$$U(s) = \frac{h}{s} \tag{2-28}$$

$$\underline{U}(s) = \frac{U(s)}{A(s)} = \frac{h}{sA(s)} = hP(s) \tag{2-29}$$

Introduce Eqs. (2-28) and (2-29) into Eq. (2-27), the Laplace domain prediction equation can be obtained as Eq. (2-30).

$$\underline{y}^I(t) = -\overline{a}_n \underline{y}^{n-1}(t) + h\overline{b}_m P^{m-1}(t-\delta) + b_0 \left[hP_c(t-\delta) + h[t-\delta] \right] + c_{n-1} P^{n-1}(t) + \xi(t) \qquad (2\text{-}30)$$

The $P^n(t)$ is defined as follows:

$$P^n(t) = \left[P_n(t) \cdots P_0(t) \right]^T \in R^{1\times(n+1)} \qquad (2\text{-}31)$$

$$P_i(t) = L^{-1} \left[s^i P(s) \right] \qquad (2\text{-}32)$$

$$P^I(t) = L^{-1} \left[\frac{P(s)}{s} \right] \qquad (2\text{-}33)$$

$$P_c(t) = L^{-1} \left[P(s)C(s) \right] \qquad (2\text{-}34)$$

For the step input $h[t-\delta] = ht - h\delta$, substituting the above formula to Eq. (2-30), the estimated equation in the form of least squares can be obtained as Eqs. (2-35) and (2-36), respectively.

$$\underline{y}^I(t) = -\overline{a}_n \underline{y}^{n-1}(t) + hb_m P_+^{m-1}(t-\delta) - b_0\delta h + c_{n-1} P^{n-1}(t) + \xi(t) \qquad (2\text{-}35)$$

$$P_+^{m-1}(t-\delta) = \left[P^{m-1}(t-\delta), P_c(t-\delta) + t \right]^T \qquad (2\text{-}36)$$

Equivalent definition the following equation.

$$\gamma(t) = \phi(t)\theta + \zeta(t) \qquad (2\text{-}37)$$

Among that:

$$\gamma(t) = \underline{y}^I(t) \qquad (2\text{-}38)$$

$$\phi(t) = \left[-\underline{y}^{n-1}(t), hP_+^{m-1}(t-\delta), -h, P^{n-1}(t) \right]^T \qquad (2\text{-}39)$$

$$\theta = \left[\overline{a}_n, b_m, b_0\delta, c_{n-1} \right] \qquad (2\text{-}40)$$

When $t = t_k$, $k = 1, 2, \ldots, N$, N is the length of the data, thus, Eq. (2-37) can be transferred as Eq. (2-41).

$$\Gamma = \Phi\theta + \zeta \qquad (2\text{-}41)$$

The whole iterative algorithm steps are as follows:

Step 1: **Initialize**. Choosing the initial parameters $A_0(s)$ and δ_0.

Step 2: **Least-squares iteration**. Build Γ and Φ at time $i = 1$, substituting $A_0(s)$ and δ_0 into $A(s)$ and δ to obtain the estimated parameters as Eq. (2-42):

$$\hat{\theta}^{LS} = \left(\Phi^T\Phi\right)^{-1}\Phi^T\Gamma \tag{2-42}$$

Let $\hat{\theta}^1 = \hat{\theta}^{LS}$, we can get $\hat{A}_1(s)$, $\hat{B}_1(s)$, and $\hat{\delta}_1$.

Step 3: **Auxiliary variable iteration**. When $i = i + 1$, build Γ, Φ and Ψ, using the $\hat{A}_{i-1}(s)$, $\hat{B}_{i-1}(s)$ and $\hat{\delta}_{i-1}$ to replace $A(s)$, $B(s)$ and δ, the auxiliary variable estimated parameters can be obtained as Eq. (2-43).

$$\hat{\theta}^{LS} = \left(\psi^T\Phi\right)^{-1}\psi^T\Gamma \tag{2-43}$$

Repeat this step until $\hat{A}_i$ and $\hat{\delta}_i$ achieve convergence.

Step 4: **Termination**. When $\hat{A}_i$ and $\hat{\delta}_i$ achieve convergence, the dynamic parameters and pure lag time can be obtained.

2.2.4.2 Verification of identification accuracy

To verify the identification efficiency, the simulation of the first-order plus pure delay time system identification has been carried out, the simulation model is set the same as before, and 10 s pure delay time has been added into the system. The model is expressed as Eq. (2-44).

$$P(s) = \frac{5}{100s+1}e^{-10s} \tag{2-44}$$

The simulation result is shown in Figure 2-5, and the identification result is as Eq. (2-45).
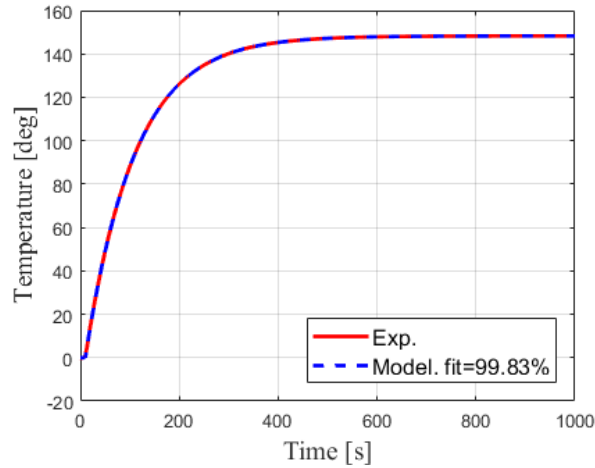
Figure 2-5 Identification result of FOPTD system.

$$P(s) = \frac{5}{99.942s + 1} e^{-10.035s} \qquad (2\text{-}45)$$

The fitness between the simulation model and the identified model is 99.83%. Thus, the efficiency of the system identification method has been verified.

2.2.5 System identification of MIMO experimental setup

After the identification method has been successfully verified, the method has been introduced into the real plant identification. The condition of the step response identification is shown in Table 2-1.

Table 2-1 Step response identification conditions

Sampling period	0.1s
Input duty	30%
Analog LPF	10Hz
Digital LPF	0.1Hz
Room temperature	25degree Celsius
Air conditioner	25degree Celsius

The 4 channels single input single output (SISO) identification results are shown in Figures 2-6 to 2-9.
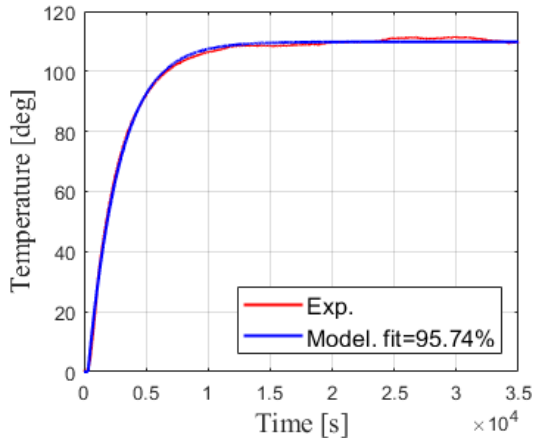
Figure 2-6 SISO identification of Ch1.
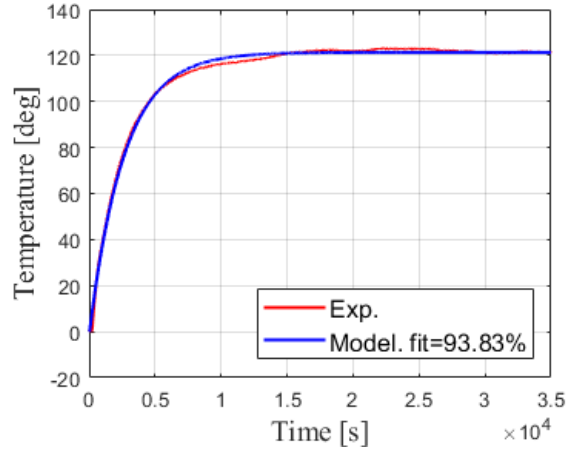
Figure 2-7 SISO identification of Ch2.
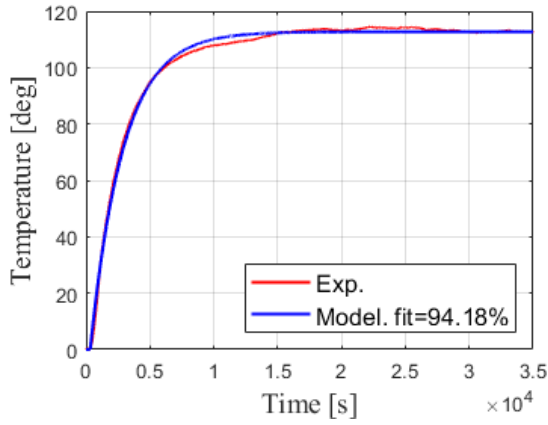
Figure 2-8 SISO identification of Ch3.
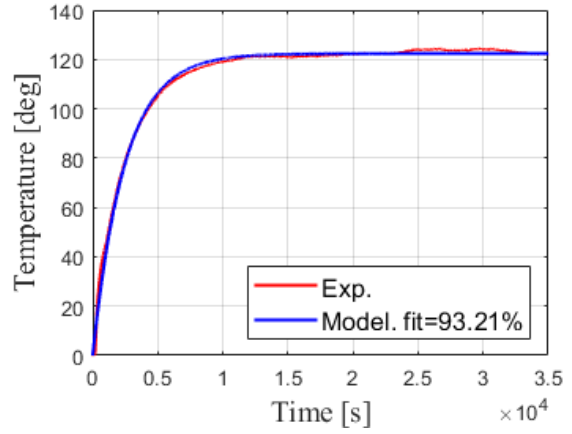
Figure 2-9 SISO identification of Ch4.

The transfer function is described as the first-order plus time delay (FOPTD), and the identified plant can be obtained as Eqs. (2-46), (2-47), (2-48) and (2-49).

$$P_{11} = \frac{4.52}{1211s+1} e^{-25s} \qquad (2\text{-}46)$$

$$P_{22} = \frac{3.59}{1307s+1} e^{-25s} \qquad (2\text{-}47)$$

$$P_{33} = \frac{4.34}{1639s+1} e^{-25s} \qquad (2\text{-}48)$$

$$P_{44} = \frac{4.38}{794s+1} e^{-10s} \qquad (2\text{-}49)$$

Also, due to the system being under strong coupling effects, all the channels are influenced

by the other channels, thus, the identification result with coupling effects has been obtained as Eq. (2-50).

$$P_{MIMO} = \begin{bmatrix} P11 & P12 & P13 & P14 \\ P21 & P22 & P23 & P24 \\ P31 & P32 & P33 & P34 \\ P41 & P42 & P43 & P44 \end{bmatrix}$$

$$= \begin{bmatrix} \dfrac{4.52}{1211s+1}e^{-25s} & \dfrac{2.40}{2907s+1}e^{-200s} & \dfrac{1.91}{5848s+1}e^{-400s} & \dfrac{0.815}{2985s+1}e^{-1400s} \\ \dfrac{2.65}{2688s+1}e^{-200s} & \dfrac{3.59}{1307s+1}e^{-25s} & \dfrac{2.84}{3677s+1}e^{-200s} & \dfrac{1.56}{2336s+1}e^{-600s} \\ \dfrac{1.67}{3984s+1}e^{-600s} & \dfrac{2.46}{3040s+1}e^{-200s} & \dfrac{4.34}{1639s+1}e^{-25s} & \dfrac{2.53}{1435s+1}e^{-200s} \\ \dfrac{1.05}{4739s+1}e^{-1000s} & \dfrac{1.69}{4608s+1}e^{-500s} & \dfrac{3.07}{3610s+1}e^{-200s} & \dfrac{4.38}{794s+1}e^{-10s} \end{bmatrix} \quad (2\text{-}50)$$

2.3 PI control of SISO system

2.3.1 PI controller design

Based on the identified plant model, the closed-loop control system for SISO system has been designed, and the PI controller is designed by the transfer function method that sets the cross over bandwidth as 400s.

The SISO compensation for each channel is explained as follows.

2.3.2 SISO control system for channel 1

Based on the transfer function of $P_{11}(s)$, the PI compensator for Ch1 can be expressed as Eq. (2-51).

$$C_{11} = \frac{1211s+1}{1778s} \quad (2\text{-}51)$$

The bode diagram of the closed-loop system is shown in Figure 2-10, where the bandwidth of the system is 400s. The step response for the closed-loop system from 0degree Celsius to 100degree Celsius is shown in Figure 2-11.
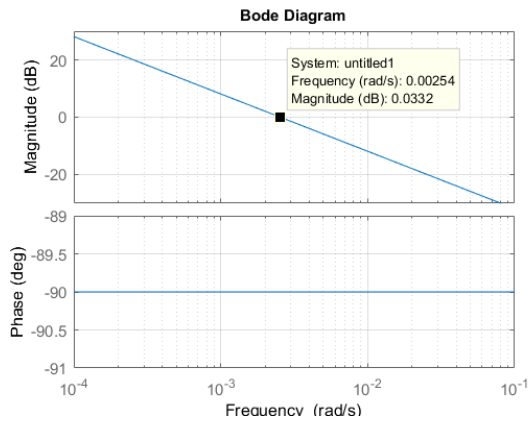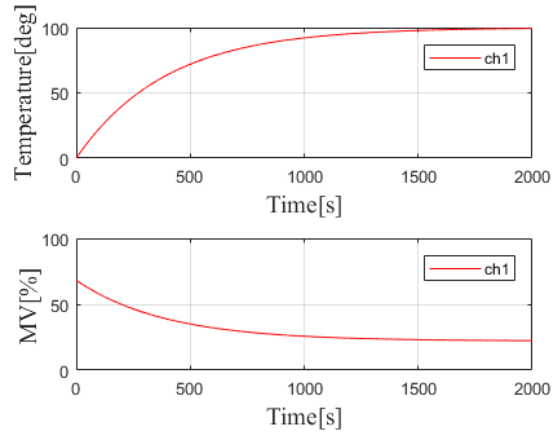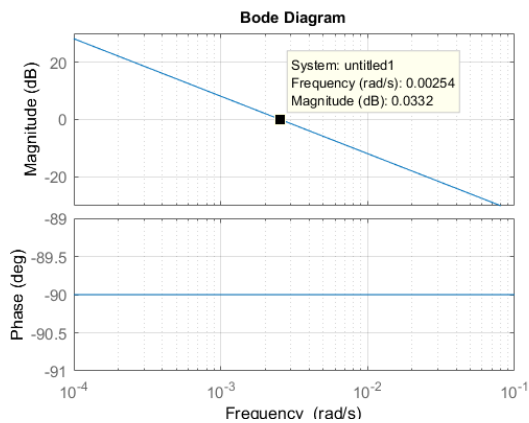
Figure 2-10 Bode diagram of closed-loop Ch1.

Figure 2-11 Step response of Ch1 closed-loop.

2.3.3 SISO control system for channel 2

Same as the Ch1 closed-loop compensation, the PI compensator for Ch2 is expressed as Eq. (2-52).

$$C_{22} = \frac{1307s + 1}{1413s} \tag{2-52}$$

The bode diagram of the closed-loop system is shown in Figure 2-12, where the bandwidth of the system is 400s. The step response for the closed-loop system from 0degree Celsius to 100degree Celsius is shown in Figure 2-13, the step response of Ch2 is same as that of Ch1.

Figure 2-12 Bode diagram of closed-loop Ch2.
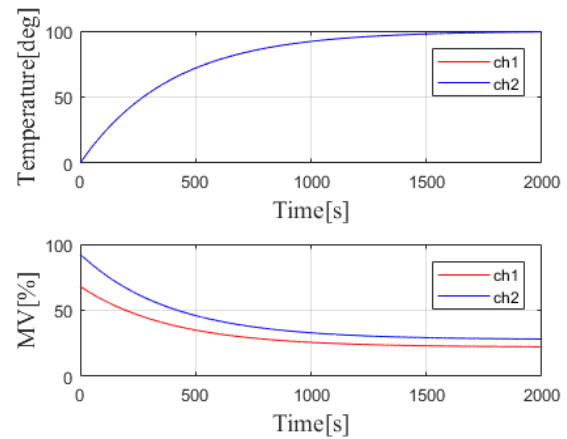
Figure 2-13 Step response of Ch2 closed-loop.

2.3.4 SISO control system for channel 3

The PI compensator for Ch3 is designed as Eq. (2-53). The bode diagram and the step

29

response result from 0degree Celsius to 100degree Celsius are shown in Figures 2-14 and 2-15, respectively.

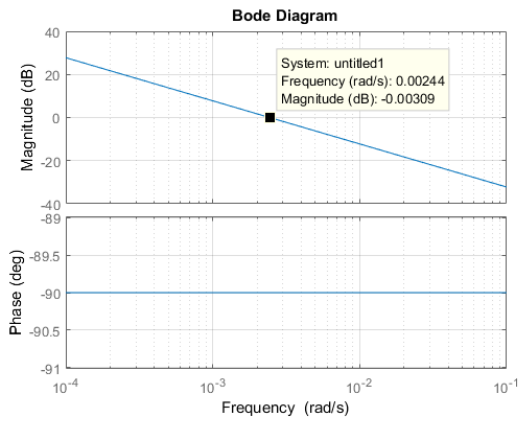$$C_{33} = \frac{1639s+1}{1778s} \qquad (2\text{-}53)$$
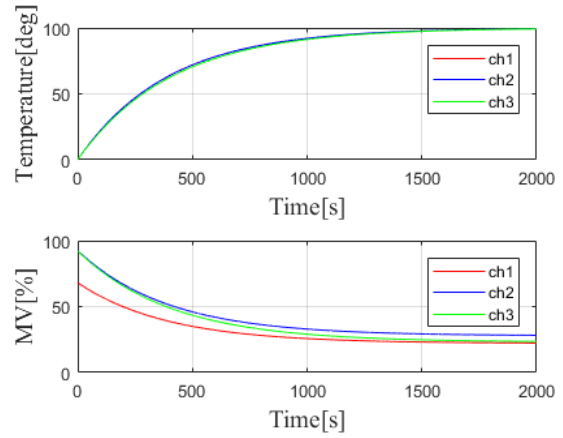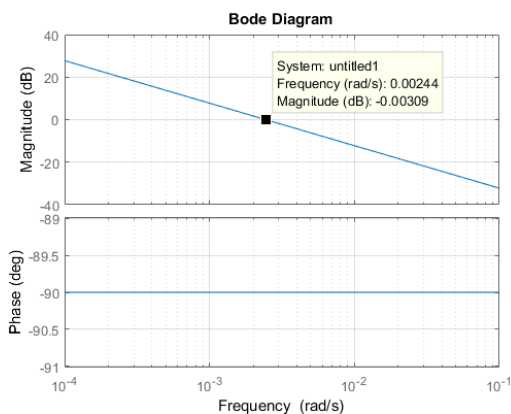

Figure 2-14 Bode diagram of closed-loop Ch3.

Figure 2-15 Step response of Ch3 closed-loop.

2.3.5 SISO control system for channel 4

The PI compensator for Ch4 is designed as Eq. (2-54). The bode diagram and the step response result from 0degree Celsius to 100degree Celsius are shown in Figures 2-16 and 2-17, respectively.

$$C_{44} = \frac{794s+1}{1738s} \qquad (2\text{-}54)$$

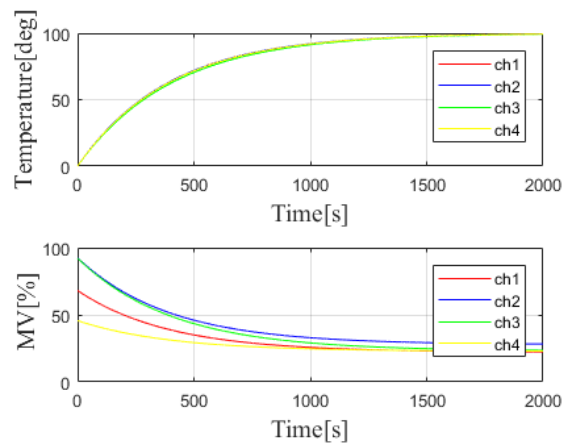Figure 2-16 Bode diagram of closed-loop Ch3.

Figure 2-17 Step response of Ch3 closed-loop.

To sum up, after setting the same bandwidth of the closed-loop systems of the four channels, the step responses of these channels are almost the same.

2.3.6 Experimental verification of SISO control system

Although the simulation results of the step response have successfully evaluated the control efficiency, the experiment still needs to be carried out to verify the control efficiency for the further step.

In the experiment, we choose Ch1 for the SISO experiment, the step response is set from room temperature (23degree Celsius) to 40degree Celsius, the response result is compared to the simulation result with the same step response, as is shown in Figure 2-18, and the control input (MV) of Ch1 is shown in Figure 2-19.
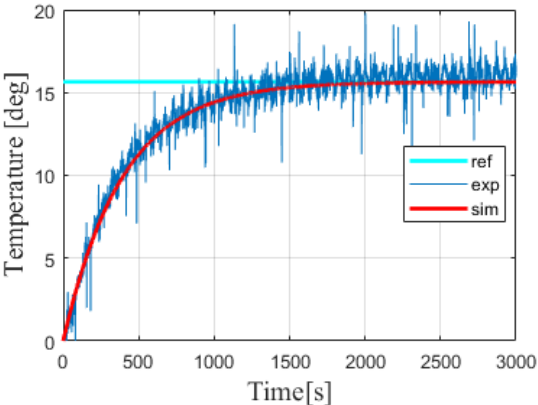

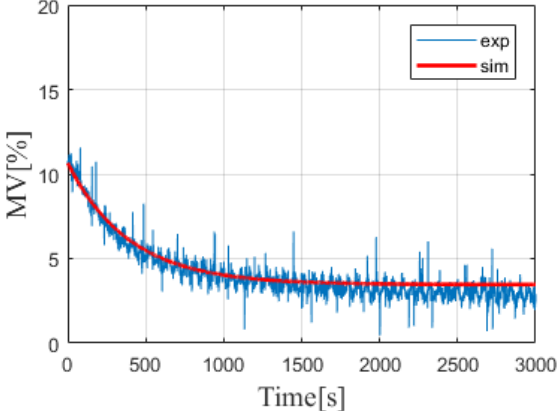Figure 2-18 Experimental step response of Ch1.　　　Figure 2-19 Control input (MV) of Ch1.

From the result, the experimental result is almost the same as the simulation, both the step response and the control input. However, the experimental result has the 60s repeated vibration, this is due to the connection noise that has been proved later.

Next, we speed up our compensation response by shortening the bandwidth of the closed-loop system to 40s, 10 times the bandwidth of normal PI compensation. The results of step response and control input are shown in Figures 2-20 and 2-21, respectively.
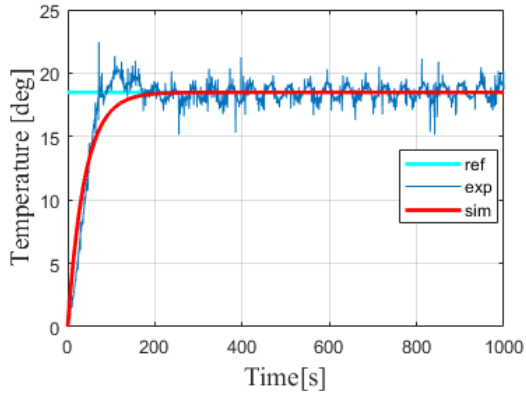
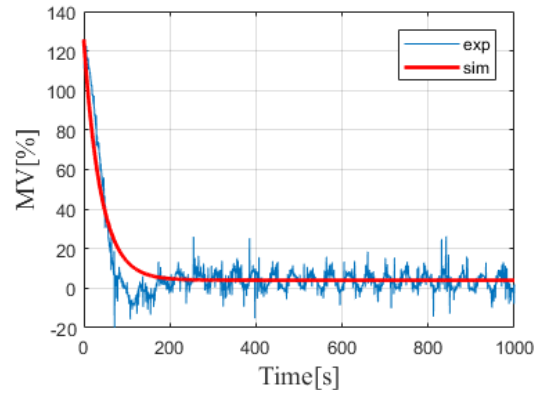Figure 2-20 Step response of 10 times PI.   Figure 2-21 Control input (MV) of 10 times PI.

From the results, the speed of the step response has been improved, but there remains a little overshoot, about 3degree Celsius. And the control input has dropped below 0, which makes no sense in this system and course the overshoot. Still, besides the overshoot, the control efficiency has been evaluated.

Thus, from the experiment result, we can state that the SISO compensation has been successfully verified.

2.4 PI control of MIMO temperature control system

In this section, the MIMO compensation based on the designed PI control above will be performed. The multi-point system has been simplified as a two-inputs two-outputs system, thus, Ch1 and Ch3 are chosen to combine the MIMO system. The controller is the same as the SISO closed-loop compensation system.

In the MIMO compensation system, the analysis will focus on the transient response and temperature difference between the chosen channels. Also, due to the system working under strong coupling effectiveness, the MIMO compensation will be divided into two steps. Step 1: MIMO compensation without decoupling. Step 2: MIMO compensation with decoupling.

2.4.1 MIMO control without decoupling compensation

The structure of conventional MIMO (2 channels) is shown in Figure 2-22. Where C_{11} and C_{33} are the controllers of Ch1 and Ch3, respectively.
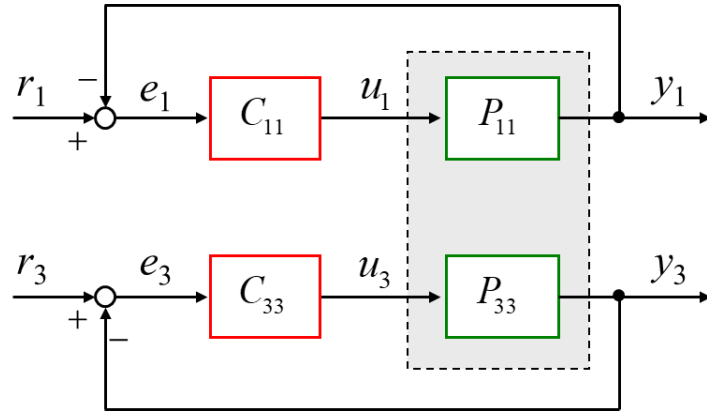
Figure 2-22 Structure of convention MIMO without decoupling control.

According to the identification results above, the transfer plant model with coupling can be expressed as Eq. (2-54), each factor is represented by FOPTD. P_{11} is defined as Ch1 while P_{33} is defined as Ch3, P_{13} and P_{31} are defined as the coupling terms between these two channels.

$$P(s) = \begin{bmatrix} P_{11} & P_{13} \\ P_{31} & P_{33} \end{bmatrix} = \begin{bmatrix} \dfrac{4.52}{1211s+1}e^{-25s} & \dfrac{1.91}{5848s+1}e^{-125s} \\ \dfrac{1.67}{3984s+1}e^{-150s} & \dfrac{4.34}{1639s+1}e^{-30s} \end{bmatrix} \tag{2-54}$$

In experiments, the reference value is set as 30degree Celsius, thus a step from room temperature (about 22degree Celsius) to 30degree Celsius reference has been added to the system, and the results have been compared to the simulation under the same conditions. The step response of these two channels is shown in Figure 2-23, while the control input is shown in Figure 2-24.
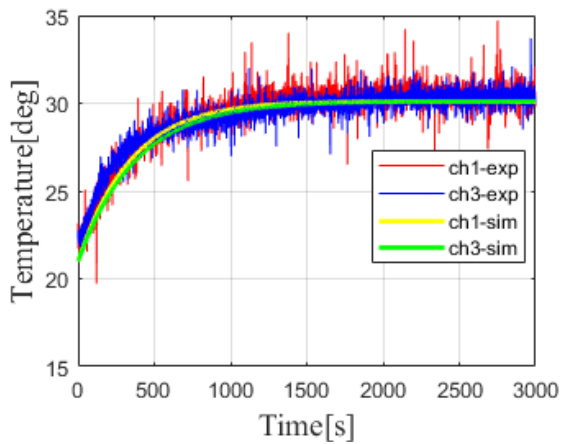

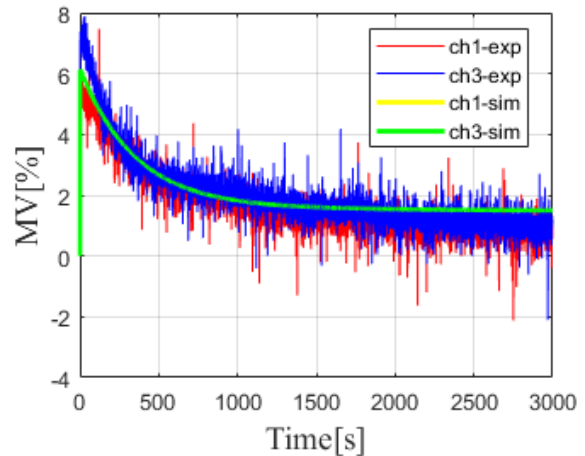Figure 2-23 Step response of Ch1 and Ch3.

Figure 2-24 Control input of Ch1 and Ch3.

33

To evaluate the control efficiency, the temperature difference and mean temperature are shown in Figures 2-25 and 2-26, respectively
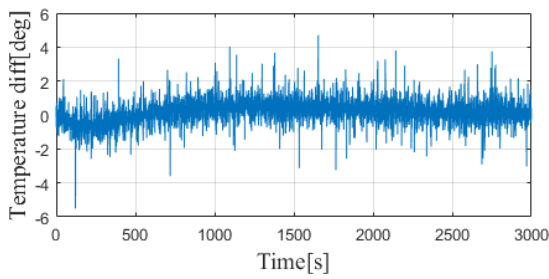

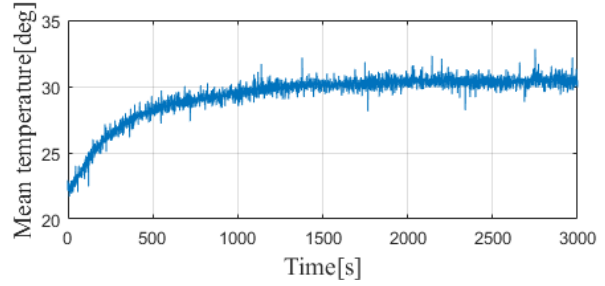Figure 2-25 Temperature difference.

Figure 2-26 Mean temperature of Ch1 and Ch3.

Also, with the same reference value, the experiments of the 10 times PI compensation are carried out, and the simulations are done under the same condition. The results of system response and control input are shown in Figures 2-27 and 2-28, respectively. The result of the temperature difference and mean temperature of these two channels are shown in Figures 2-29 and 2-30, respectively.
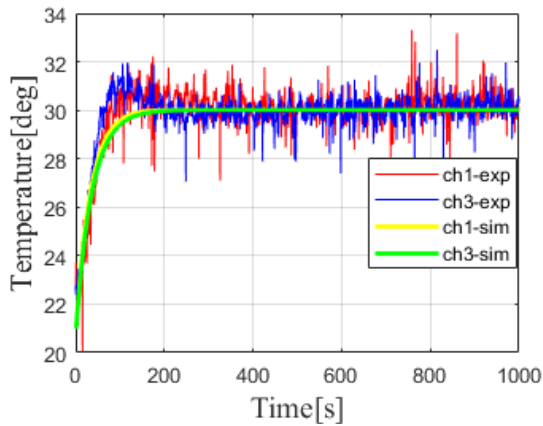

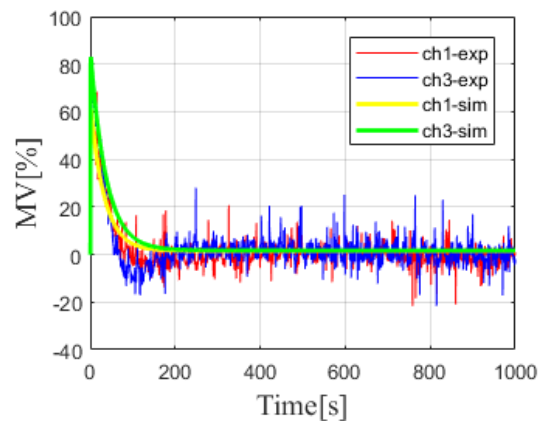Figure 2-27 DIDO response with 10 times PI.

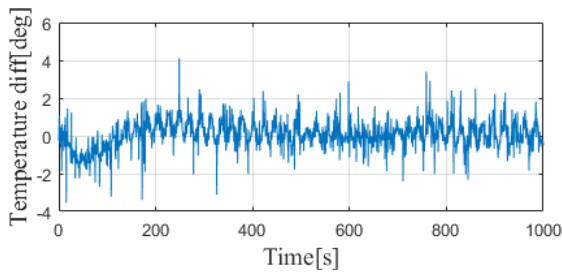Figure 2-28 Control input of 10 times PI.

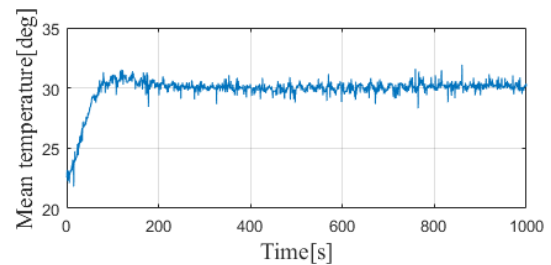Figure 2-29 Temperature difference of 10 times PI.

Figure 2-30 Mean temperature of 10 times PI.

The analysis of the experiment result is focused on the transient response and maximum temperature difference between these two coupled channels, which could be divided into two

34

phases. Phase 1: Transient response, from the result, both normal PI compensation system and 10 times bandwidth PI compensation system have a similar response compared to the simulation results, although the 10 times bandwidth PI compensation system has a little overshoot in both two channels. Phase 2: Maximum temperature difference, the absolute value of the maximum temperature difference between these two channels is about 2degree Celsius, while the normal PI compensation is a little smaller than the 10 times bandwidth PI compensation system but not so clarified, this phenomenon is caused by the coupling terms between these two channels. Thus, it can be stated that the coupling effect needs to be compensated.

2.4.2 MIMO control system with decoupling compensation

Due to the problems caused by the coupling terms, the decoupling compensation needs to be introduced into the MIMO temperature control system. The structure of MIMO system with decoupling compensation is shown in Figure 2-31, Where C_{13} and C_{31} are the decoupling compensators of Ch3 and Ch1, respectively. And after the decoupling compensation, the equivalent system is shown in Figure 2-32.
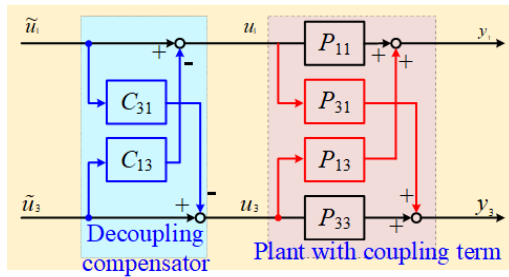

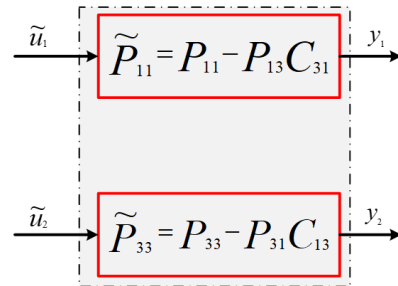Figure 2-31 Structure of decoupling compensation.   Figure 2-32 Equivalent system compensation.

Thus, to compensate for the coupling effect, the compensator C_{13} and C_{31} can be expressed as Eqs. (2-55) and (2-56), respectively.

$$C_{13} = P_{13} * P_{11}^{-1} \qquad (2\text{-}55)$$

$$C_{31} = P_{31} * P_{33}^{-1} \qquad (2\text{-}56)$$

2.4.2.1 Design of decoupling compensators

There remain three kinds of compensators that are designed for the decoupling compensation.

1) Full state compensation

In this method, the compensation of the decoupling considers the steady-state gains, time constants and pure delay time of both channel plants and the coupling terms. Thus, the decoupling compensators C_{13} and C_{31} can be designed as Eqs. (2-57) and (2-58), respectively. Where K_{13} and K_{11} respectively indicate the steady-state gain of Ch1 and coupling term P_{13}, while T_{11} and T_{13} indicate the time constant of Ch1 and P_{13}. The delay time of each plant can be indicated as L_{11} and L_{13}, respectively.

$$C_{13} = P_{13} * P_{11}^{-1} = \frac{K_{13}}{T_{13}s+1}e^{-L_{13}s} \cdot \frac{T_{11}s+1}{K_{11}}e^{-L_{11}s} = \frac{K_{13}}{K_{11}}\frac{T_{11}s+1}{T_{13}s+1}e^{-(L_{13}-L_{11})s} \tag{2-57}$$

$$C_{31} = P_{31} * P_{33}^{-1} = \frac{K_{31}}{T_{31}s+1}e^{-L_{31}s} \cdot \frac{T_{33}s+1}{K_{33}}e^{-L_{33}s} = \frac{K_{31}}{K_{33}}\frac{T_{33}s+1}{T_{31}s+1}e^{-(L_{31}-L_{33})s} \tag{2-58}$$

2) High-frequency gain plus delay time compensation

In this method, only the high-frequency gain and delay gain are considered, thus the compensators C_{13} and C_{31} can be expressed as Eqs. (2-59) and (2-60), respectively.

$$C_{13} = \frac{K_{13}}{K_{11}}\frac{T_{11}}{T_{13}}e^{-(L_{13}-L_{11})s} \tag{2-59}$$

$$C_{31} = \frac{K_{31}}{K_{33}}\frac{T_{33}}{T_{31}}e^{-(L_{31}-L_{33})s} \tag{2-60}$$

3) High-frequency gain compensation

This is the simplest compensation, only the high-frequency gain is considered, the delay time can't be compensated. In this way, the compensators C_{13} and C_{31} can be expressed as Eqs. (2-61) and (2-62), respectively.

$$C_{13} = \frac{K_{13}}{K_{11}}\frac{T_{11}}{T_{13}} \tag{2-61}$$

$$C_{31} = \frac{K_{31}}{K_{33}}\frac{T_{33}}{T_{31}} \tag{2-62}$$

2.4.2.2 Experiment verification

After the decoupling compensation has been designed, the experiments need to be carried out to verify the effectiveness of the decoupling compensation. In the experiments, the simplest decoupling compensation which only considers the high-frequency gain is used. The compensators C_{13} and C_{31} are calculated as Eqs. (2-63) and (2-64), respectively.

$$C_{13} = 0.0875 \tag{2-63}$$

$$C_{31} = 0.158 \tag{2-64}$$

The experiments are divided into two steps. Step 1: The normal PI control with decoupling compensation. In this experiment, the PI controllers are the same as the controllers designed before which has a bandwidth of 400s. Step 2: 10 times bandwidth PI control with decoupling compensation. The step response and control input of step 1 is shown in Figures 2-33 and 2-34, respectively. While the temperature difference between these two channels and the mean temperature of these two channels are respectively shown in Figure 2-35 and 2-36.
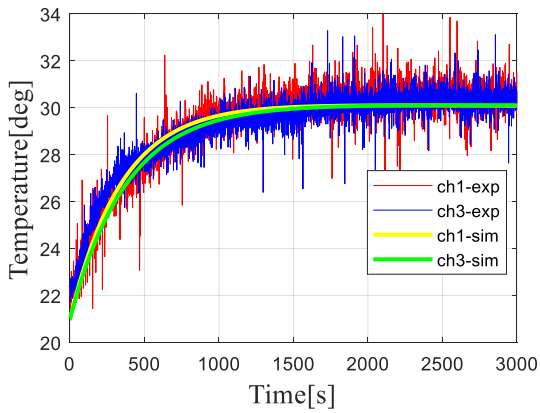

Figure 2-33 DIDO with decoupling compensation.
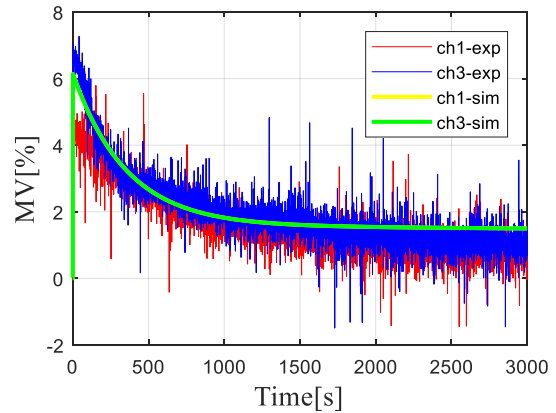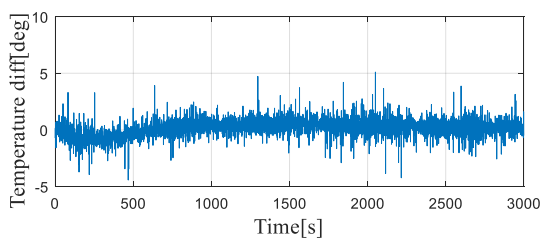

Figure 2-34 Control input.

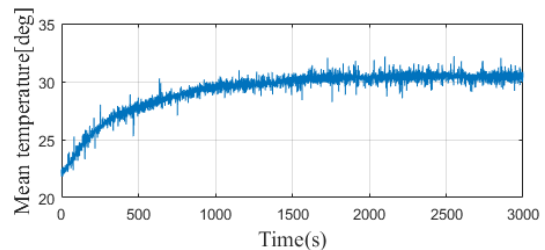Figure 2-35 Temperature difference.

Figure 2-36 Mean temperature.

Figures 2-37 and 2-38 show the results of the step response and control input of step 2 with

10 times bandwidth PI control, respectively. And the temperature difference between these two channels and the mean temperature of them are shown in Figures 2-39 and 2-40, respectively.
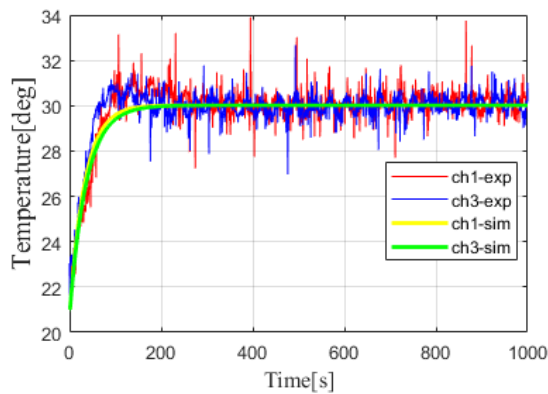

Figure 2-37 Result of 10 times PI.
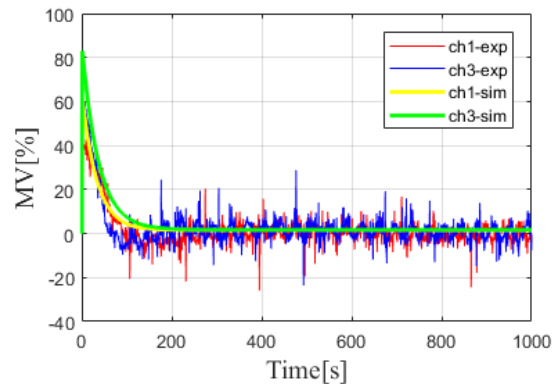
Figure 2-38 Control input of 10 times PI.
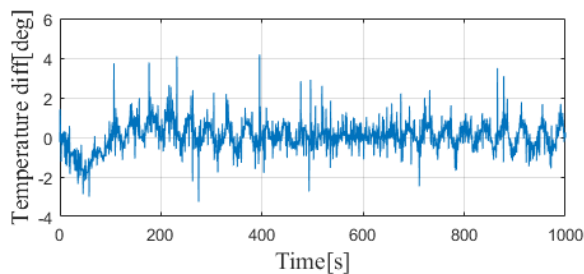
Figure 2-39 Temperature difference of 10 times PI.
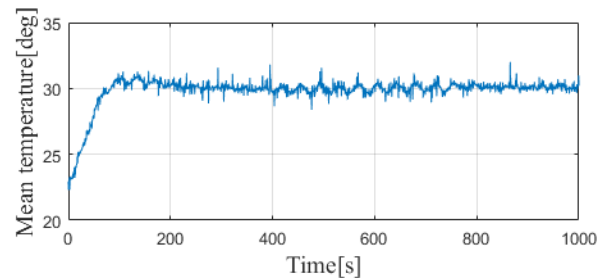
Figure 2-40 Mean temperature of 10 times PI.

From these results, the analysis is focused on the transient response and temperature difference. For the transient response, although the experimental results are similar to those of the simulations, there still remains a little overshoot in the results of 10 times PI control with decoupling compensation. For the temperature difference, both the absolute maximum value of the two-step experimental results is about 1.5degree Celsius, a little improved compared to the former experimental results without the decoupling compensation. Thus, compensation effectiveness has been successfully evaluated.

2.5 Pole-zero cancellation method for MIMO temperature control system

To solve the dead (delay) time and coupling influence of the MIMO temperature control system, based on the previous research, only decoupling compensation may not fully compensate for the effect of the coupling term and other influence between the channels. Hence,

we propose a new advanced control method for the MIMO temperature control system with the pole-zero cancellation method to improve the transient response of each point without any overshoot and to reduce the temperature difference between multi-points at the same time. Figure 2-41 shows the block diagram of the proposed MIMO control system. For simplicity of design and explanation, the controlled object is considered as a two-inputs two-outputs temperature system. In the figure, r_1 and r_2 indicate the reference of the MIMO system while y_1 and y_2 are the output temperature, respectively. The control system configuration can be divided into five parts: Part 1 describes the simplified controlled objects; Part 2 will somewhat compensate the coupling effect and dead time difference of the two channels; Part 3 will introduce the pole-zero cancellation with reference model to convert the complex system to almost equal to the reference model; Part 4 is the main controller of the system; Part 5 indicates the anti-wind-up compensation that will not only compensate for the saturation of the control input but also ensure the uniformity of the temperature by setting difference maximum saturation.
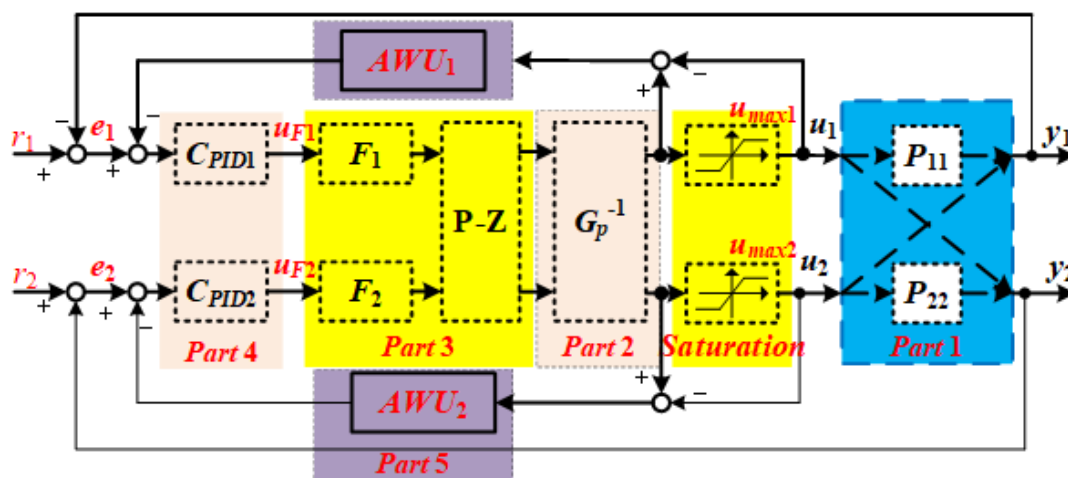
Figure 2-41 Block diagram of pole-zero cancellation for two-input two-output system.

2.5.1 Part 1: MIMO plant with coupling effect

The control system is designed based on a multi-input multi-output (MIMO) temperature system with a strong coupling influence. The schematic block diagram of the coupled system is shown in Figure 2-42, where u_1 and u_2 are defined as the inputs of Ch1 and Ch2, respectively. In addition, y_1 and y_2 indicate the output of Ch1 and Ch2, respectively. The coupling terms

between the two channels are obtained as P_{21} and P_{12}, respectively.
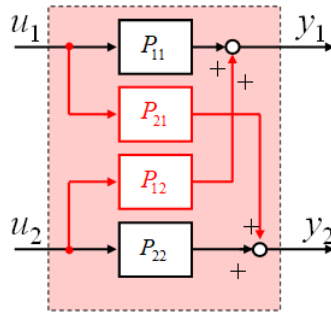
Figure 2-42 Block diagram of coupled system.

2.5.2 Part 2: Compensation for dead time difference and coupling

In this paper, the controlled objects can be defined as a first-order plus time delay (FOPTD) system, shown as Eq (2-65), and can be approximated to Eq. (2-66) based on the Pade approximation method, which leads to ease of dead-time compensation. Considering the characteristic of the transient response of the temperature system, there is a difference in the delay time d between the multipoint temperature outputs. As a result, a temperature difference remains in the outputs of different channels.

$$P(s) = \frac{K}{Ts+1} e^{-ds} \tag{2-65}$$

$$P(s) \approx \frac{K}{Ts+1} \cdot \frac{1}{ds+1} \tag{2-66}$$

Same as the delay time difference, since the coupling influence also affects the temperature of both channels, compensation of the coupling term needs to be introduced, the same as already introduced above.

In this method, a matrix gain compensation method has been introduced to compensate delay time difference and coupling effects together. Taking G_p as the system characteristic matrix, including the coupling and delay time gain of the system. The compensation of the G_p based on the inverse of the matrix $G_p{}^{-1}$, the matrix can be obtained by giving the step signal to the two channels one by one after natural cooling. The measurement method of the characteristic G_p for the MIMO-controlled object is shown in Figure 2-43.
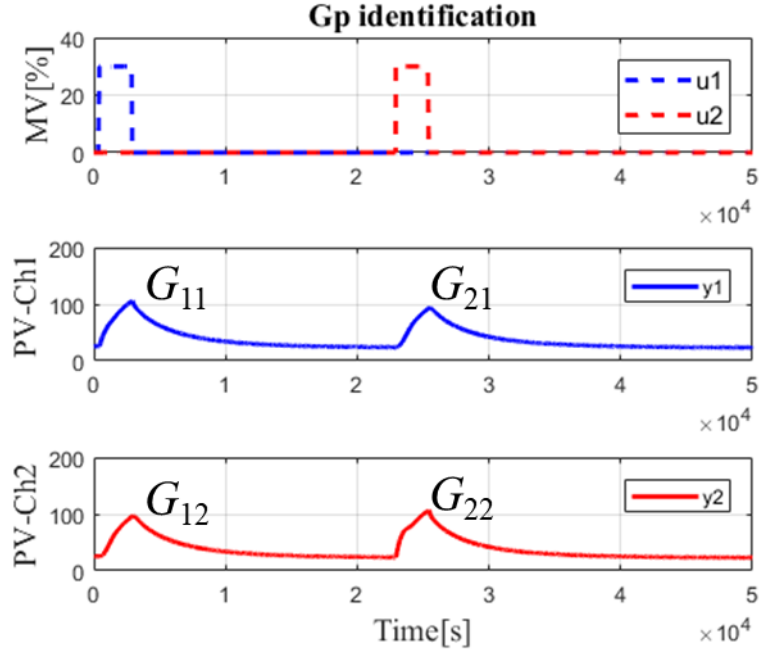
Figure 2-43 System matrix gain Gp identification.

Thus, the matrix gain G_p can be calculated as Eq. (2-67), and the delay time difference and coupling compensator G_c can be obtained as Eq. (2-68) by the inverse of the G_p.

$$G_p = \begin{bmatrix} G_{11} & G_{12} \\ G_{21} & G_{22} \end{bmatrix} \tag{2-67}$$

$$G_c = G_p^{-1} \tag{2-68}$$

For this compensation gain matrix G_c, it can somewhat compensate delay time difference and coupling influence together, therefore, the temperature difference can be reduced.

2.5.3 Part 3: Pole-zero cancelation with feedforward reference model

As introduced above, after the matrix compensation, the MIMO-controlled object can be treated as a non-interference system, therefore the feedforward reference model with pole-zero cancellation is designed for this system. The block diagram and the simplified system are shown in Figure 2-44, where the F_1 and F_2 are reference models which can provide an expected response reference for the controlled systems, by using this, after the pole-zero cancellation, the system can be equaled as the reference model. In addition, u_{F1} and u_{F2} are the inputs of two

41

channels, respectively, while y_1 and y_2 indicate the outputs of Ch1 and Ch2 respectively. The F_1 and F_2 can be designed as Eqs. (2-69) and (2-70), respectively, and the order of the controllers is decided by the inverse of the plant transfer function (in this paper 1st order). In this proposal, to make it easy for the design of the controllers, F_1 and F_2 are designed as $F_1 = F_2$, thus, $w_1 = w_2$.

$$F_1 = \frac{\omega_1}{s + \omega_1} \tag{2-69}$$

$$F_2 = \frac{\omega_2}{s + \omega_2} \tag{2-70}$$
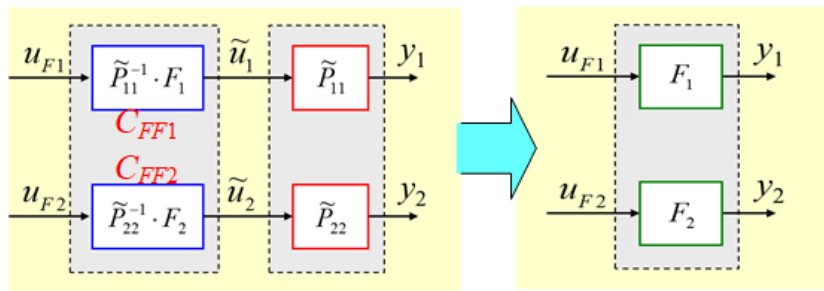
Figure 2-44 Block diagram of feedforward reference model with pole-zero cancellation and simplified system.

2.5.4 Part 4: PID controller design

In part 3, defining the equivalent plant as $F_1 = F_2$, the same PID controllers can be designed ($C_{PID1} = C_{PID2}$). Hence, one of the most important factors is the stability of the controller, and there have already existed several methods for controller stability analysis. However, the PID controller in this proposed system is designed based on the Ziegler-Nichols method (step response tuning method), where the stability has been ensured. The PID control system diagram is shown in Figure 2-45.
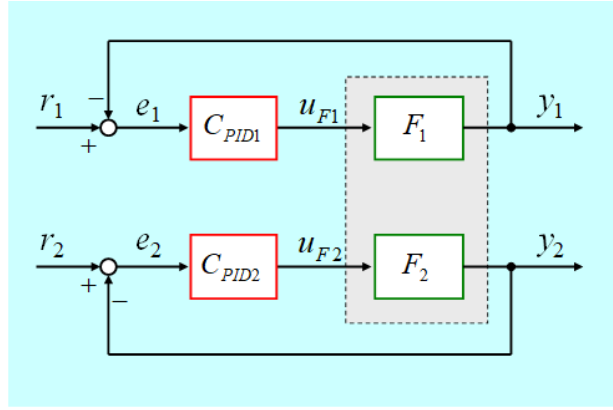
Figure 2-45 Block diagram of PID control system.

2.5.5 Part 5: Anti-wind-up compensation for control input saturation

In system design, the control inputs u_1 and u_2 are under a saturation from 0 to u_{max}, thus, to improve the effectiveness of the controller, the anti-wind-up compensation has been added to the control loop. The structure of the anti-wind-up compensation is shown in Figure 2-46. In addition, due to the difference transient response characteristics of the two channels, the relationship between these two channels is as Eq. (2-71), where u_{max1} and u_{max2} indicate the maximum saturation of Ch1 and Ch2, respectively, K_{11} and K_{22} indicate the steady-state gain of Ch1 and Ch2, respectively. By setting this, it can somewhat make the two channels' response be precisely the same even the controllers are working under the saturation.

$$u_{\max 1} = \frac{K_{11}}{K_{22}} u_{\max 2} \tag{2-71}$$
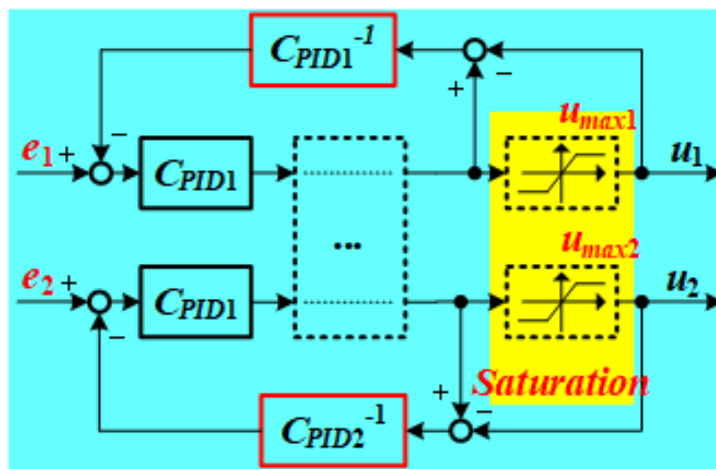
Figure 2-46 Structure of anti-wind-up compensation.

2.5.6 Simulation results

In the simulation, the control object $P(s)$ of the MIMO temperature system is defined as a two-input and two-output vectors as Eq. (2-72), which is identified by the step response method, and Ch1 and Ch2 are chosen to build this two-input and two-output system.

$$P(s) = \begin{bmatrix} P_{11} & P_{12} \\ P_{21} & P_{22} \end{bmatrix} = \begin{bmatrix} \dfrac{4.0992}{2627s+1}e^{-200s} & \dfrac{3.7036}{2536s+1}e^{-326s} \\ \dfrac{2.2805}{2580s+1}e^{-324s} & \dfrac{4.1268}{2461s+1}e^{-150s} \end{bmatrix} \quad (2\text{-}72)$$

Each factor is represented by FOPTD, in which the parameters are calculated by the step response system identification method, the factor (1,1) can be defined as Ch1 while the factor (2,2) can be defined as Ch2. Figure 2-47 shows the setpoint tracking results for the control inputs and temperature outputs for the system obtained using the conventional PI control method.
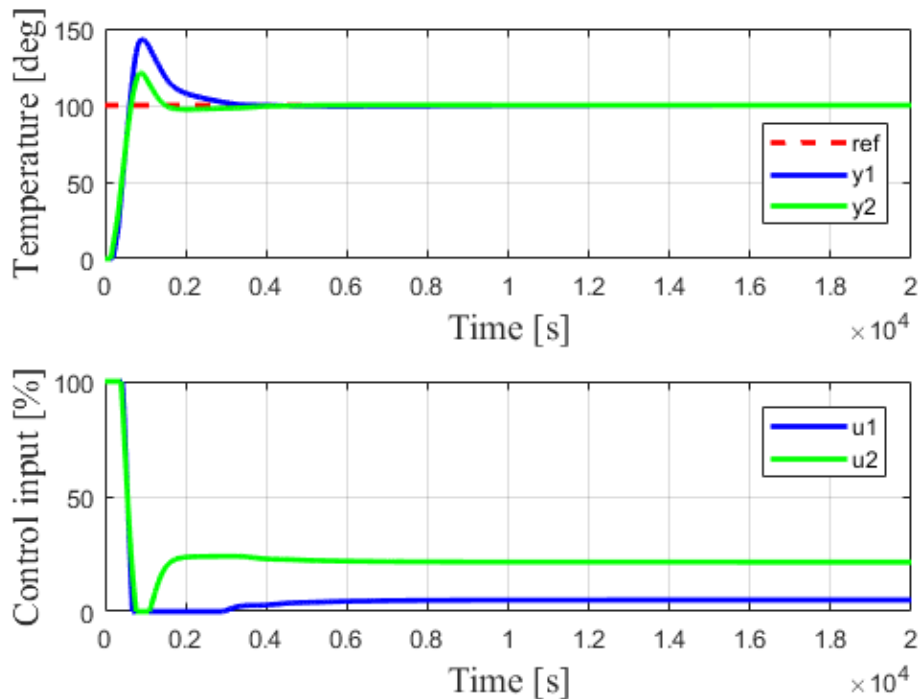
Figure 2-47 Tracking results for conventional PI control.

Figure 2-48 shows the temperature difference, $(y_1 - y_2)$, and the mean temperature, $(y_1 + y_2)/2$. As is shown in Figure 2-48, the overshoot of the mean temperature reaches 45%, and the

maximum temperature difference becomes 23degree Celsius.
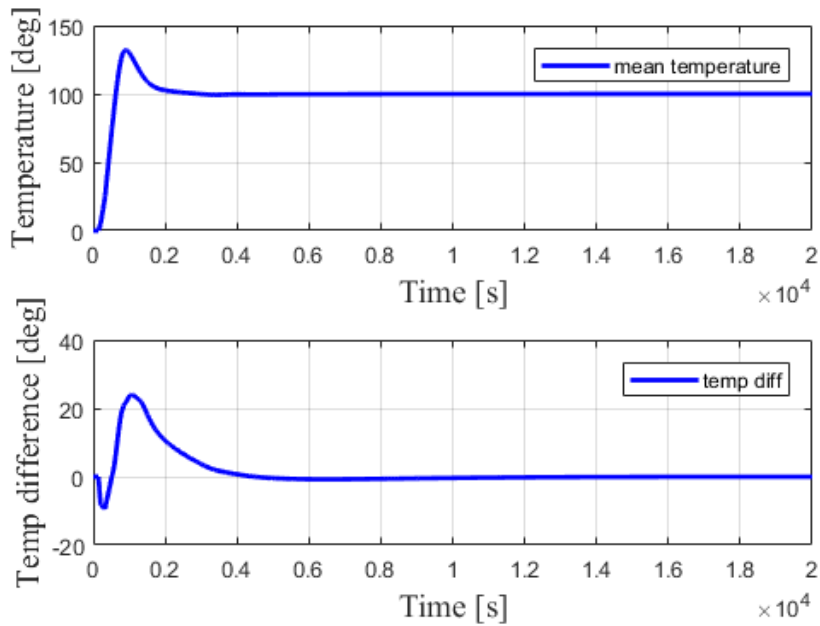
Figure 2-48 Mean temperature and temperature difference results for conventional PI control.

On the other hand, the set point tracking results of the proposed pole-zero cancellation method are shown in Figure 2-49, and Figure 2-50 shows the mean temperature and temperature difference, where there is no overshoot of the mean temperature, and the maximum temperature difference is also controlled to 8degree Celsius.
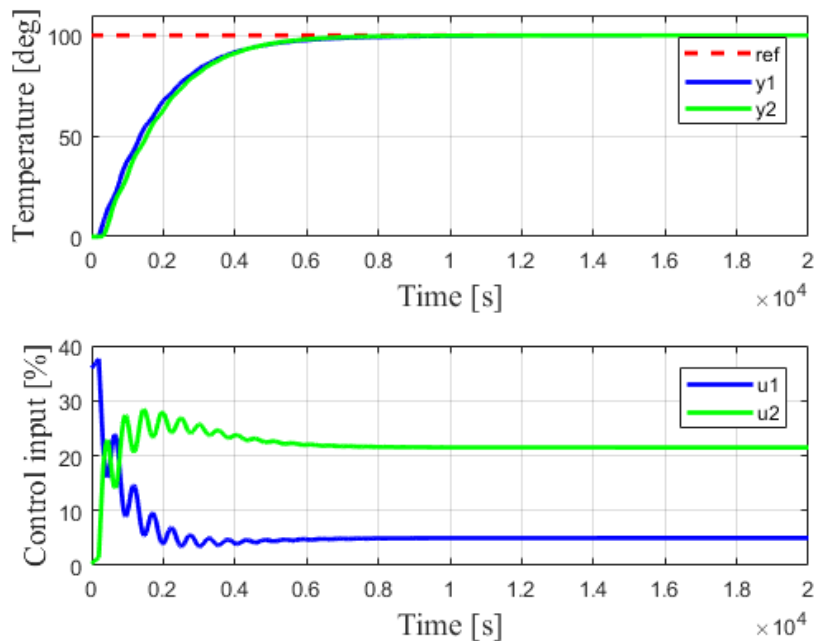
Figure 2-49 Tracking results for proposed pole-zero cancellation method.

45
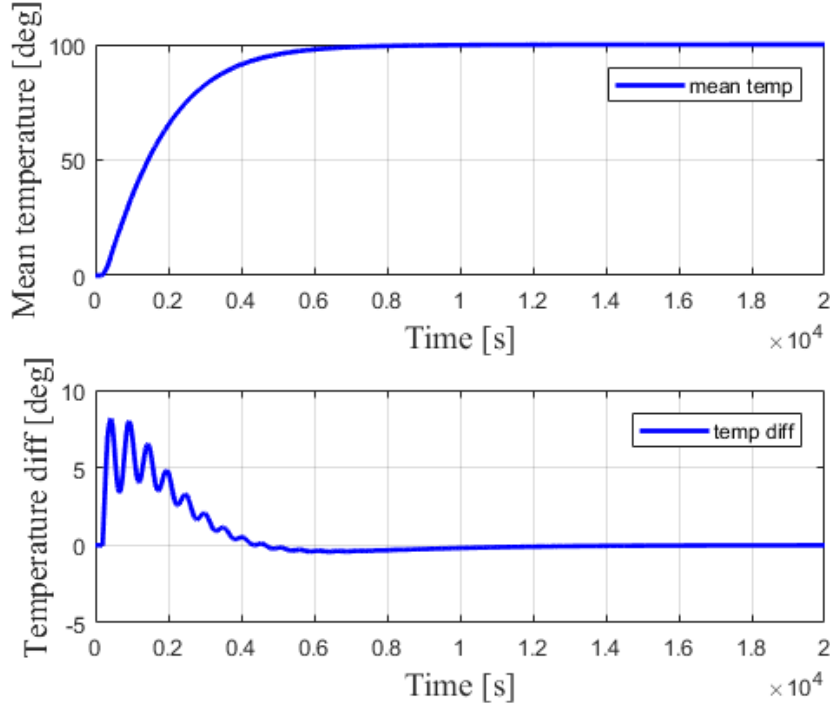
Figure 2-50 Mean temperature and temperature difference results for proposed pole-zero cancellation method.

2.5.7 Experimental results

Experiments with the proposed pole-zero cancelation control method were carried out using parameter values identical to those used in the simulation. the control objects can be identified as Eq. (2-73).

$$P(s) = \begin{bmatrix} P_{11} & P_{12} \\ P_{21} & P_{22} \end{bmatrix} = \begin{bmatrix} \dfrac{4.0992}{2627s+1}e^{-200s} & \dfrac{3.7036}{2536s+1}e^{-326s} \\ \dfrac{2.2805}{2580s+1}e^{-324s} & \dfrac{4.1268}{2461s+1}e^{-150s} \end{bmatrix} \tag{2-73}$$

According to the identified plant model, the two channels are under strong coupling effects, and with 50s delay time difference between them.

The matrix compensator G_c is designed by only considering the steady-state gain of each part as Eq. (2-74).

$$Gc = \begin{bmatrix} 0.0979 & -0.0901 \\ -0.0901 & 0.0970 \end{bmatrix} \tag{2-74}$$

After the matrix compensation, the feedforward reference models F_1 and F_2 can be designed

as Eq. (2-75). As introduced previously, the feedforward reference models F_1 and F_2 are designed to provide an expected reference response. In this proposal, to simplify the controlled system, the reference models are designed as $F_1 = F_2$.

$$F1 = F2 = \frac{0.2}{s + 0.2} \tag{2-75}$$

Thus, the controllers of these two channels are designed by Ziegler-Nichols method (step response method), $C_{PID1} = C_{PID2}$ as (12).

$$C_{PID1} = C_{PID2} = \frac{0.04s + 1}{25s} \tag{2-76}$$

In the experiments, to verify the control efficiency of the proposed method, the results were compared to the well-tuned conventional PI control system and conventional PI plus decoupling compensation system. The experiments were carried out by controlling the temperature of the two channels from room temperature (24degree Celsius) to 100degree Celsius. The results of the conventional PI control are shown in Figure 2-51, while the results of the conventional PI plus decoupling compensation are shown in Figure 2-52, the experiment results of the proposed pole-zero cancelation method are shown in Figure 2-53. In addition, the results of the compared mean temperature and the temperature difference between the two channels are shown in Figure 2-50.

Figure 2-51 Experimental results of conventional PI control.

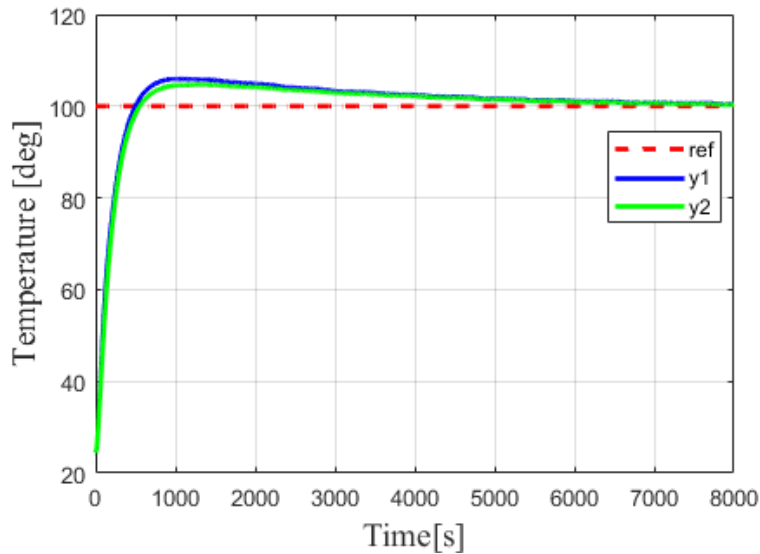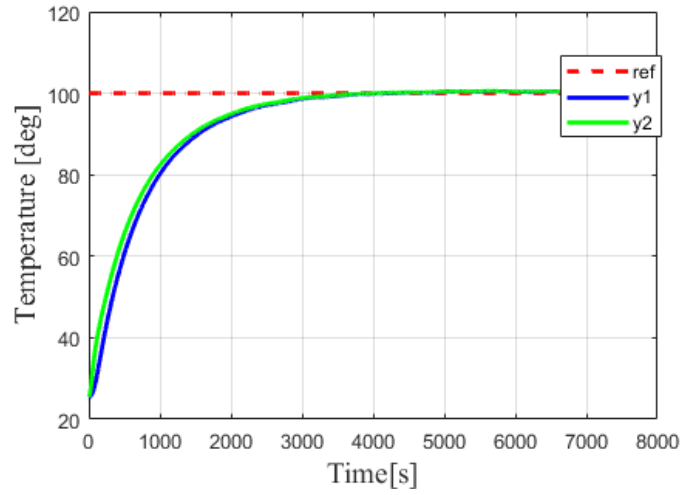Figure 2-52 Experimental results of conventional PI plus decoupling compensation.
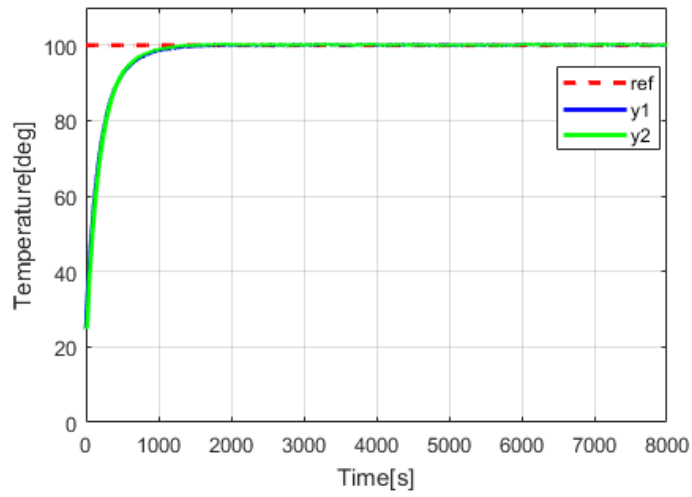

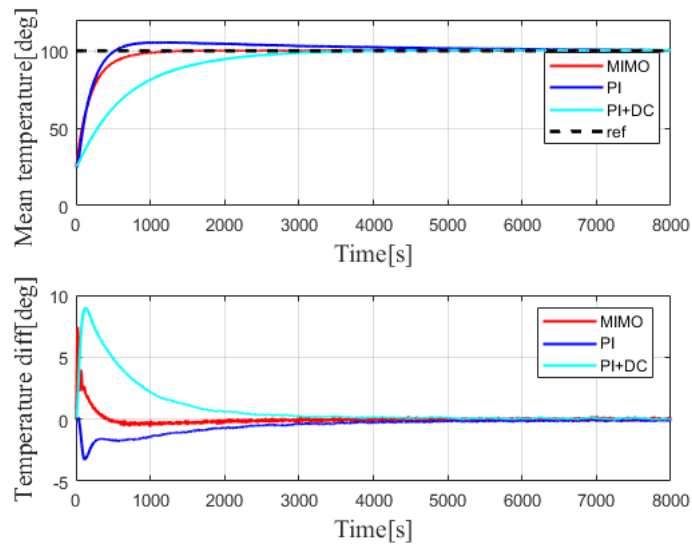Figure 2-53 Experimental results of proposed pole-zero cancelation control.

Figure 2-54 Compared results of mean temperature and temperature difference.

From the experimental results, the well-tuned conventional PI control system has the fastest transient response, while the conventional PI plus decoupling compensation system has the slowest response. However, the conventional PI control has an overshoot of 8degree Celsius (8% of the reference value), and the conventional PI plus decoupling compensation has the biggest maximum temperature difference as 9degree Celsius (9% of the reference temperature). By introducing the proposed pole-zero cancelation method, the overshoot and the maximum temperature difference can be improved. As shown in the figures above, the transient response of the proposed pole-zero cancelation control system is as fast as the well-tuned conventional PI control system about 250s rising time while the PI plus decoupling compensation has almost 1000s rising time. In addition, the proposed method has no overshoot, the maximum temperature difference has been reduced to 4degree Celsius (4% of the reference value), and quickly drops to 0degree Celsius, hence the temperature uniformity has been realized.

2.5.8 Discussion

In this proposal, compared to the conventional PI and PI plus decoupling compensation, the advantages of the proposed pole-zero cancellation method with feedforward reference model can be divided into two phases. Phase 1: The transient response has been improved to about 250s rising time as fast as the well-tuned PI control, almost 750s shortened compared to the PI plus decoupling compensation, and no overshoot compared to the conventional PI control (8% overshoot); Phase 2: The maximum temperature difference between these two channels has been minified almost half that of PI plus decoupling compensation, and the temperature difference quickly goes down to zero compared to the conventional PI control, temperature uniformity has been realized. However, if the system has plant perturbation, the proposed method may not work as efficiently as expected. Otherwise if the poles and zeros are not correctly identified, the controlled system may have some certain deviations, including overshoot, unexpected transient response, etc. Therefore, online system identification method needs to be introduced in case of perturbed systems.

2.6 Conclusions

In this chapter, the pole-zero cancellation method for the multi-point temperature control system has been introduced. Before that, the theoretical introduction of the system identification has been performed and applied to the real experimental setup. The PI controller of each channel has been designed based on the plant model obtained by the step response system identification method, and the SISO closed-loop control experiments have been carried out, the results were compared to those of simulation. Then the MIMO closed-loop control experiments have been carried out both without or with decoupling compensation, the results were compared of the simulation results. Finally, the proposed pole-zero cancellation method has been introduced and applied to the experimental setup, both simulations and experiments of the proposed pole-zero cancellation method have been carried out, and the results were compared to the conventional PI and gradient control system, the analysis of the results was focused on the transient response of both channel and the maximum temperature difference between the controlled two channels. The control efficiency of the proposed pole-zero cancellation method has been successfully verified through the comparison of the results.

Reference

[1] Engelhart. D, Boonstra.T .A, Aarts. R. G. K. M, Comparison of closed-loop system identification techniques to quantify multi-joint human balance control, Annual Reviews in Control, 2016, 41,58-70.

[2] Hassselt. G, Iyengar. R, Systems pharmacology-based identification of pharmacogenomic determinants of adverse drug reactions using human iPSC-derived cell lines, Current Opinion in Systems Biology, 2017, 4, 9-15.

[3] Sirca. G, Adeli. H, System identification in structural engineering, Scientia Iranica, 2012, 19, 6, 012, 1355-1364.

[4] Suda, N. PID Control; Asakura Publishing, Tokyo, Japan, 1992.

[5] Oshima, M. Process Control Systems, Corona Publishing: Tokyo, Japan, 2003.

[6] Goodwin, G.C, Fraebe, S.F, Salgado, M.E. Control System Design, Prentice Hall: Upper Saddle River, NJ, USA, 2001.

[7]   Morari, M, Zafiriou, E. Robust Process Control, Prentice Hall: Upper Saddle River, NJ, USA, 1992.

[8]   Maciejowski, J.M. Multivariable Feedback Design, Addison Wesley, Boston, MA, USA, 1989.

[9]   Ko, J.-S, Huh, J.-H, Kim, J.-C, Improvement of Temperature Control Performance of Thermoelectric, Dehumidifier Used Industry 4.0 by the SF-PI Controller, Processes 2019, 7, 98.

[10] Ganesh, H.S, Edgar, T.F, Baldea, M, Model Predictive Control of the Exit Part Temperature for an Austenitization Furnace, Processes 2016, 4, 53.

[11] Garrido, J, Lara, M, Ruz, M.L, Vazquez, F, Alfaya, J.A, Morilla, F. Decentralized PID control with inverted decoupling and superheating reference generation for efficient operation, Application to the Benchmark PID, 2018. IFAC-Papers OnLine 2018, 51, 710–715.

[12] Gilbert, A.F, Yousef, A, Natarajan, K, Deighton, S, Tuning of PI controllers with one-way decoupling in MIMO systems based on finite frequency response data, J. Process Control 2003, 13, 553–567.

[13] Waller, M, Waller, J.B, Waller, K.V, Decoupling revised. Ind. Eng. Chem. Res. 2003, 42, 4575–4577.

[14] Deng, M, Bi, S, Operator-based robust nonlinear control system design for MIMO nonlinear plants with unknown coupling effects. Int. J. Control 2010, 83, 1939–1946.

[15] Wang, Q.G, Zou, B, Zhang, Y. Decoupling Smith delay compensator design for multivariable systems with multiple time delays. Chem. Eng. Res. Des. 2000, 78 Pt. A, 565–572.

[16] Wang, Q.G, Zhang, Y, Chiu, M.S. Decoupling internal model control for multi-variable systems with multiple time delays. Chem. Eng. Sci. 2002, 57, 115–124.

[17] Pop, C.I, Ionescu, C.M, Keyser, R.D. Time delay compensation for the secondary processes in a multivariable carbon isotope separation unit. Chem. Eng. Sci. 2012, 80, 205–218.

[18] Coakley, D, Raftery, P, Keane, M. A review of methods to match building energy simulation models to measured data. Renew. Sustain. Energy Rev. 2014, 37, 123–141.

[19] Yao, Y, Yang, K, Huang, M, Wang, L. A state-space model for dynamic response of indoor air temperature and humidity. Build. Environ. 2013, 64, 26–37.

[20] Seong, Y.B, Cho, Y.H, Development and evaluation of applicable optimal terminal box control algorithms for energy management control systems. Sustainability 2016, 8, 1151.

[21] Jeng, J.C, Chang, Y.J, Lee, M.W, Novel design of dynamic matrix control with enhanced decoupling control performance. Comput. Aided Chem. Eng. 2014, 44, 541–546.

[22] Nanno, I, Tanaka, M, Matsunaga, N, Kawaji, S, On Performance of the Gradient Temperature Control

Method for Uniform Heating. IEEJ Trans. EIS 2004, 124, 1606–1612.

[23] Matsunaga, N, Kawaji, S, Tanaka, M, Nanno, I, A Novel Approach of Thermal Process Control for Uniform Temperature. IFAC Proc. Vol. 2005, 38, 111–116.

[24] Tomaru, T, Mori, Y, Design Method of Minimum-Phase State Decoupling Control with Feedforward Compensation. In Proceedings of the SICE Annual Conference 2007, Takamatsu, Japan, 17–20 September 2007; IEEE: Takamatsu, Japan, 2007; 1C07-1. Processes 2019, 7, 497 12 of 12

[25] Ishii, Y, Masuda, S, Data-driven Update of The Free Parameter of The Youla-Kucera Parametrization in Disturbance Attenuation FRIT based on Variance Evaluation. In Proceedings of the 2016 International Conference on Advanced Mechatronic Systems (ICAMechS), Melbourne, VIC, Australia, 30 November– December 2016; IEEE: Melbourne, Australia, 2016; pp. 11–16.

[26] Gao, Z, Saxen, H, Gao, C, Data-driven approaches for complex industrial systems. IEEE Trans. Ind. Inform. 2013, 9, 2210–2212.

[27] Gao, Z, Nguang, S.K, Kong, D.X, Advances in Modelling, Monitoring, and Control for Complex Industrial Systems. Complexity 2019.

[28] Gao, R, Gao, Z, Pitch control for wind turbine systems using optimization, estimation and compensation. Renew. Energy 2016, 91, 501–515.

[29] Wang, J, Tse, N, Gao, Z, Synthesis on PI-based pitch controller of large wind turbines generator. Energy Convers. Manag. 2011, 52, 1288–1294.

[30] Ziegler, J.G, Nichols, N.B, Optimum settings for automatic controllers. Trans. ASME 1942, 64, 759–768.

Chapter 3

Reference-Model-Based Artificial Neural Network Control Method for Temperature Control System

Intelligent control, as an important development part of the modern advanced control field, can achieve automation via the emulation of biological intelligence. The combinations of the intelligent control field have already been introduced in Chapter 1. In this study, the artificial neural network is applied.

3.1 Artificial neural network

Artificial Neural Network (ANN) is a research hot spot that has emerged in the field of artificial intelligence since the 1980s. It abstracts the human neuron network from the perspective of information processing, establishes some simple model, and forms different networks according to different connection methods. In engineering and academia, it is often referred to as a neural network or neural networks. A neural network is a computing model that consists of a large number of nodes (or neurons) connected to each other. Each node represents a specific output function, called an activation function. The connection between every two nodes represents a weighted value for the signal passing through the connection, called the weight, which is equivalent to the memory of an artificial neural network. The output of the network varies depending on how the network is connected, the weight value and the excitation function. The network itself is usually an approximation of an algorithm or function in nature, or it may be an expression of a logical strategy.

In the past ten years, the research work of artificial neural network has been continuously deepened, and great progress has been made. It has successfully solved many problems in the fields of pattern recognition, intelligent robots, automatic control, prediction and estimation, biology, medicine, and economics. The practical problems that modern computers are difficult to solve have shown good intelligent characteristics.

3.2 Advantages of artificial neural network

The characteristics and advantages of artificial neural networks are mainly manifested in three aspects:

1). **Self-learning function.** For example, when image recognition is implemented, only many different image templates and corresponding recognition results should be input into the artificial neural network first, and the network will slowly learn to recognize similar images through self-learning function. The self-learning function is particularly important for prediction. It is expected that artificial neural network computers in the future will provide economic forecasts, market forecasts, and profit forecasts for human beings, and their application prospects are very promising.

2). **Lenovo memory function.** This kind of association can be realized with the feedback network of the artificial neural networks.

3). **Ability to find optimal solutions at high speed.** Finding an optimal solution to a complex problem often requires a large amount of calculation. Using a feedback-type artificial neural network designed for a certain problem and using the computer's high-speed computing capabilities, it may quickly find an optimal solution.

3.3 Algorithm of artificial neural network

In this section, the forward calculation and backpropagation algorithms of the neural network will be introduced. The forward algorithms will be introduced from the single-input single-layer neural network to the multi-input multi-layer neural network, while the backpropagation algorithm will focus on the multi-input multi-layer neural network.

3.3.1 Single-input neuron

The single-neuron is shown in Figure 3-1, where p is the scalar input of the neuron and w is the weight of the neuron, wp is the gradient value of the neuron and b is the bias of the neuron. f is the activation function of the neuron. Thus, the output of the neuron can be calculated as
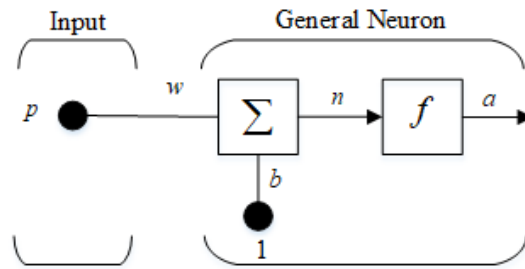
Eq. (3-1).

Figure 3-1 Single-Input neuron.

$$a = f(wp+b)$$

<div align="right">(3-1)</div>

Note that w and b are both scalar parameters of the neuron, and the activation function is chosen freely by the user and then the parameters w and b will be trained by some learning rules so that the relationship between input and output can reach some specific goal. The activation functions will be introduced later.

3.3.2 Multi-input neuron

Usually, the inputs of one neuron are more than one, that is, each neuron may have multi-input signals. The typical structure of the multi-input neuron with R inputs is shown in Figure 3-2, where the individual inputs $p_1, p_2, p_3, \ldots, p_n$ are respectively weighted by the corresponding elements $w_1, w_2, w_3, \ldots, w_n$ of the weight matrix W.
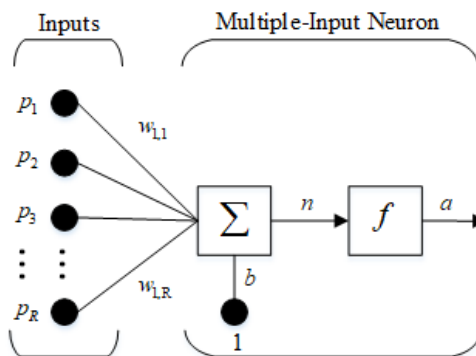

Figure 2-3 Multi-input neuron.

In this figure b is the bias of the neuron, and f is the activation function of the neuron. Thus, the neuron output can be expressed in matrix form and calculated as Eq. (3-2).

$$a = f(Wp+b)$$

<div align="right">(3-2)</div>

3.3.3 Multi-input multi-layer neural network

Consider that in practical application, the multi-layer neural network performs better than the single-layer neural network, thus most of the control application will choose to use the multi-input multi-layer neural network to improve the system performance. Take a three-layer neural network as an example, the calculation structure is shown in Figure 3-3, where the network has n input signals. W_1, W_2 and W_3 indicate the weights of each layer, respectively. b_1, b_2 and b_3 respectively indicate the bias of each layer. f is the activation function of the neurons.

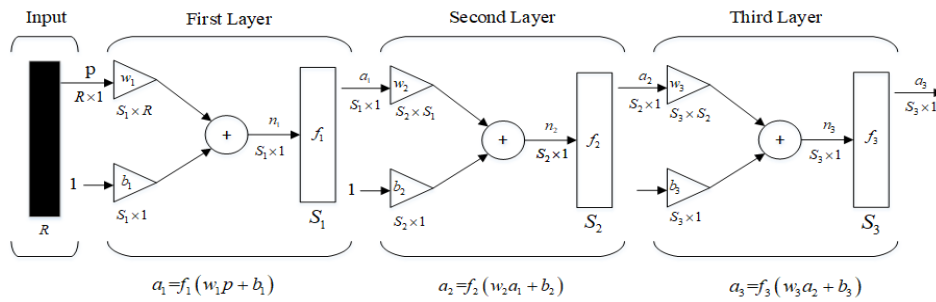$$a_1 = f_1(w_1 p + b_1) \qquad a_2 = f_2(w_2 a_1 + b_2) \qquad a_3 = f_3(w_3 a_2 + b_3)$$

Figure 3-3 Three-Layer Network.

Thus, for a three-layer neural network, the output of the network can be calculated as Eq. (3-3).

$$a_3 = f_3(W_3 f_2(W_2 f_1(W_1 p + b_1) + b_2) + b_3) \tag{3-3}$$

3.4 Activation functions of neural network

The activation function is one of the most important parts in the neural network iteration, it can decide the learning speed and the output of each neuron. So, the correct choice of the activation function will have a direct impact on the performance of the neural network. Here three widely used activation functions are introduced.

3.4.1 Sigmoid activation function

As one of the earliest used activation functions in the neural network history, the *sigmoid* function takes any real value and squashes it into the range between 0 and 1. The mathematical expression of the *sigmoid* function is as Eq. (3-4).

$$f(x) = \frac{1}{1 + e^{-x}} \tag{3-4}$$

From the equation, it is easy to see that the *sigmoid* is a smooth and differentiable function. The dynamic output curves of the *sigmoid* function and its differential are shown in Figures 3-4 and 3-5, respectively.
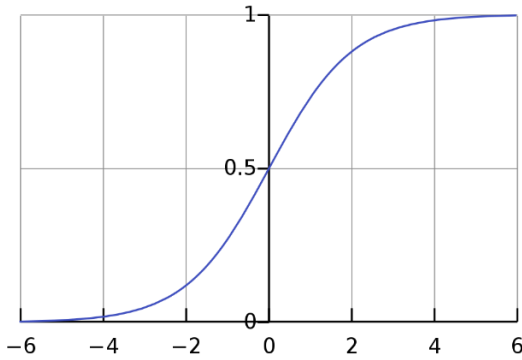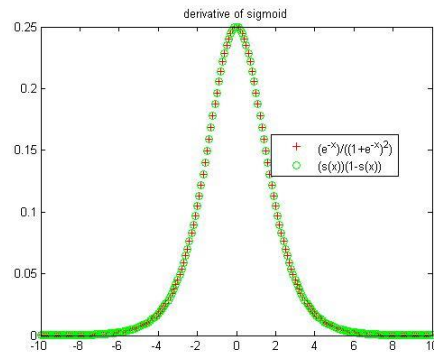

Figure 3-4 Sigmoid function output.   Figure 3-5 Output of sigmoid differential function.

As can be observed from the figures, the *sigmoid* function can saturate (produce extremely valued outputs) very quickly and for a majority of inputs. However, this may become a problem, due to it may lead to the gradients becoming either zero or diverging to an overflowing floating-point value. These two problems are defined as vanishing gradient problem and exploding gradient problem, respectively. As a result, it is rare to apply the sigmoid in the neural networks other than at the output.

3.4.2 Tanh activation function

The *tanh* activation function is a cosmetically different variant of the *sigmoid* activation function. The tanh activation function can be expressed as Eq. (3-5).

$$f(x) = \tanh x = \frac{e^{x} - e^{-x}}{e^{x} + e^{-x}} \tag{3-5}$$

Except the little bit of wrangling, the *tanh* can be convinced simply as a linear transform of the sigmoid function, the response of the *tanh* function and its differential are shown in Figures 3-6 and 3-7, respectively.
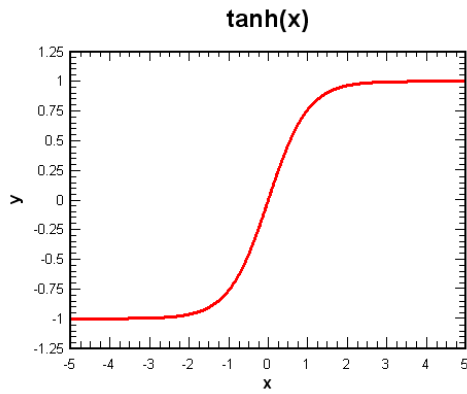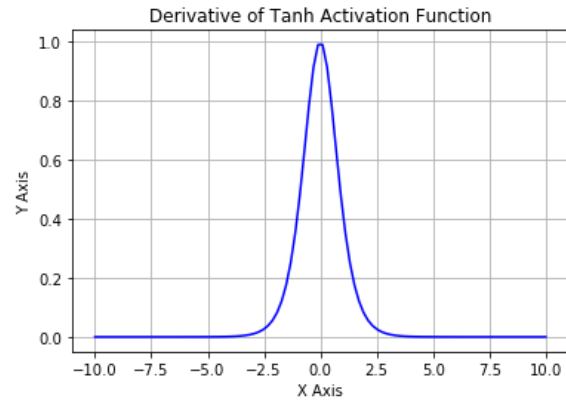
Figure 3-6 Sigmoid function output.　　　　Figure 3-7 Output of sigmoid differential function.

Notice that, the *tanh* function like the sigmoid is also a "squashing" function, except that it maps the set of real values from (-∞, +∞) to the range [-1, 1].

3.4.3 ReLU activation function

ReLU function stands for the rectified linear unit. This is arguably the most important of the activation function that in recent innovations in deep learning, there would have been impossible without the use of ReLU activation function. The expression of the ReLU function is as the Eq. (3-6).

$$f(x) = \max(0, x)$$

(3-6)

From the equation, what the ReLU unit is doing is to clip the negative values to zero and the positive values being kept the same. The output characteristic of ReLU unit is shown in Figure 3-8.
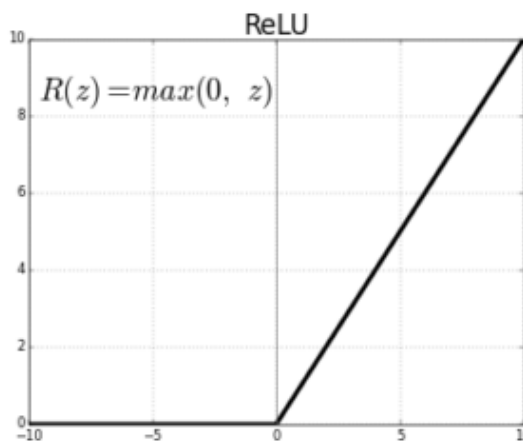

Figure 3-8 Output characteristic of ReLU function.

Utill now, the typical three kinds of the activation functions have been introduced. The ReLU function can simply help with the vanishing gradient problem of the neuron. Thus, in this study, ReLU function is chosen as the activation function.

3.5 Backpropagation for neural network training

Regarding self-learning, the backpropagation algorithm is applied for the weight training and neuron bias update. Assuming that neuron j is a neuron in the hidden layer that connected to the output neuron k, the signal flow graph of the nth iteration (i.e., nth training sample) is shown in Figure 3-9.
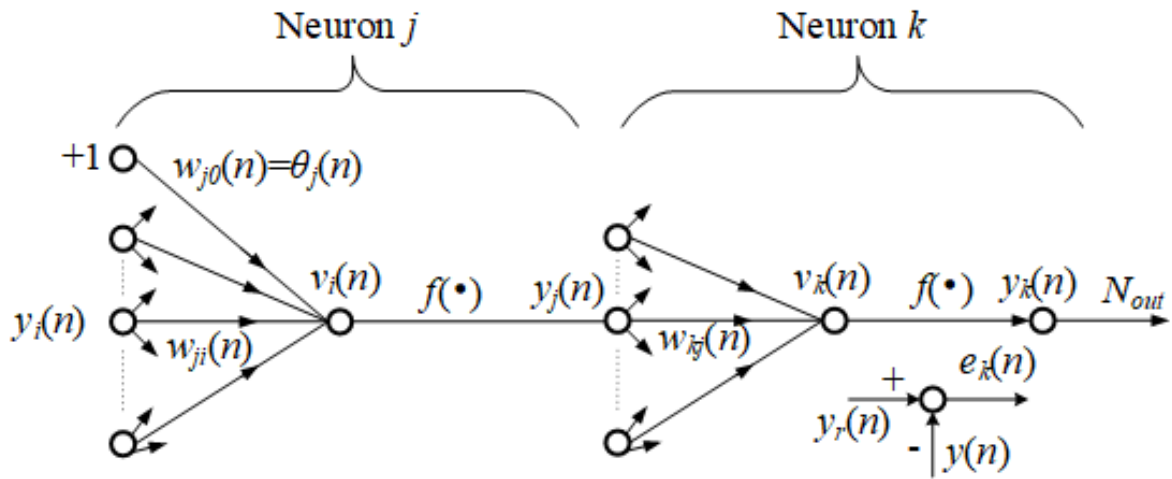

Figure 3-9 Signal flow graph highlighting the details of output neuron k connected to hidden neuron j.

From Figure 3-9, neuron j is fed by a set of function signals produced by a layer of neurons to its left. Thus, the local gradient values of the neuron j and k can be obtained as Eqs. (3-7) and (3-8), respectively. Where m is the total number of the number of inputs (excluding the bias) applied to neuron j. the synaptic weight $w_{j0}(n)$ (corresponding to the fixed input $y_0 = +1$) equals the bias θ_j applied to neuron j.

$$v_j(n) = \sum_{i=0}^{m_{L-1}} w_{ji}(n) y_i(n) \tag{3-7}$$

$$v_k(n) = \sum_{j=0}^{m_{K-1}} w_{kj}(n) y_j(n) \tag{3-8}$$

The activation function will apply to the local gradient of the neurons, and then the output of neurons j and k can be obtained as Eqs. (3-9) and (3-10), respectively.

$$y_j(n) = f\left(\sum_{i=0}^{m} w_{ji}(n) y_i(n)\right) \tag{3-9}$$

$$y_k(n) = f\left(\sum_{j=1}^{m} w_{kj}(n) y_j(n)\right) \tag{3-10}$$

The backpropagation begins at the output layer of the NN controller, so the signal will flow from neuron k to neuron j. The error signal is used as the teaching signal for the neurons, the error signal at n^{th} iteration is defined as Eq. (3-11).

$$e_k(n) = d_k(n) - y_k(n) \tag{3-11}$$

We define the instantaneous value of the error energy of the output neuron k as $\frac{1}{2}\sum e_k^2(n)$. Then the entire instantaneous error energy $\varepsilon(n)$ of the output layer at n^{th} iteration is the sum of the instantaneous error energy of all neurons in the output layer, and $\varepsilon(n)$ is used as the cost function of network training. The $\varepsilon(n)$ can be obtained as Eq. (3-12).

$$\varepsilon(n) = \frac{1}{2}\sum_{k=1}^{m_K} e_k^2(n) \tag{3-12}$$

According to the backpropagation algorithm, the correction of the weight w_{kj} is that in Eq. (3-13) and Δw_{kj} is obtained as shown in Eq. (3-14), where α is the learning gain.

$$w_{kj}(n+1) = w_{kj}(n) + \Delta w_{kj}(n) \tag{3-13}$$

$$\Delta w_{kj}(n) = -\alpha \frac{\partial \varepsilon(n)}{\partial w_{kj}(n)} \tag{3-14}$$

Considering the chain rule of the differential function, the negative gradient of $\varepsilon(n)$ to $w_{kj}(n)$ can be expressed as Eq. (3-15).

$$-\frac{\partial \varepsilon(n)}{\partial w_{kj}(n)} = \left(-\frac{\partial \varepsilon(n)}{\partial v_k(n)}\right)\frac{\partial v_k(n)}{\partial w_{kj}(n)} = \delta_k(n)\frac{\partial v_k(n)}{\partial w_{kj}(n)} \tag{3-15}$$

Here we define $\delta_k(n)$ as the local gradient, which is the negative gradient of cost function

to the local domain induced by the neuron. By the differential chain rule, the local gradient of neuron k can be obtained as Eq. (3-16).

$$\delta_k(n) = -\frac{\partial \varepsilon(n)}{\partial v_k(n)} = -\frac{\partial \varepsilon(n)}{\partial e_k(n)} \frac{\partial e_k(n)}{\partial y_k(n)} \frac{\partial y_k(n)}{\partial v_k(n)} = e_k(n) \varphi_k'(v_k(n)) \tag{3-16}$$

From the equation, the local gradient of the output neuron k equals to the production of the error signal of neuron k and the derivative $\varphi_k'(v_k(n))$ of the corresponding activation function. Thus, differentiate $w_{kj}(n)$ on both sides of the Eq. (3-8), we can get Eq. (3-17).

$$\frac{\partial v_k(n)}{\partial w_{kj}(n)} = y_j(n) \tag{3-17}$$

Take Eqs. (3-16) and (3-17) into Eq. (3-14), the correction formula of the weight adjustment is obtained as Eq. (3-18).

$$\Delta w_{kj}(n) = \eta \delta_k(n) y_j(n) \tag{3-18}$$

For the neuron j, the local gradient of this neuron can be obtained as Eq. (3-19), according to the definition of the local gradient shown in Eq. (3-16).

$$\delta_j(n) = -\frac{\partial \varepsilon(n)}{\partial v_j(n)} = -\frac{\partial \varepsilon(n)}{\partial y_j(n)} \frac{\partial y_j(n)}{\partial v_j(n)} = -\frac{\partial \varepsilon(n)}{\partial y_j(n)} \varphi_j'(v_j(n)) \tag{3-19}$$

To obtain the partial derivative $\partial \varepsilon(n)/\partial y_j(n)$, we re-modify Eq. (3-11) as Eq. (3-20).

$$\varepsilon(n) = \frac{1}{2} \sum_{k=1}^{m_K} e_k^2(n) \tag{3-20}$$

Partial derivative of function signal $y_j(n)$ on both sides, Eq. (3-21) can be obtained.

$$\frac{\partial \varepsilon(n)}{\partial y_j(n)} = \sum_{k=1}^{m_K} e_k(n) \frac{\partial e_k(n)}{\partial y_j(n)} \tag{3-21}$$

Note that, due to the fully connected nature of the neural network, the hidden layer neurons are responsible for the errors of each neuron in the output layer, that is, the output of the hidden layer neurons is the hidden function of the output error, so there is a sum in Eq. (3-21).

And then, introducing the chain rule into partial derivative $\partial e_k(n)/\partial y_j(n)$, the Eq. (3-21) can be equivalently expressed as Eq. (3-22).

$$\frac{\partial \varepsilon(n)}{\partial y_j(n)} = \sum_{k=1}^{m_K} e_k n \frac{\partial e_k(n)}{\partial v_k(n)} \frac{\partial v_k(n)}{\partial y_j(n)} \tag{3-22}$$

For the output neuron k, Eqs. (3-23) and (3-24) may work. Where $w_{k0}(n)$ is the bias of neuron k.

$$e_k(n) = d_k(n) - y_k(n) = d_k(n) - \varphi_k(v_k(n)) \tag{3-23}$$

$$v_k(n) = \sum_{k=0}^{m_{K-1}} w_{kj}(n) y_j(n) \tag{3-24}$$

Partial derivative of $v_k(n)$ and $y_j(n)$ on both sides of Eqs. (3-23) and (3-24), respectively, we can obtain the Eqs. (3-25) and (3-26).

$$\frac{\partial e_k(n)}{\partial v_k(n)} = -\varphi_k'(v_k(n)) \tag{3-25}$$

$$\frac{\partial v_k(n)}{\partial y_j(n)} = w_{kj}(n) \tag{3-26}$$

Take these two equations into Eq. (3-22), we can get Eq. (3-27).

$$\frac{\partial \varepsilon(n)}{\partial y_j(n)} = -\sum_{k=1}^{m_K} \left[e_k(n) \varphi_k'(v_k(n)) \right] w_{kj}(n) = -\sum_{k=0}^{m_K} \delta_k(n) w_{kj}(n) \tag{3-27}$$

According to the Eq. (3-16), the relationship of Eq. (3-28) can be found in Eq. (3-27).

$$\delta_k(n) = e_k(n) \varphi_k'(v_k(n)) \tag{3-28}$$

Finally, take Eq. (3-27) into Eq. (3-19), the local gradient of the hidden neuron j can be obtained as Eq. (3-29).

$$\delta_j(n) = \varphi_j'(v_j(n)) \sum_{k=1}^{m_K} \delta_k(n) w_{kj}(n) \tag{3-29}$$

Thus, the weight correction of neuron j is obtained as shown in Eq. (3-30), and $\Delta w_{kj}(n)$ is expressed as is shown in Eq. (3-31).

$$w_{ji}(n+1) = w_{ji}(n) + \Delta w_{ji}(n) \tag{3-30}$$

$$\Delta w_{ji}(n) = --\alpha \frac{\partial \varepsilon(n)}{\partial w_{kj}(n)} = \alpha \delta_j(n) y_j(n) \tag{3-31}$$

Also, the neuron bias needs to be adjusted. The correction is also determined by the local

gradient $\delta_j(n)$. The bias correction of neuron j at n^{th} iteration is expressed as Eq. (3-32), where β is the bias training gain.

$$\theta_j(n+1) = \theta_j(n) - \beta\delta_j(n) \tag{3-32}$$

To improve the self-learning ability of the NN controller, here we choose ReLU activation function as the activation function. The function can be expresses as Eq. (3-33) and its derivative is shown in Eq. (3-34).

$$f(x) = \begin{cases} x, x > 0 \\ 0, x \leq 0 \end{cases} \tag{3-33}$$

$$f'(x) = \begin{cases} 1, x > 0 \\ 0, x \leq 0 \end{cases} \tag{3-34}$$

3.6 Reference-model-based artificial NN control method for temperature control system

After the theoretical introduction of the artificial neural network, we proposed a reference-model-based artificial neural network control method for the temperature control system. The configuration of the proposed system is shown in Figure 3-10.
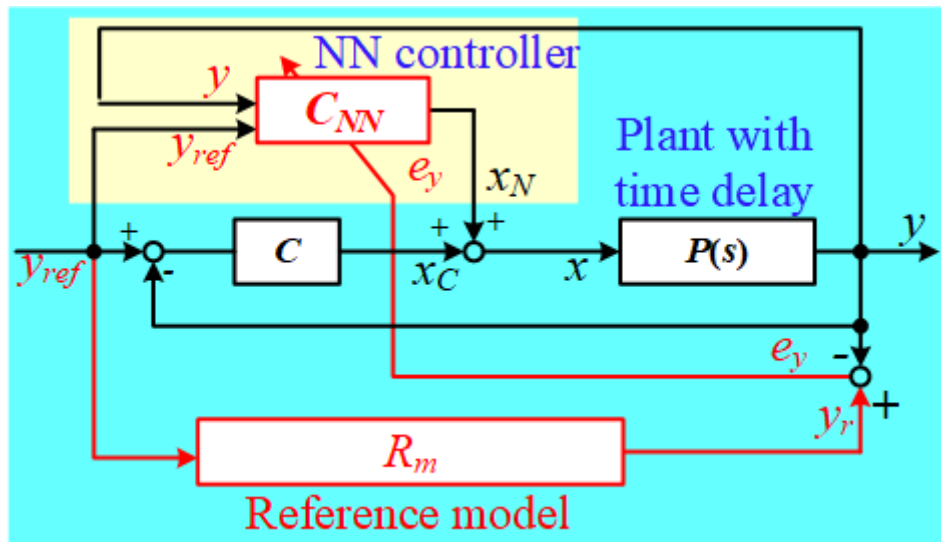

Figure 3-10 Block diagram of reference-model-based neural network control system.

For simplicity, the controlled object is expressed as a first order plus time delay (FOPTD)

model. In Figure 3-10, y_{ref} is the set reference value for the system, e_y is the teaching signal for the NN controller, which is calculated as the error between the output y_r of reference model R_m and the output temperature y, C is a conventional PID controller (in this paper, an I-PD configuration is employed), and x is the control input, which is the sum of the NN controller output x_N and I-PD output x_C. The reference model R_m is designed based on the control object, thus it can provide the reference output temperature with the same time delay. The explanation of the control system is divided into four main parts.

3.6.1 Control object with time delay

The controlled object is the thermal processing system, which can be represented as a FOPTD system. With its large delay time, the transfer function of the plant can be expressed as Eq. (3-35), where K is the steady-state gain of the output temperature against the input signal, T is the time constant of the plant, and t is the delay time of the response. The step response of the plant is shown in Figure 3-11. Since this model is only suitable for the autotuning method of the I-PD controller, it is not required to design the NN controller itself.
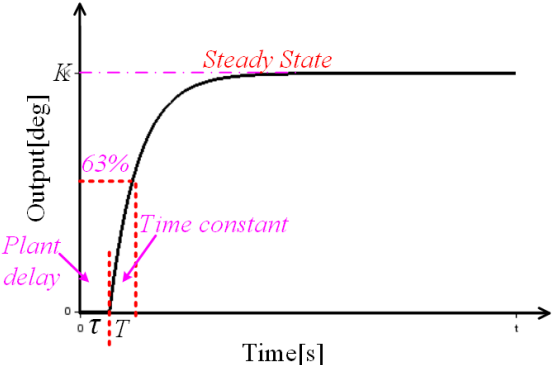
$$P(s) = \frac{K}{Ts+1} e^{-\tau s} \tag{3-35}$$

Figure 3-11 Step response of FOPTD plant.

3.6.2 Conventional I-PD control

Considering that the NN controller needs time to learn and train its parameters, and will mainly act after finishing training, a conventional I-PD controller is designed for the control of

the initial state. The block diagram of I-PD controller is shown in Figure 3-12, where k_f is the feed-forward gain used to decide the system response speed (0: slow; 0.5: middle; 1: fast), T_i is the integral time constant, T_d is the differential time constant, η is the gain of the low-pass filter (LPF) which is necessary for the feasibility of the derivative action. This part is the derivative part of the controller and can introduce an effective early correction signal in the system before the deviation signal changes too much hence making it possible in speeding up the system's action speed. K_p is the proportional gain of the controller. Compared to the conventional PID control structure, the I-PD control structure can prevent sharp rising of the control input which means that if there is a sudden change in the error signal, the mutation will not happen in the output of the I-PD controller. The control input will be smoothly adjusted instead of a step change.
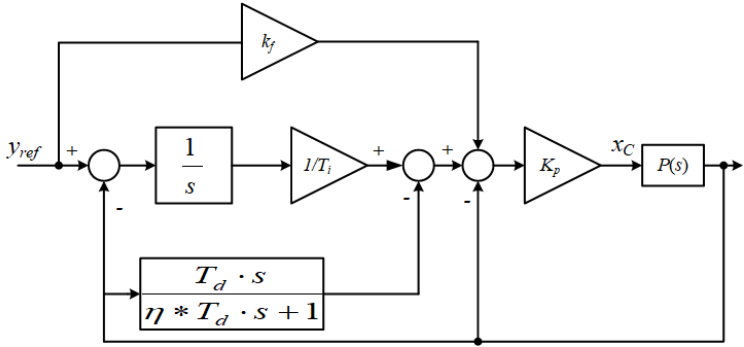

Figure 3-12 Structure of conventional I-PD control.

Stability is one of the most important factors of a controller. Several methods have been proposed for controller stability analysis. Because the parameters of the I-PD controller are designed based on the Ziegler-Nichols rule (step response method), stability is ensured. These values are determined by τ, K and T in Eq. (3-35). The I-PD parameters K_p, T_i and T_d can be calculated as Eqs. (3-36). (3-37) and (3-38), respectively.

$$K_p = 1.2\frac{T}{\tau} \tag{3-36}$$

$$T_i = 0.5T \tag{3-37}$$

$$T_d = 0.5\tau \tag{3-38}$$

65

3.6.3 Artificial NN controller

In order to realize model-free control and auto-learning for reference model output tracking, a multi-layer NN controller is introduced into the I-PD control system. In the proposed system, the NN controller has one input layer, two hidden layers, and one output layer. The two hidden layers have 10 neurons, and thus the structure of the NN controller is 2-10-10-1 as is shown in Figure 3-13.
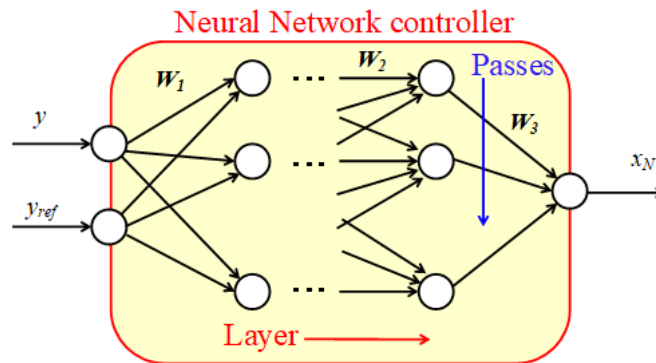

Figure 3-13 Structure of multi-layer neural network controller.

In this system, the reference value of the system y_{ref} and the output temperature y are set as the input signal of the neural networks. x_N is the output value of the neural networks. The calculation process from the input N_{in} to the output N_{out} can be shown in Figure 3-14. Where the W is the weight of neurons, θ is the offset value of every neuron, $f(\cdot)$ is the neuron activation function.
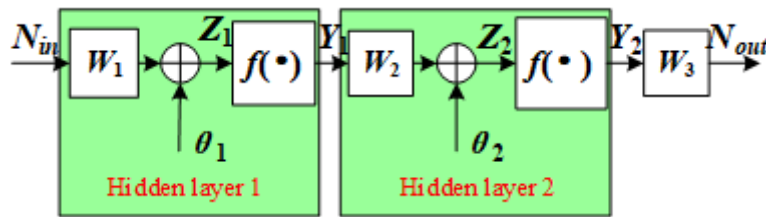

Figure 3-14 Calculation process of neural network controller.

From the calculation process the output of the neural networks can be derived as Eq. (3-39).

$$NN_{out} = W_3 * f(W_2 * f(W_1 * NN_{in} + \theta_1) + \theta_2)$$

(3-39)

Regarding the self-learning, the backpropagation has been introduced as Section 3.5, and also the ReLU function is applied as the activation function.

3.6.4 Reference-model-based NN control system

The reference model, which is based on the plant transfer, has been applied to provide the training signal of the NN controller and also help to prevent the over learning of the NN controller. Reducing the memory required to store the output can make the controller realization easy, thus the approximation of the dead time needs to be introduced. There are several approximation methods, such as graphical approximation and Pade approximation. Here, the Pade approximation method is applied, the basic rule of the Pade approximation method is shown in Eq. (3-40).

$$e^{-\tau s} = \frac{e^{-\frac{\tau}{2}s}}{e^{\frac{\tau}{2}s}} = \frac{1 - \frac{\tau s}{2} + \frac{\tau^2 s^2}{2} + \cdots + \frac{(-\frac{\tau s}{2})^k}{k!}}{1 + \frac{\tau s}{2} + \frac{\tau^2 s^2}{2} + \cdots + \frac{(\frac{\tau s}{2})^k}{k!}} \tag{3-40}$$

In some cases, a very crude approximation given by a first-order lag is also acceptable, in this study our approximation is shown as Eq. (3-41).

$$e^{-\tau s} \approx \frac{1}{(\frac{\tau s}{2} + 1)^2} \tag{3-41}$$

Thus, the reference model setting is based on the approximated plant model, which is to improve the transient response speed by adding a gain R to the plant time constant, the approximated model is shown as Eq. (3-42). Approximation of dead time to 2nd order transfer function makes the controller realization much easier, i.e. the memory to store the output can be saved.

$$R(s) \approx \frac{1}{T * Rs + 1} \bullet \frac{1}{(\frac{\tau s}{2} + 1)^2} \tag{3-42}$$

The step response and open-loop bode diagram of the original FOPTD plant and the approximated plant are shown in Figures 3-15 and 3-16, respectively.

In this proposal, the reference model is proposed to provide the teaching signals for the NN controller, to provide efficient teaching signal, the reference model should include exactly the same dead time of the controlled plant as well as the real plant model.
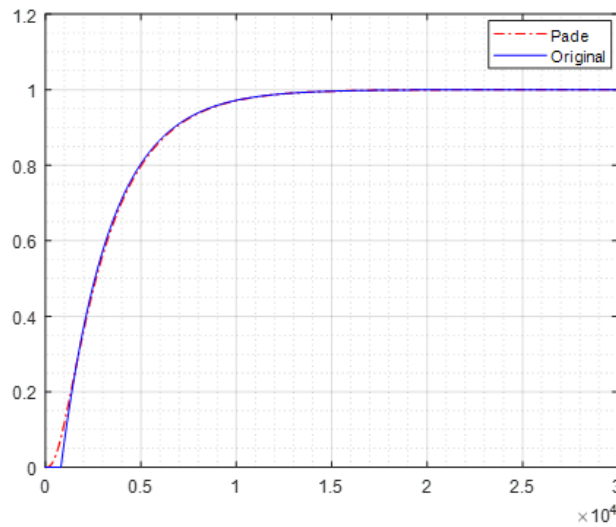
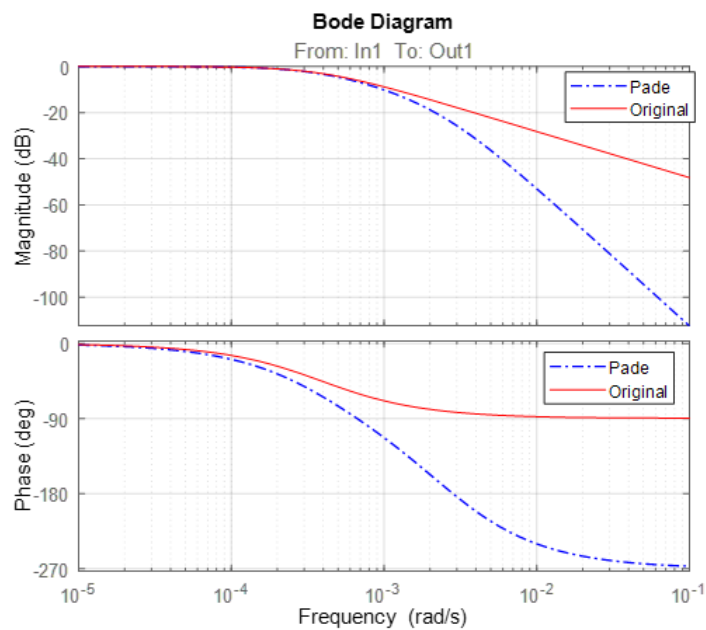Figure 3-15 Step response of the original model and approximated model.

Figure 3-16 Bode diagram of the original and approximated model.

From the step response figure, we can see that the approximate plant is similar to the original plant model both in the transient response and steady-state characteristics. And for the FOPTD plant model, the bode diagram can only show the plant without delay time part, but after approximated, the whole characteristic can be shown.

3.7 Simulation comparison to conventional error feedback NN control method

To verify the effectiveness of the proposed control method, the comparison with conventional error feedback NN control method needs to be carried out. The structure of the conventional error feedback NN control method is shown in Figure 4, where the output of the IPD controller is used as the learning signal of the NN controller. In this comparison simulation, the control object is freely chosen as Eq. (3-43), which only has 1s delay time, and the reference model is designed as introduced above shown as Eq. (3-44). Both the conventional error feedback NN control method and the proposed reference-model-based NN control method has been applied to this control object, a step reference from 100 to 105 is applied as the reference value which will be repeated several times, and have both first step response and the last step response compared.
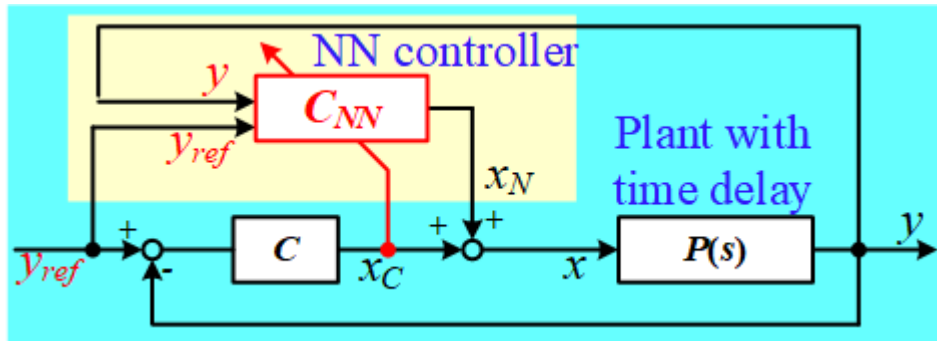

Figure 3-17 Structure of conventional error feedback NN control system.

$$P(s) = \frac{540}{225s+1}e^{-s} \qquad (3\text{-}43)$$

$$R(s) = \frac{1}{s+1}e^{-s} \qquad (3\text{-}44)$$

In the conventional error feedback NN control system, since the output of the conventional PID controller is used as the teaching signal of the NN controller, considering that the controlled object has a big time lag, the output of the conventional feedback controller reaches the saturation at the beginning and the NN controller starts training at the same time even when the

plant has no output, which easily causes the overlearning of the NN controller. In the proposed reference-model-based NN control system, the training signal is provided by the error between the reference mode output and the real plant output. Due to the reference mode having the same dead time as the plant, the training signal before the plant has output signal is set as zero, thus, the NN controller starts training after the plant has output. As a result, the teaching signal is much smoother with no sudden change, which can help prevent the over training of the NN controller. This difference mainly affects the learning efficiency of the NN controller.

Figure 3-18 (a) and 3-18 (b) respectively show the time response of the conventional error feedback NN control system and the proposed reference-model-based NN control system. From the simulation results, the first step response and the last step response of the conventional error feedback NN control are almost the same, which means that after repeating several times the conventional feedback NN control method can't improve the system response. However, by introducing the proposed reference-model-based NN method, compared with the first step response the last step response has been improved by the overshoot and transient response. Thus, we state that our proposed reference-model-based NN control method is better than the conventional error feedback NN method.

(a) Control result of conventional error feed-back ANN control system   (b) Control result of proposed reference-model-based ANN control system
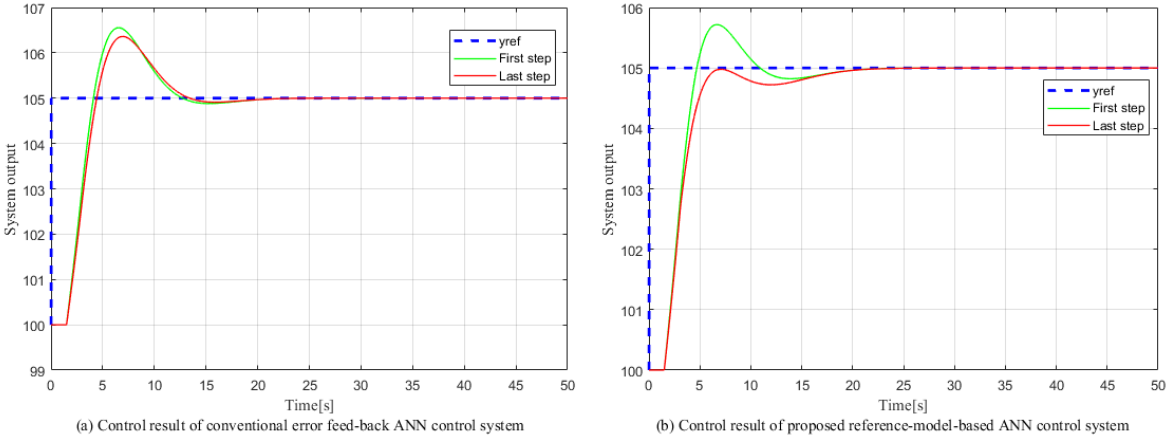
Figure 3-18 Comparison simulation results. (a) Time response of the conventional error feedback NN control system and (b) Time response of the proposed reference-model-based NN control system.

For detailed showing, the repeated response of the reference-model based NN control result is shown in Figure 3-19 with the FBA and NN output.
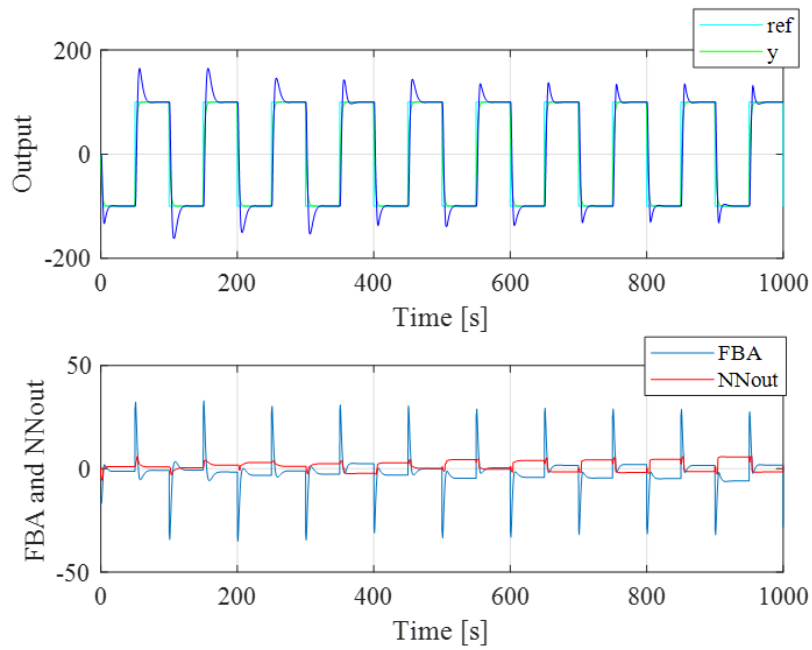
Figure 3-19 Repeated output and control output of FBA controller and NN controller.

Also, the reference model output and error between the reference model output and real plant output is shown in Figure 3-20.
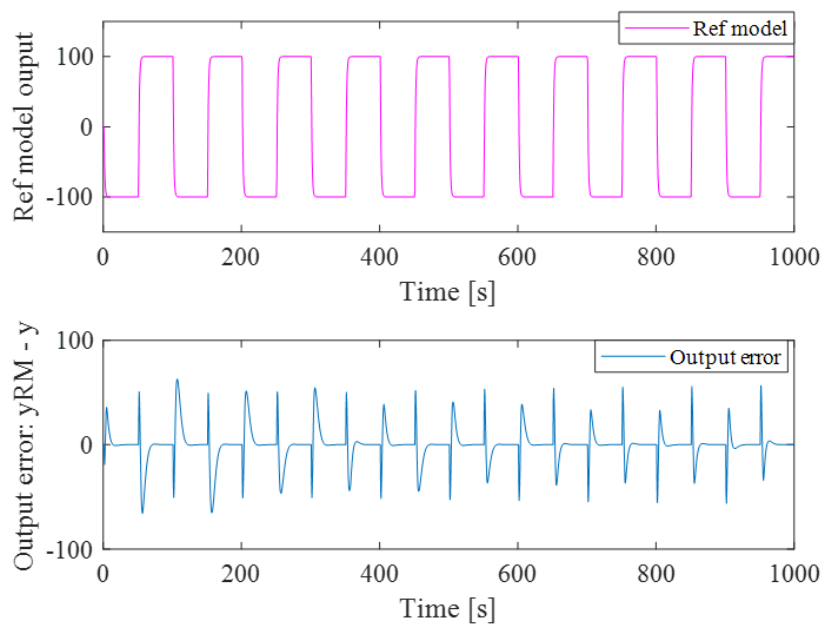

Figure 3-20 Reference model output and error signal.

Next, the training comparison between the conventional feedback NN control system and reference-model-based NN control is focused on both positive direction and negative direction.

The training results of these two control systems are shown in Figures 3-21 and 3-22, respectively.
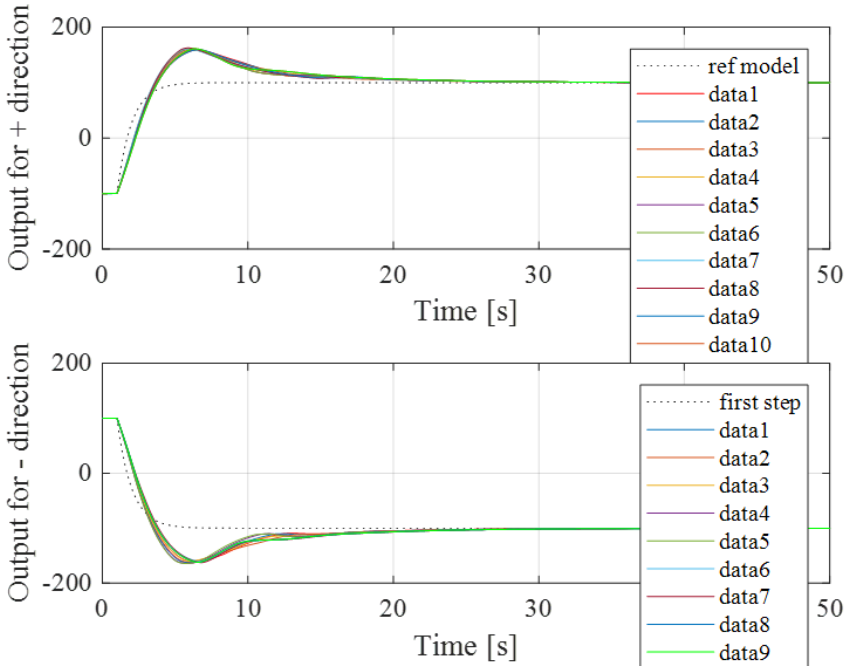

Figure 3-21 Training result of conventional error feedback NN control system.
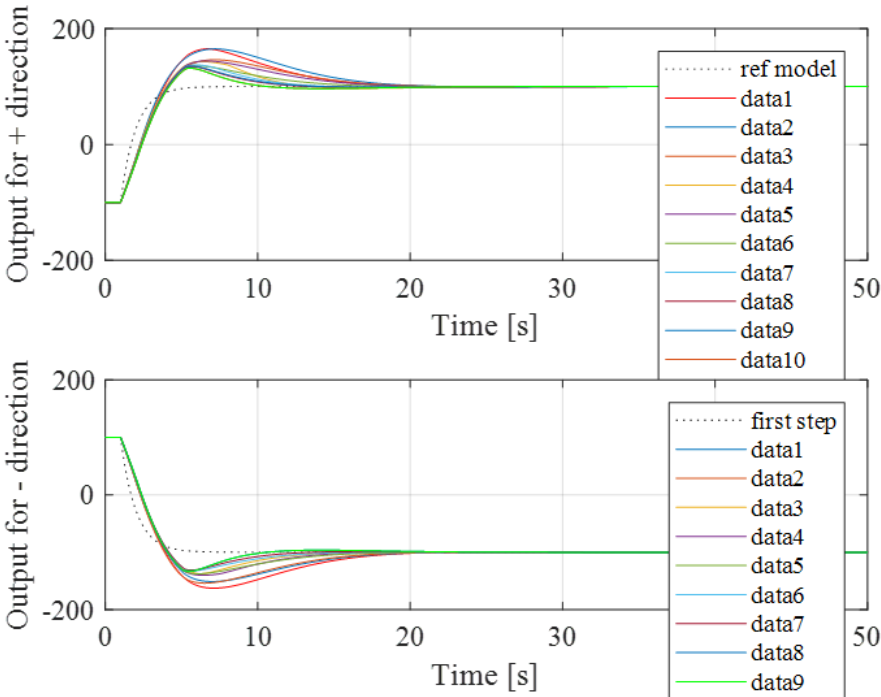

Figure 3-22 Training results of reference-model-based NN control system.

From the results of both positive direction control and negative direction control, it can be concluded that, for the conventional error feedback NN control system, there is no obvious

improvement after several repetitions, while for the reference-model-based NN control system, after repeating several times, the response has been improved in both positive direction and negative direction control.

3.8 System identification

To make the system worse and hard to be controlled, both the time constant and delay time of the system need to be larger. Thus, as is shown in Figure 3-23, Ch1 is chosen as the heater, and Ch4 is chosen as the temperature output. The step response identification result can be expressed as Eq. (3-45), and the reference model can be designed as Eq. (3-46). According to the approximation method, the reference model can be approximated as Eq. (3-47).
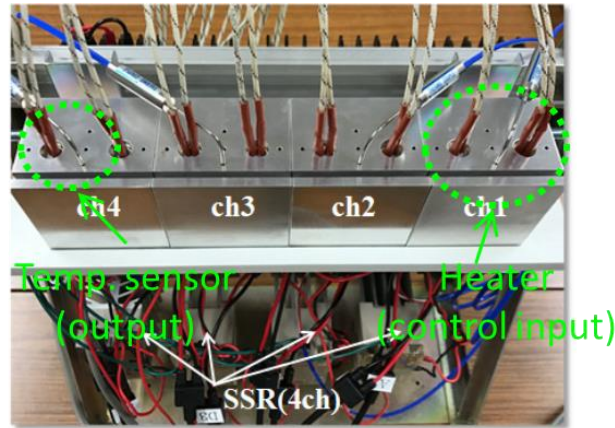

Figure 3-23 Experimental setup.

$$P(s) = \frac{2.36}{2626s + 1} e^{-524s} \qquad (3\text{-}45)$$

$$R(s) = \frac{2.36}{2626 * Rs + 1} e^{-524s} \qquad (3\text{-}46)$$

$$R(s) \approx \frac{2.36}{26.26s + 1} \cdot \frac{1}{(\dfrac{524}{2}s + 1)^2} \qquad (3\text{-}47)$$

3.9 Simulation results

The simulation was carried out in the MATLAB/SIMULINK environment. The simulation

can be divided into three phases. Phase 1: Basic feedforward NN (FNN) simulation. Phase 2: Robustness of the Reference-model-based NN control system. Phase 3: Recurrent type NN control system simulation.

3.9.1 Basic feedforward NN simulation results

For the conventional feedforward NN controller, the multi-layer network structure and its calculation relationship are shown in Figure 3-24. In this type of NN controller, the algorithm has already been introduced before as a typical NN network controller.
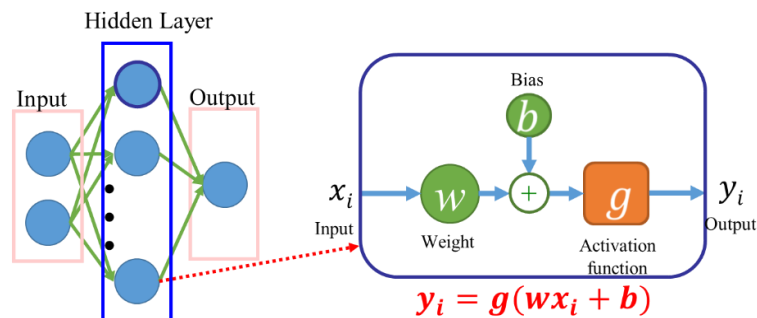

Figure 3-24 Basic feedforward type NN controller.

In the simulation, the control object transfer is expressed as a FOPTD system as Eq. (3-45). Hence the reference model can be represented as Eq. (3-46), wherever R is set as 0.01.

The I-PD parameter was decided by the plant parameter as described before. The parameters were K_p = 10.3, T_i = 838, T_d = 209. Moreover, the hyperparameters of the neural network are decided as $\alpha = 1 \times 10\text{-}9$, $\beta = 2 \times 10\text{-}5$, these two parameters are designed by try and error method. The initial value of the weight was set to a random value between -1 and 1.

The simulation has been carried out with the following condition: the control performance was evaluated both in a positive direction and a negative direction. The reference value of the temperature was set as a repetitive step signal with an amplitude of 5 degree Celsius, the offset of the reference is 100 degree Celsius. The time response is shown in Figure 3-25.
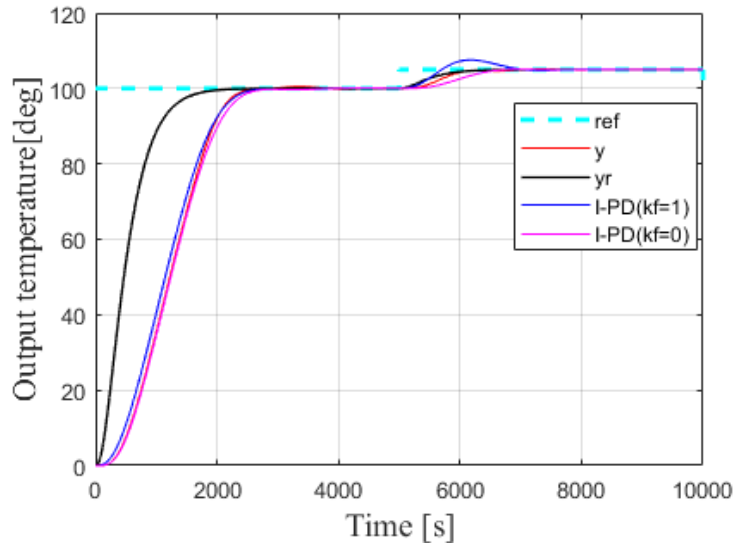
Figure 3-25 Time response of the controlled system.

Changes from 100 degree Celsius to 105 degree Celsius are defined as the positive direction control, while 105 degree Celsius to 100 degree Celsius are defined as the negative direction control. These two direction controls will be repeated several times to compare the first step and last step response as is shown in Figure 3-26.
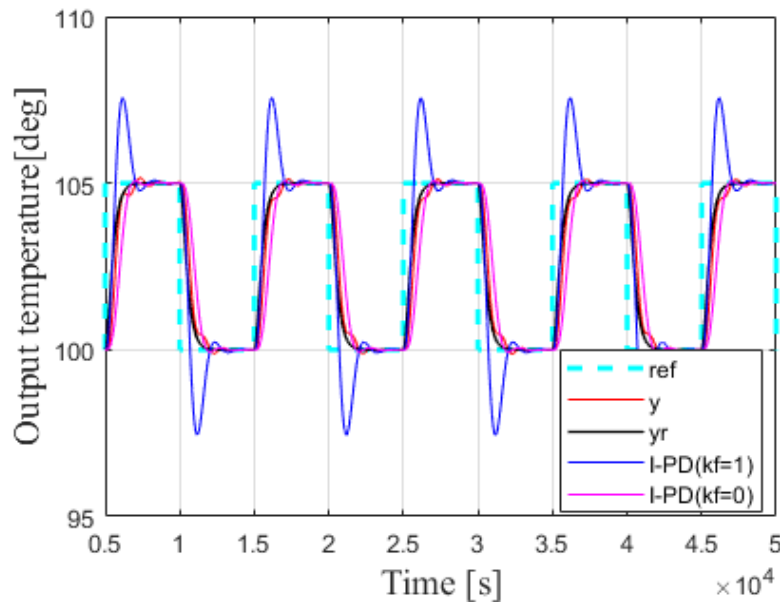

Figure 3-26 Repeated time response between 100 *degree Celsius* and 105 *degree Celsius.*

The output of the NN and I-PD controllers are shown in Figure 3-27, while the control input with the summation of the neural network output and the I-PD output is shown in Figure 3-28.
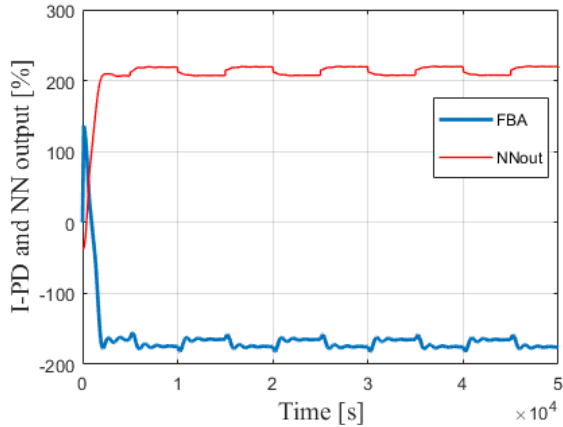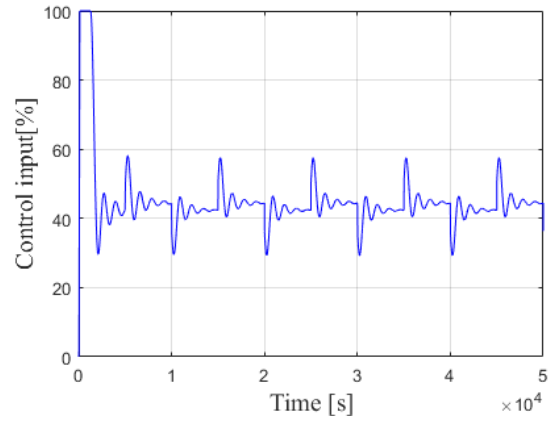
75

Figure 3-27 NN and I-PD output.

Figure 3-28 Control input.

As shown above, the output of the I-PD controller is initially positive, about 140%, and that of the NN controller is initially negative, about -40%. In this condition, the I-PD controller plays a dominant role. As the system approaches the setpoint, the output of the I-PD controller becomes negative, about -180%, and that of the NN controller becomes positive, about 225%. The control efficiency switches from the I-PD controller to the NN controller. The control input respects the sum of the I-PD and NN output; the steady-state value is about 45%.

Focusing on the reference from 100 degree Celsius to 105 degree Celsius as the positive direction and 105degree Celsius to 100degree Celsius as the negative direction, each step response is plotted on the same figure as in Figures 3-29 and 3-30, respectively.
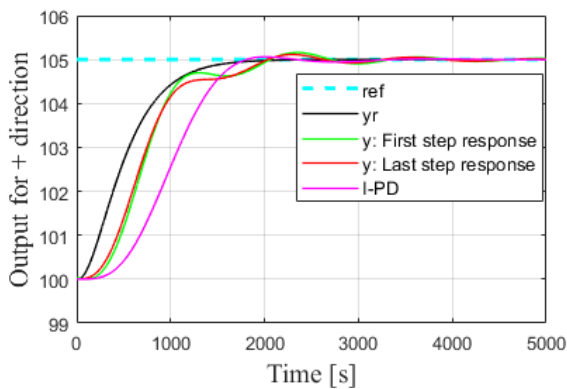

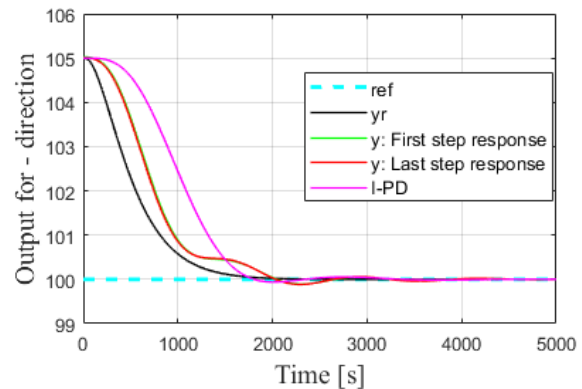Figure 3-29 Positive direction control result.

Figure 3-30 Negative direction control result.

From the simulation results, regardless of the positive direction control or the negative direction control, the system response with the neural network control in regards to rising time and settling time is improved from the conventional I-PD control. Moreover, since the first step

76

response is almost the same as the last step response, the learning process has been done at the beginning of the first step. The system response follows the reference model, although there is a little deviation. As a result, the control efficiency has been improved by comparing to the conventional I-PD control.

3.9.2 Robustness of artificial NN control system

For the temperature control system, when the control object is defined as a FOPTD system, there always remains plant perturbation. Here, assuming that L is the delay time of the system and T is the time constant of the control object, the ratio L/T is defined as the plant perturbation. When the value of L/T is small, it is easy to control the system, while it is hard to control the system when L/T is big. According to the identified plant model shown as Eq. (3-45), we will divide the control object into 4 classifications, shown as Table 3-1.

Table 3-1 4 kinds of model parameters

①	K=2.36	T=2626	L=524	LT ratio 1:5
②	K=2.36	T=262.6	L=52.4	LT ratio 1:5 (T and L are both smaller as 1/10)
③	K=2.36	T=2626	L=52.4	LT ratio 1:50
④	K=2.36	T=2626	L=524	LT ratio 1:1.6

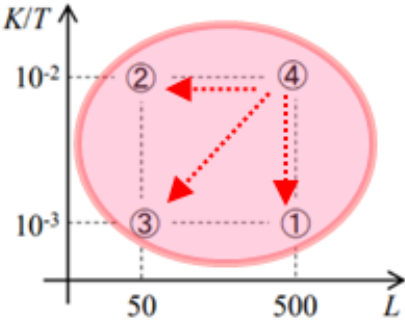The possibility of the NN control range of these 4 kinds models is shown in Figure 3-32.

Figure 3-32 The plant perturbation of NN control system.

From the diagram, the plant ④ has the biggest L/T ratio, that makes this kind of plant most difficult to control, and plant ③ has the smallest L/T ratio, this kind of plant is the easiest to be controlled. Based on these plant parameters, the parameters of the conventional I-PD controllers can be obtained as shown in Table 3-2.

Table 3-2 I-PD Parameters of each control object

Control object	①	②	③	④
K_p	5.1546	1.754	16.1	0.1754
T_i	921.8	74.7	125.4	961.8
T_d	209	186.8	31.4	240.45

The simulation has been carried out in MATLAB/SIMULINK environment, and the simulation condition is same as before in Section 3.9.1, only the parameters of the I-PD controllers are based on Table 3-2, the simulation results of these four kinds of plants are shown in Figures 3-33, 3-34, 3-35 and 3-36, respectively. Only positive control will be analyzed.
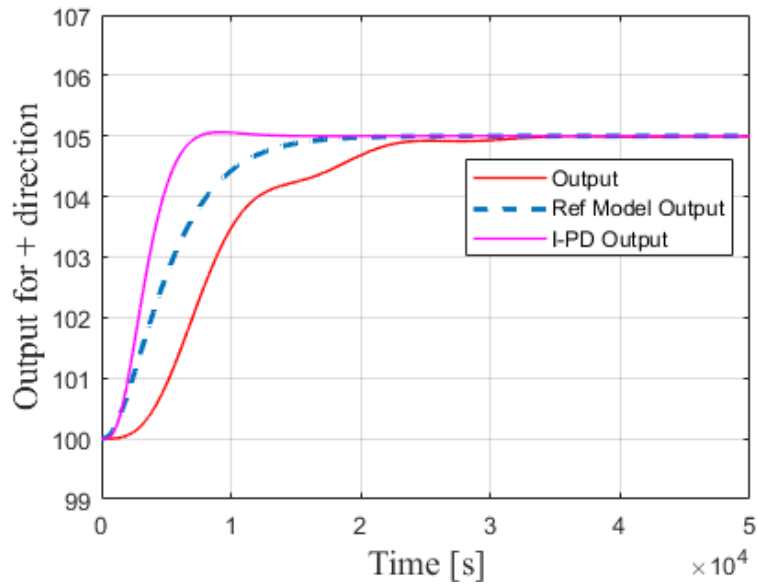

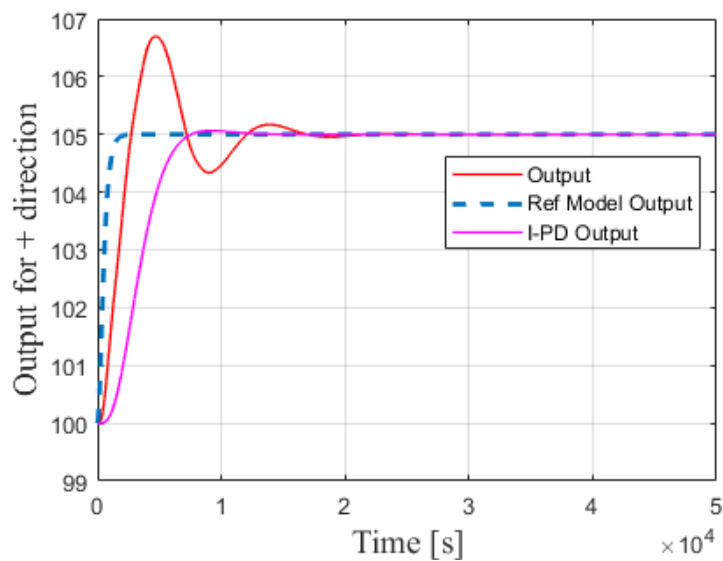Figure 3-33 Simulation result of NN control for plant ①.

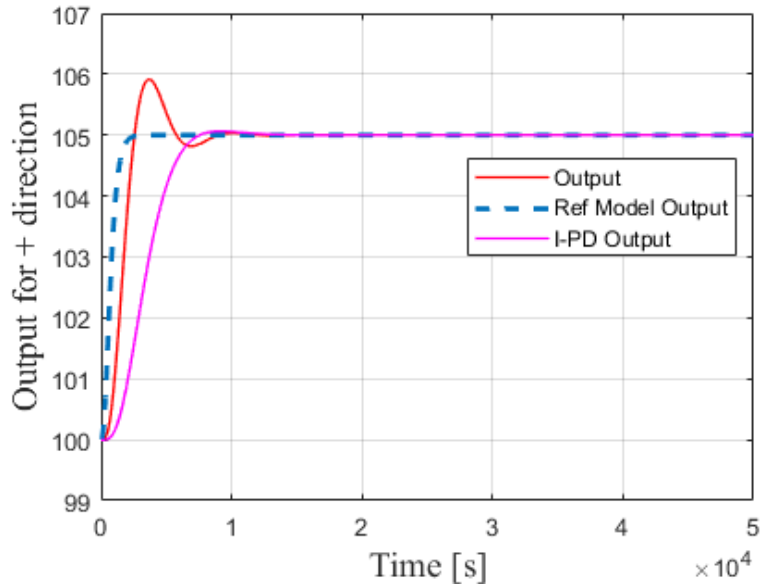Figure 3-34 Simulation result of NN control for plant ②.

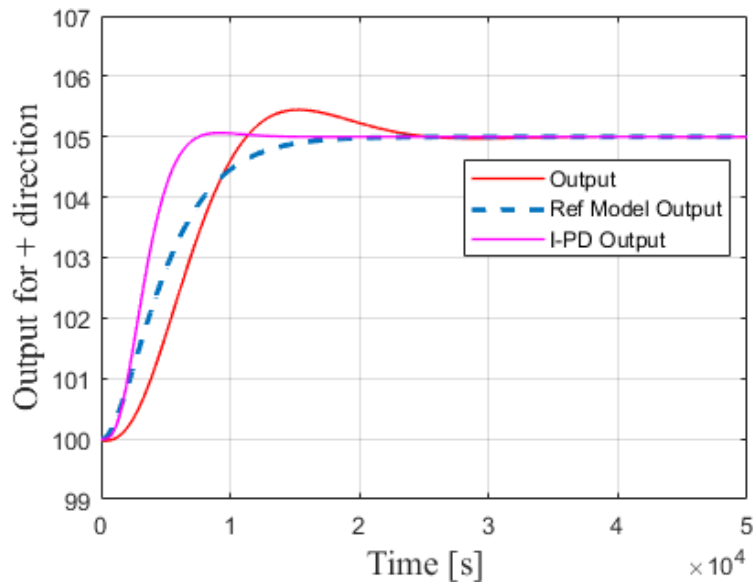Figure 3-35 Simulation result of NN control for plant ③.

Figure 3-36 Simulation result of NN control for plant ④.

From the tracking results, although the response of plant ② to ④ has a little overshoot, the response of the NN control system can still track the reference model, and can control the system to the steady-state stable state. Thus, we can state that the reference-model-based NN control system has somehow the robustness of the plant perturbation.

Besides the plant perturbation, the disturbance is also one of the most effective influences of the temperature system and it has a direct impact on the output temperature. Thus, the control system needs to have the robustness of the system disturbance, and the simulation has been

carried out to test the robustness of the reference-model—based NN control system to disturbance. In the simulation, a 2degree Celsius disturbance has been added to the controlled stable system at time 32500s, all the four kinds of the control objects have been simulated, the simulation tracking results are shown in Figures 3-37, 3-38, 3-39 and 3-40, respectively. Same as the plant perturbation robustness simulation, only the positive direction control responses are shown.
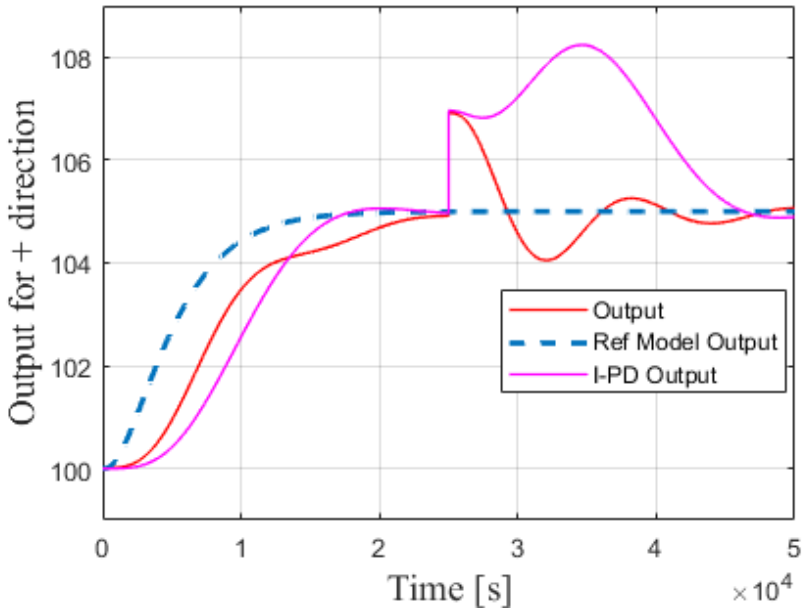

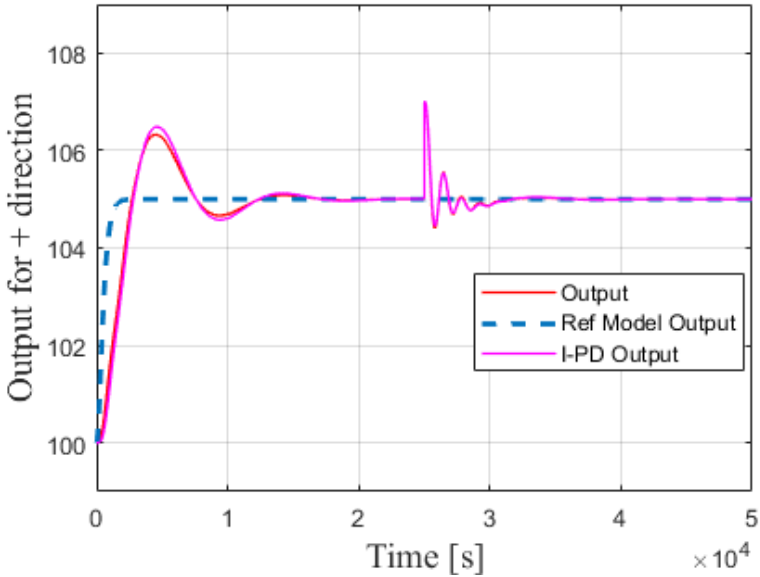Figure 3-37 Simulation result of NN control for plant ① with disturbance.

Figure 3-38 Simulation result of NN control for plant ② with disturbance.
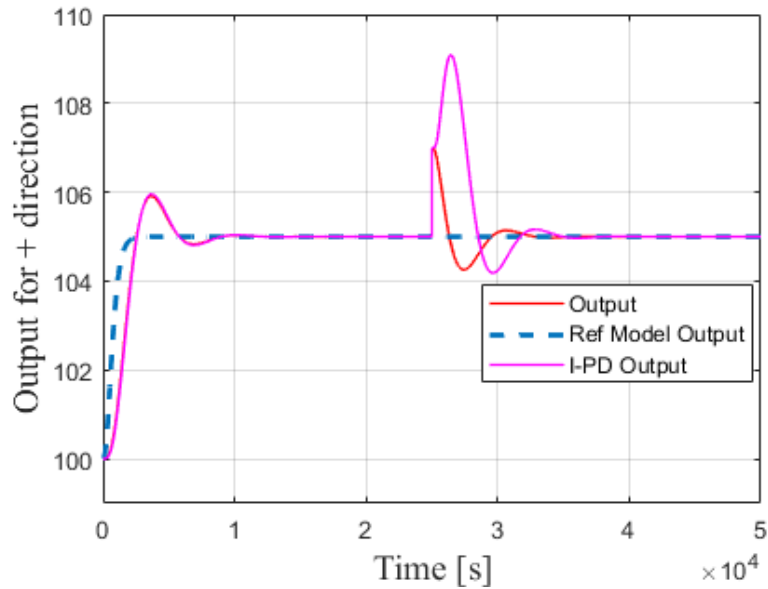
Figure 3-39 Simulation result of NN control for plant ③ with disturbance.
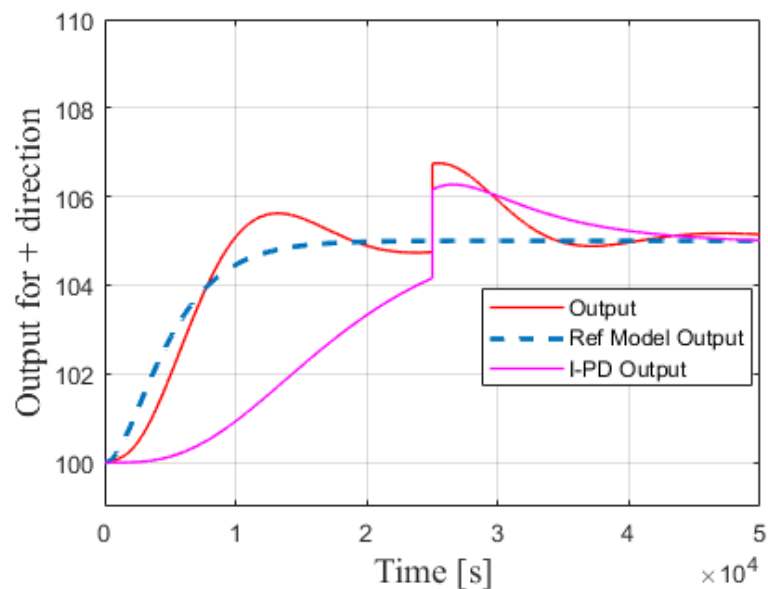
Figure 3-40 Simulation result of NN control for plant ④ with disturbance.

From the results, for all the kinds of the plants, after the disturbance has been introduced, the controlled system can return back to the steady-state after a few seconds. Here we can conclude that the control method for all the kinds of the plants has the robustness of the disturbance.

3.9.3 Recurrent NN control system

In this section, we try to change the conventional feedforward NN structure to the recurrent

NN (RNN) structure. The diagram of the RNN is shown in Figure 3-41.

$$y_i = g(wx_i + uy_{i-1} + b)$$

Figure 3-41 Recurrent NN controller structure.

Unlike the feedforward neural networks, RNN can use their internal state (memory) to process sequences of inputs. This makes them applicable to tasks such as unsegmented, connected handwriting recognition or speech recognition. The weight or gradi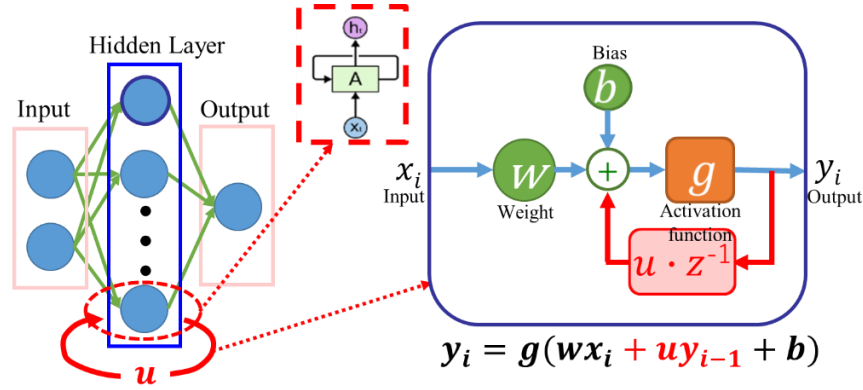ent error update of the RNN is related to the number of state retention τ, the weight and bias updating can be changed into Eqs. (3-48), (3-49) and (3-50), respectively.

$$W_2(t+1) = W_2(t) - \alpha_2 \sum_{z=0}^{\tau} \Delta_2(t-z) Y_1(t-z)^T \tag{3-48}$$

$$U_2(t+1) = U_2(t) - \alpha_2 \sum_{z=0}^{\tau} \Delta_2(t-z) Y_1(t-z-1)^T \tag{3-49}$$

$$\theta_2(t+1) = \theta_2(t) - \beta_2 \sum_{z=0}^{\tau} \Delta_2(t-z) \tag{3-50}$$

The simulation has been carried out to evaluate the control efficiency of the RNN control method and comparing it to the basic FNN control method, the simulation condition is the same as before, and the plant model is same as the identified model shown in Eq. (3-45). The simulation result is compared to that of conventional FNN control system under the same condition, the result of FNN is shown in Figure 3-42. To evaluate the improvement of the RNN control method, the response lag behind the reference model J is used as the judgment.
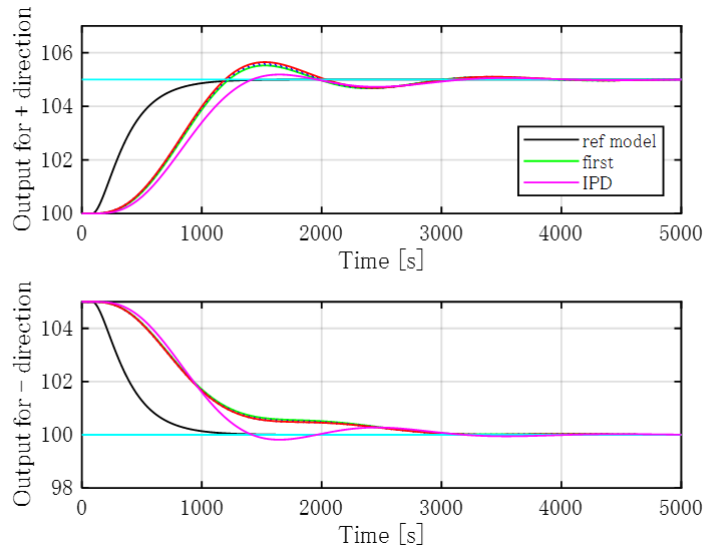
Figure 3-42 Positive and negative control result of FNN controller.

From the response results of the FNN control system, the overshoot of the positive direction control is about 0.9 degree Celsius and the response lag behind the reference model $J = 4291$, which means 4291 simulation steps behind the reference model.

The step response of the RNN control system can be divided into three kinds which are determined by the number of state retention τ, the simulation result of $\tau = 2$ (2 steps state retention) is shown in Figure 3-43. From the result, it can be easily seen that the overshoot and transient response speed have been improved, and $J = 3115$ smaller than the FNN control system.
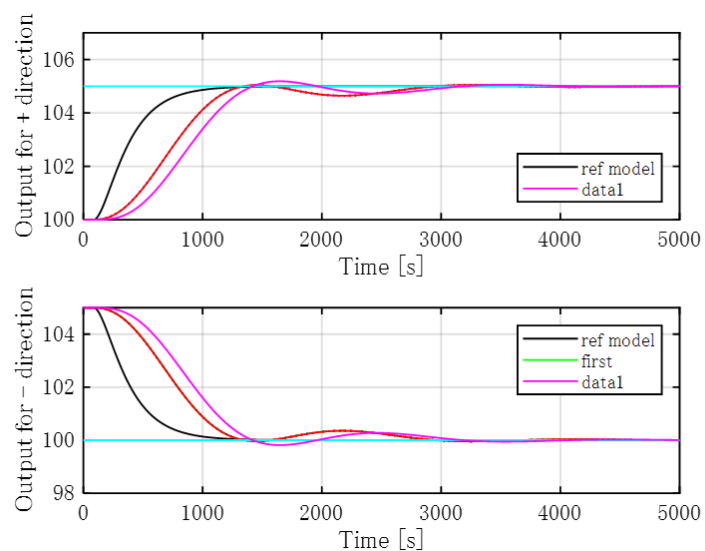
Figure 3-43 Positive and negative control result of RNN controller ($\tau = 2$).

The tracking result of $\tau = 5$ (5 steps state retention) is shown in Figure 3-44, although the overshoot is smaller than the FNN control system, still remains, and the judgment $J = 1517$ almost half that value of RNN ($\tau = 2$).
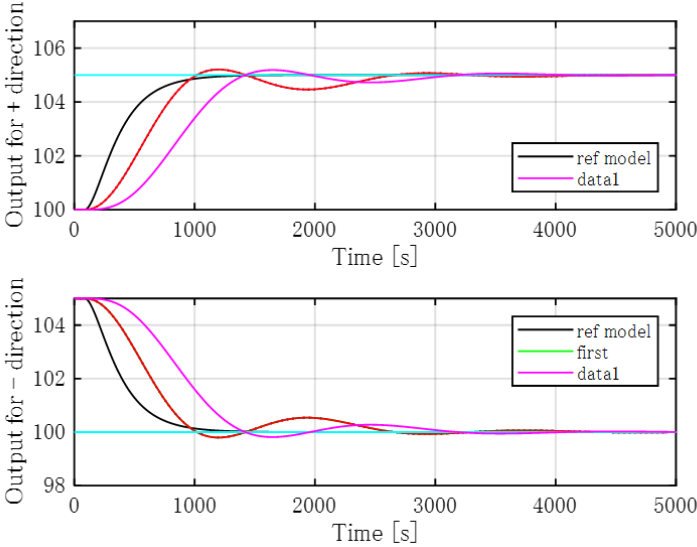
Figure 3-44 Positive and negative control result of RNN controller ($\tau = 5$).

Keeping on enlarging the $\tau = 10$ (10 steps state retention), the tracking result is shown in Figure 3-45, the judgment value $J = 1516$, only 1 step improved compared to RNN ($\tau = 5$) system.
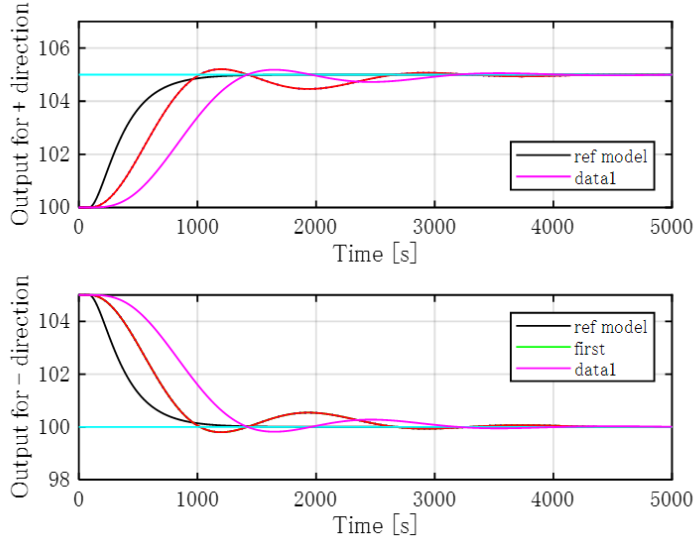
Figure 3-45 Positive and negative control result of RNN controller ($\tau = 10$).

The simulation result of RNN ($\tau = 20$) is shown in Figure 3-46, both positive and negative transient response including overshoot and response time are improved. However, the judgment

value $J = 2057$ is bigger than RNN ($\tau = 5$ and $\tau = 10$), the system response is a little slower than before.

Figure 3-46 Positive and negative control result of RNN controller ($\tau = 20$).

And the RNN $\tau = 50$ simulation result is shown in Figure 3-47, the judgment value $J = 3536$, the system response is slower than RNN with a smaller τ system.
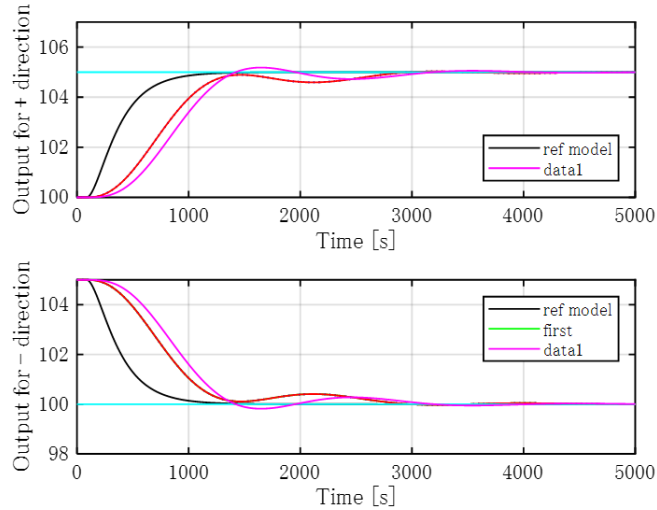
Figure 3-47 Positive and negative control result of RNN controller ($\tau = 50$).

From these results, we can conclude that the transient response and overshoot can be improved by RNN control method, and the value of τ has a significant impact on the output of the controlled system, but the system works under the best state is with $\tau = 10$.

Take the RNN ($\tau = 10$) as the best simulation system, the test of n control cycle 1 NN

calculation has been carried out. The sampling time of the simulation is set as 0.5, so $\tau = 10$ means 5s state retention, thus one control cycle may have 5s state retention. The numbers of control cycle will choose as 10, 20, 50 and 100, still, J will be the judgment.

The result of $n = 10$ simulation is shown in Figure 3-48, where the overshoot is a little big and $J = 1626$ the response is a little slower.
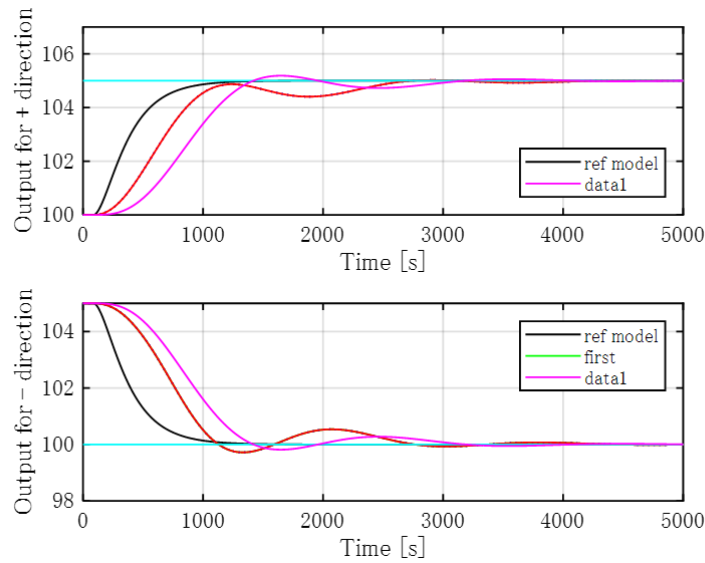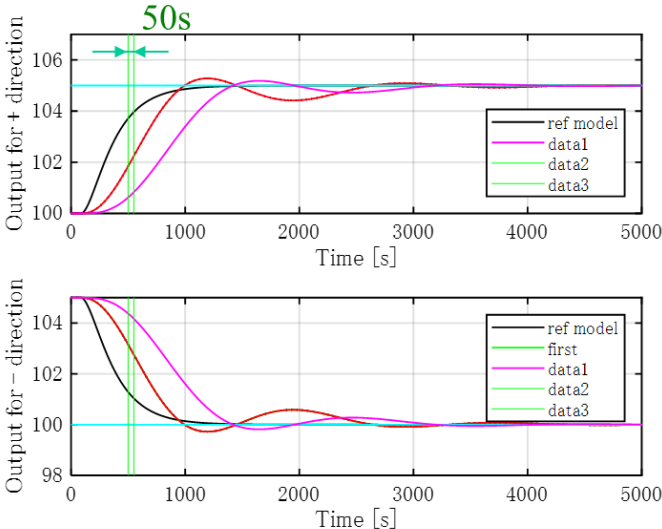

Figure 3-48 Positive and negative control result of RNN controller ($\tau = 2$, $n = 10$).

The result of $n = 20$ simulation is shown in Figure 3-49, the judgment value $J = 1960$, bigger than $n = 10$, the system response with a slight overshoot and down shoot.
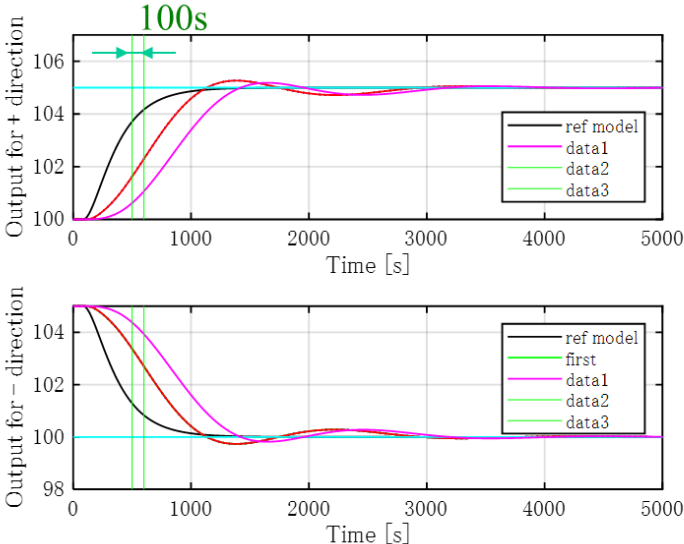
Figure 3-49 Positive and negative control result of RNN controller ($\tau = 2$, $n = 20$).

The simulation results of $n = 50$ and 100 are shown in Figures 3-50 and 3-51, respectively.

With the larger n, the J also becomes larger, that is the system response becomes slower. The judgment value J of these two systems are 2079 and 2965, respectively.
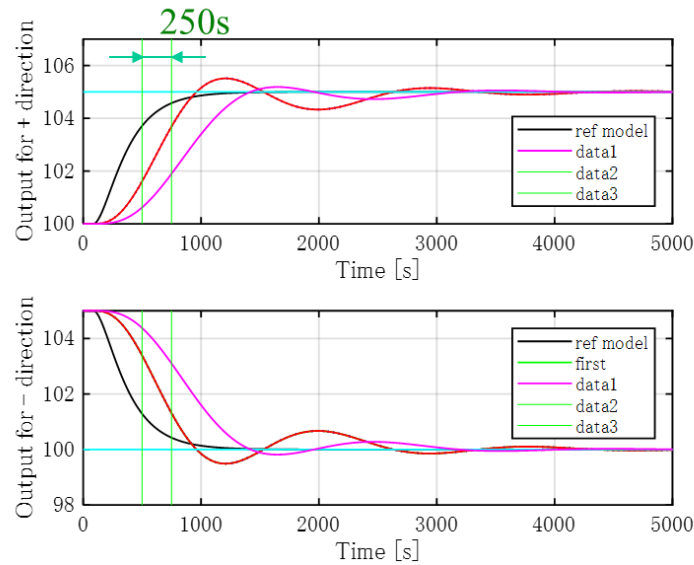
Figure 3-50 Positive and negative control result of RNN controller ($\tau = 2$, $n = 50$).
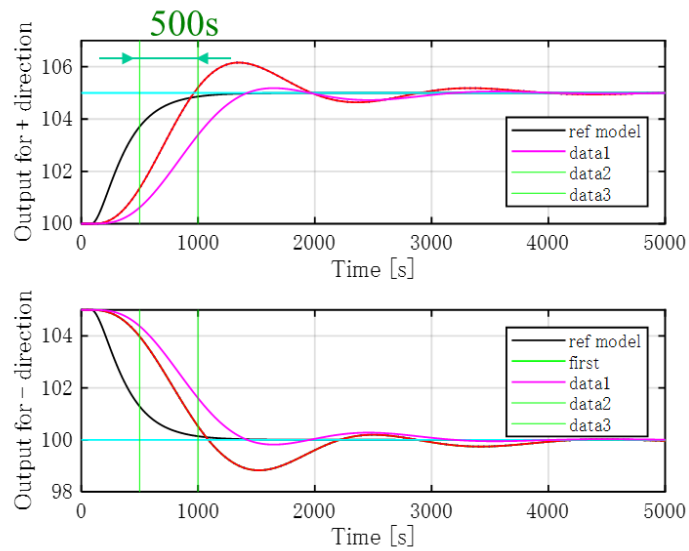
Figure 3-51 Positive and negative control result of RNN controller ($\tau = 2$, $n = 100$).

As a result, the best system response can be obtained through the NN controller calculates in every control cycle.

3.10 Experimental results

Experiments with the proposed reference-model-based NN control method were carried out using parameter values identical to those used in the simulation. The experimental setup was

the same as that shown in Figure 3-23. The condition of experiments is as the following: sampling period is 0.1s, controller sampling bit is 12bits, sensor resolution is 0.1degree Celsius and the air conditioner is set as 25degree Celsius. In the experiments, as in the simulation, to verify the control efficiency of the proposed method, the results were compared with those for a conventional I-PD control system with feed-forward gain $k_f = 0$ (slow) and $k_f = 1$ (fast). The experiments were carried out by controlling the temperature of Ch1 from 100degree Celsius to 105degree Celsius. The results for the output temperature are shown in Figure 3-52. The temperature change from room temperature to 100degree Celsius is defined as the learning period of the NN controller, and the temperature change from 100degree Celsius to 105degree Celsius is the control result for the controlled system as is shown in Figure 3-53.
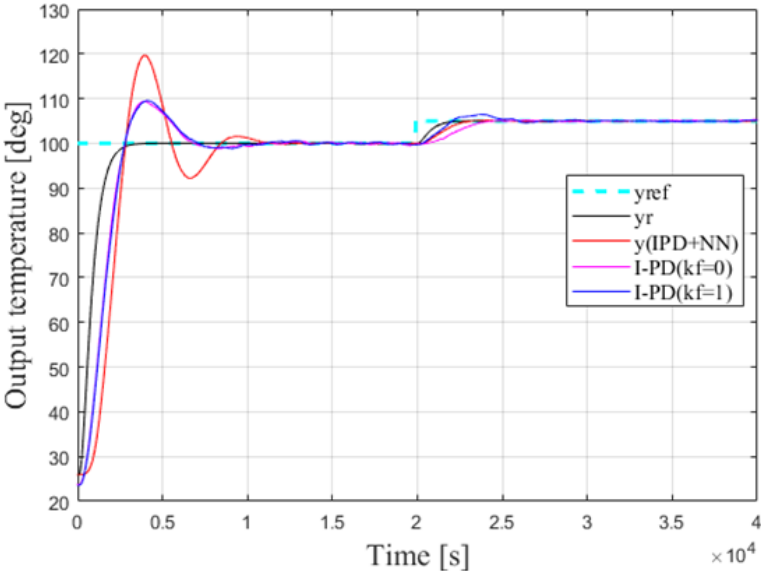
Figure 3-52 Experiment results of time response for the controlled system.
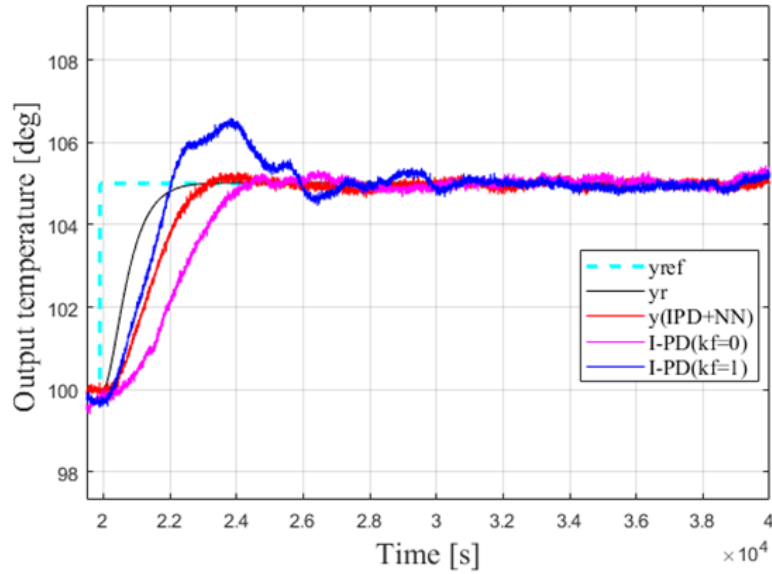
Figure 3-53 Experimental results of positive direction control for proposed control system.

The response time of the controlled system is about 2300s and about 1900s for the conventional I-PD system with $k_f = 0$ and $k_f = 1$, respectively, and about 2000s for the proposed NN control system. Although the response time for the proposed system is 5% slower than that for the I-PD ($k_f = 1$) system, it is 15% faster than that for the I-PD ($k_f = 0$) system. Although the I-PD ($k_f = 1$) system has the fastest response, it exhibits an overshoot of 1.5degree Celsius, which is about 30% of the reference value. The proposed NN control system and the I-PD ($k_f = 0$) system do not exhibit overshoot. Thus, control effectiveness is improved by the proposed method.

Figures 3-54 and 3-55 respectively show the output of the NN and I-PD controllers and the control input, which is expressed as the sum of the NN and I-PD output. As shown, the output of the I-PD controller is initially positive, about 140%, and that of the NN controller is initially negative, about -120%. Under this condition, the I-PD controller plays a dominant role. As the system approaches the setpoint, the output of the I-PD controller becomes negative, about -25%, and that of 152% the NN controller becomes positive, about 63%. The control efficiency switches from the I-PD controller to the NN controller. And the control input respects the sum of the I-PD output and NN output; the steady-state value is about 38%.

89
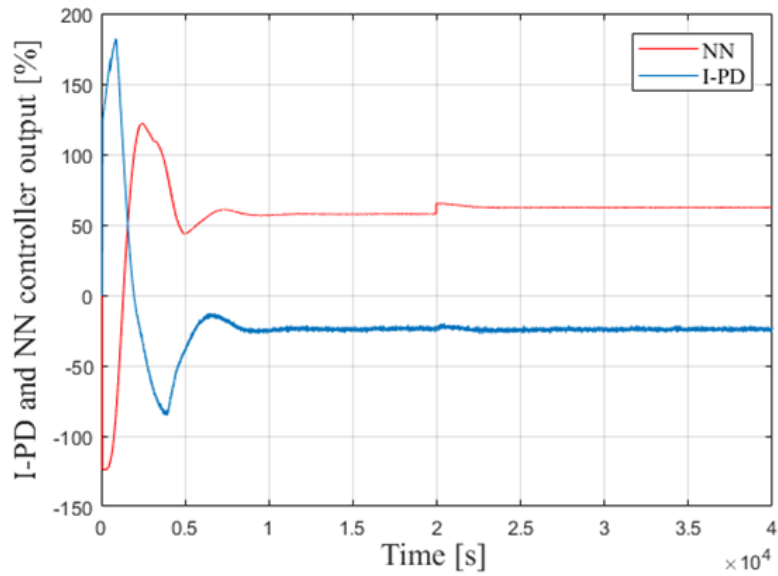
Figure 3-54 Outputs of NN controller and I-PD controller.
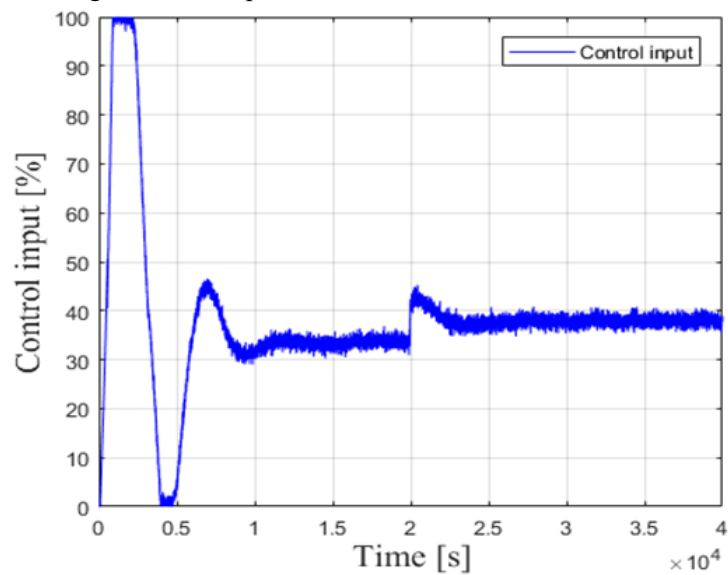
Figure 3-55 control input obtained from experiments.

From the experimental results compared with the simulation results shown above, the system improvement has been verified, thus we can conclude that, by introducing the reference-model-based NN control method, the transient response of the temperature control system can be improved as well as the overshoot compared to the conventional I-PD control system. Also, from the simulations results, it can be easily concluded that the NN control method is a model-free method what has the robustness of the plant perturbation and disturbance.

3.11 Conclusion

In this chapter, a reference-model-based NN control method for the temperature control system has been proposed. First, a brief introduction of artificial neural network and its advantages have been performed. Second, the forward algorithm of three kinds of neural structure has been introduced as well as the introduction of three kinds of most used neuron activation functions. Third, the backpropagation which is used to train the weight of every neuron has been presented in detail. Finally, the reference-model-based method has been introduced, the step by step design of the method was performed, and the advantage of the proposed method compared to the conventional error feedback NN method has been successfully evaluated through simulations. The simulation of the reference-model-based method has been carried out based on the identified control object, and the robustness of the proposed NN control method has been verified. Also, changing the NN type into recurrent NN yielded a better simulation result of the transient response. The experiments of the reference-model-based NN control method have been carried out, the results were compared to those of convention I-PD control system (both fast and slow control system). The effectiveness of the reference-model-based NN control method has been successfully evaluated through simulations and experiments.

Reference

[1] Suda, N. PID Control, Asakura Publishing: Tokyo, Japan, 1992.

[2] Oshima, M. Process Control Systems, Corona Publishing: New York, NY, USA, 2003.

[3] Goodwin, G.C, Fraebe, S.F, Salgado, M.E, Control System Design; Prentice Hall: Upper Saddle River, NJ, USA, 2001.

[4] Morari, M, Zafiriou, E. Robust Process Control, Prentice Hall: Upper Saddle River, NJ, USA, 1992.

[5] Maciejowski, J.M. Multivariable Feedback Design, Addison Wesley: Boston, MA, USA, 1989.

[6] Ko, J.S, Huh, J.H, Kim, J.C, Improvement of Temperature Control Performance of ThermoelectricDehumidifier Used Industry 4.0 by the SF-PI Controller, Processes 2019, 7, 98.

[7] Song, B.Q, Mills, J.K, Liu, Y.H, Fan, C. Z, Nonlinear Dynamic Modeling and Control of a Small-Scale

Helicopter, Int. J. Control Automat. Syst. 2010, 8, 534–543.

[8] Fujimori, A, Ohara, S, Order Reduction of Plant and Controller in Closed Loop Identification based on Joint Input-Output Approach, Int. J. Control Automat. Syst. 2017, 15, 1217–1226.

[9] Yao, Y, Yang, K, Huang, M, Wang, L, A state-space model for dynamic response of indoor air temperature and humidity, Build. Environ. 2013, 64, 26–37.

[10] Yao, Y, Yang, K, Huang, M, Wang, L, A technique for identification of linear systems, IEEE transactions on Automatic Control. 1965, AC-10, 461–464.

[11] Fliess. M, Marquez. R, Mounier. H, An extension of predictive control, PID regulators and Smith predictors to some linear delay systems. Int. J. Control. 2002, 75, 728–743.

[12] Bai. J, Wang. S, Zhang. X, Development of an adaptive Smith predictor-based self-tuning PI controller for an HVAC system in an experiment room, Energy Build. 2008, 40, 2244–2252.

[13] Xu. M, Li. S, Practical generalized predictive control with decentralized identification approach to HVAC systems. Energy Convers, Manage. 2007, 48, 292–299.

[14] Zhang. J, Experimental study on a novel fuzzy control method for static pressure reset based on the maximum damper position feedback, Energy Build. 2015, 108, 215–222.

[15] Afram. A, Janabi-Sharifi, Theory and applications of HVAC control systems - Areview of model predictive control (MPC). Build, Environ. 2014, 72, 343–355.

[16] Gao, Z, Nguang, S.K, Kong, D.X. Data-driven approaches for complex industrial systems, IEEE Trans. Ind. Inform. 2013, 9, 2210–2212.

[17] Gao, Z, Nguang, S.K, Kong, D.X, Advances in Modelling, Monitoring, and Control for Complex Industrial Systems, Complexity 2019, doi:10.1155/2019/2975083.

[18] Ryu. S. H, Moon. H. J, Development of an occupancy prediction model using indoor environmental data based on machine learning techniques, Build. Environ. 2016, 107, 1–9.

[19] Megri. A.C, Naqa. I. EI, Prediction of the thermal comfort indices using improved support vector machine classifiers and nonlinear kernel functions, Indoor Built Environ. 2016, 25, 6–16.

[20] Badia. M, McCarthy. R, Data estimation methods for predicting temperatures of fruit in refrigerated containers, Biosystems Engineering. 2016, 151, 251–272.

[21] Mercier. S, Marcos. B, Identification of the best temperature measurement position inside a food pallet for the prediction of its temperature distribution, International Journal of Refrigeration. 2017, 76, 147–

159.

[22] Badia. M, Qian. J. P, Fan. B. L, Artificial neural networks and thermal image for temperature prediction in apples, Food and Bioprocess Technology. 2012, 9, 1089–1099.

[23] Nunes. M. C. N, Nicometo. M, Emond. J. P, Badia-Melis. R, Uysal. Improvement in fresh fruit and vegetable logistics quality, Berry logistics field studies. Philosophical Transactions of the Royal Society A: Mathematical, Physical and Engineering Sciences. 2014, 372, 20130307.

[24] Raab. V, Petersen. B, Kreyenschmidt. J, Temperature monitoring in meat supply chains, British Food Journal. 2011, 113, 1267–1289.

[25] Katic. K, Li. R. L, Verharrt. J, Zeiler. W, Neural network based predictive control of personalized heating systems, Energy Build. 2018, 174, 199–213.

[26] Li. X. M, Zhao. T. Y, Zhang. J. L, Chen. T. T, Predication control for indoor temperature time-delay using Elman neural network in variable air volume system, Energy Build. 2017, 154, 545–552.

[27] Mercier. S, Uysal. I, Neural network models for predicting perishable food temperatures along the supply chain, Biosystems Engineering 2018, 171, 91–100.

[28] Thenozhi. S, Yu. W, Stability analysis of active vibration control of building structures using PD/PID control, Engineering Structures 2014, 81, 208–218.

[29] Guerrero. J, Torres. J, Creuze. V, Chemori. A, Campos. E, Saturation based nonlinear PID control for underwater vehicles: Design, stability analysis and experiments. Mechatronics 2019, 61, 96–105.

[30] Ziegler, J.G, Nichols, N.B, Optimum settings for automatic controllers, Trans. ASME 1942, 64, 759–768.

Chapter 4

Summary and Future Work

4.1 Summary

This thesis is focused on the advanced control strategies and its application in the industrial processes. Two advanced control methods for the temperature control systems have been proposed.

1. Model-based advanced control

In this method, the pole-zero cancellation method for the multi-point temperature control system has been introduced. In order to realize the model-based advanced control, the system identification method was performed to obtain the plant model of the control object, the detailed introduction of the system identification method for first order plus time delay (FOPTD) system has been presented. Based on the identified plant model, the PI controllers with normal bandwidth and 10 times bandwidth for each channel were designed, and then the SISO experiments of the PI control system have been carried out. Comparing it to the simulation results, PI control performance has been verified. After this evaluation, the MIMO PI control system has been designed. Due to strong coupling effect of the controlled object, the decoupling compensation has been added into the MIMO PI control system. In the same way as the SISO experiments, both MIMO PI control system with and without decoupling compensation have been investigated. Upon these foundations, the pole-zero cancellation method has been proposed for the MIMO temperature control system to ensure proper transient response and to provide more closely controlled temperatures. In the proposed method, the temperature difference and transient response of all points can be controlled by considering the delay time difference and coupling term together with matrix gain compensation, and by investigating the pole-zero cancellation with feedforward reference model to the control loop. The simulations were carried out in the MATLAB/SIMULINK environment, and the experiments were performed based on the DSP controlled system platform. The effectiveness of the proposed

pole-zero cancellation method was evaluated by comparing the results to those for a well-tuned conventional PI control system and PI plus decoupling compensation system.

2. Model-free intelligent control

In this method, a reference-model-based artificial neural network (NN) control method has been proposed for the temperature control system. Several types of neural network structure and activation function are investigated, and the multi-layer NN structure is chosen with the ReLU function as its activation function. The control system is driven by using the error signal between system output and reference model output as the teaching signal of the NN controller. The proposed method is a reference-model-based NN system combined with I-PD control structure. The reference model and I-PD parameters are designed based on the FOPTD system. The simulation has been carried out in MATLAB/SIMULINK environment to evaluate the control performance of the proposed method by comparing with the conventional feedback error learning NN control system. The effectiveness of the proposed method has been evaluated by focusing on the overshoot and transient response of the controlled system. Also, the robustness of the proposed reference model-based NN control method for the plant perturbation and disturbance, has been successfully verified. In addition, the recurrent type NN structure has been introduced to the control system, and simulations have been carried out to compare with the feedforward type NN control system. Finally, the experiments of the proposed control method have been carried out on a DSP-based temperature system platform. The results are quantitively evaluated by taking the transient response into account.

4.2 Future works

Although the proposed methods have successfully improved the control performance, there still remain some shortcomings that need to be improved. Followings will be the future works.

1). Plant model: In this thesis, the plant model of the temperature control system is expressed as a first-order plus time delay (FOPTD) system. However, the thermal process is a very complex process, only by using the FOPTD model it may not indicate all the characteristics of the plant. Thus, in further research, the higher-order model is expected to be applied to the control system.

2). The proposed pole-zero cancellation method currently is just applied to a simplified two-inputs two-outputs temperature control system, further research is needed to extend the control points of the system.

3). The proposed reference-model-based NN control method is applied to a SISO plant, for further research this method is expected to be applied to the multi-point temperature control system. Also, the reference model we designed is just a model based on the control plant and there is no control loop in the reference model. Thus, future research needs to improve the reference model by adding closed-loop control.

Publication Papers

Journal publications

Related journal publications

➢ Song Xu, Seiji Hashimoto and Wei Jiang: "Pole-Zero Cancellation Method for Multi Input Multi Output (MIMO) Temperature Control in Heating Process System," *Processes*, Vol. 7, No. 8, 497, pp.1-12, 2019. (Impact Factor: 1.963 (2018)) (DOI: 10.3390/pr7080497)

➢ Song Xu, Seiji Hashimoto, Yuqi Jiang, Katsutoshi Izaki, Takeshi Kihara, Ryota Ikeda and Wei Jiang:" A Reference-Model-Based Artificial Neural Network Approach for Temperature Control System," *Processes*, Vol. 8, No. 1, 50, pp.1-11, 2020. (Impact Factor: 1.963 (2018)) (Doi:10.3390/pr8010050)

Reference journal publications

➢ Song Xu, Wei Jiang and Seiji Hashimoto: "Analysis and Design of an Air-Coupled DC Transformer with a Hybrid Modulation Control Method," *Energies*，Vol. 12, No.13, 2570, pp.1-19, 2019. (Impact Factor: 2.707 (2018); 5-Year Impact Factor: 2.990 (2018)) (DOI: 10.3390/en12132570)

➢ Wei Jiang, Jieyun Wang, Qianglong Wang, Song Xu, Seiji Hashimoto and Zhong Liu:"Design and Implementation of a Low Power Low Cost Digital Current-Sink Electronic Load," *Energies*, Vol. 12, No. 13, 2611, pp.1-14, 2019. (Impact Factor: 2.707 (2018); 5-Year Impact Factor: 2.990 (2018)) (doi:10.3390/en12132611)

➢ Song Xu, Seiji Hashimoto, Wei Jiang: "DC Micro-Grid Contactless Power Supply System with Active Load Detecting Control Method," Journal of Technology and Social Science, Vol. 2, No. 2, pp.36-44, 2018.

International conference papers

- Song Xu, Seiji Hashimoto and Wei Jiang, "A Novel Reference Model-Based Neural Network Approach to Temperature Control System", 2019 International Conference on Industrial Application of Big Data and Artificial Intelligence (BDAI 2019), D004, Oct, 2019.

- Song Xu, Seiji Hashimoto, "Pole-Zero Cancelation Method for Multi-input Multi-output Temperature Control System", International Conference on Mechanical, Electrical and Medical Intelligent System 2018 (ICMEMIS 2018), IPS06-02, Nov. 2018.

- Song Xu, Seiji Hashimoto, etc., "Experimental Verification of Slow Mode Based Control Method with Decoupling Compensation for MIMO System", International Conference on Technology and Social Science 2018 (ICTSS 2018), Apr. 2018.

- Song Xu, S. Hashimoto, Wei Jiang, "DC Micro-Grid Contactless Power Supply System with Load Detecting Control Method", International Conference on Mechanical, Electrical and Medical Intelligent System 2017 (ICMEMIS 2017), ID: I08-06, 2017.

- Seiji Hashimoto, Song Xu, etc., "A High Positioning Control and State Estimation Based on Learning Algorithm, International Conference on Mechanical", Electrical and Medical Intelligent System 2018 (ICMEMIS 2018), KL09-01, Nov. 2018.

- Seiji Hashimoto, Yu Fujimura, Song Xu, "Sliding Mode Observer-based Precise Vehicle State Estimation for EPS Systems", International Conference on Mechanical, Electrical and Medical Intelligent System 2017 (ICMEMIS 2017), ID: I08-01, Nov 29, 30 & Dec 1, 2017.

- Y. Jiang, L. Yuan, S. Xu et al. "Disturbance Rejection Evaluation of Slow-Mode Based Control for MIMO Delay System", International Conference on Mechanical, Electrical and Medical Intelligent System 2017 (ICMEMIS 2017), ID: I08-04, Nov 29, 30 & Dec 1, 2017.

Domestic conference papers

- Song Xu, Seiji Hashimoto and Wei Jiang. Experimental Verification of Slow Mode Based

Control Method for MIMO System with Dead Time,平成 29 年度第 8 回電気学会栃木

・群馬支所合同研究発表会, Mar. 2018.